NTNU – Trondheim
Norwegian University of
Science and Technology

Earthquake Analysis of Concrete Gravity Dams

Review and Modernization of Two Analysis Procedures

Arnkjell Løkke

Civil and Environmental Engineering
Submission date: June 2013
Supervisor: Svein N Remseth, KT
Co-supervisor: Anil K. Chopra, University of California, Berkeley

Norwegian University of Science and Technology
Department of Structural Engineering

NTNU
Norwegian University of Science and Technology

Faculty of Engineering Science and Technology
Department of Structural Engineering

MASTER THESIS SPRING 2013

For

Arnkjell Løkke

"Earthquake Analysis of Concrete Gravity Dams"

Earthquake analysis and earthquake resistant design of dams is of major importance because of the catastrophic consequences if such a structure is to fail. For this purpose, rigorous response history analysis (RHA) procedures have been developed to accurately compute stresses and deformations in concrete gravity dams subjected to earthquake ground motion, and simplified response spectrum analysis (RSA) procedures have been developed for use in the preliminary phase of design and safety evaluation of existing dams. However, since the early 1990's, few advances have been made to the procedures applicable for analysis of concrete gravity dams.

The purpose of this master's thesis is to review the analysis procedures and software available for computing the earthquake response of concrete gravity dams, and investigate how the procedures can be updated to ensure consistency with recent research and how the software can be modernized to improve its accessibility and user-friendliness. In particular, this includes:

- Literature study of the above mentioned RHA and RSA procedures that are available for concrete gravity dams.
- In depth study of how these analysis procedures are implemented in available computer software.
- Modernize the RHA and RSA procedures to account for advances in recent research.
- Modernize and improve user-friendliness of available computer software by computing new data to be used in the programs and programming new modules for pre- and post-processing of input and output.

- Perform comprehensive evaluation of the accuracy of the RSA procedure by comparing its results with those obtained from RHA of an actual dam modeled as a finite element system.

The student will conduct the research and preparation of his master's thesis during a six-month stay as a visiting student researcher at the University of California, Berkeley. The thesis must be written according to the requirements set forth by the Department of Structural Engineering at NTNU.

Supervisors are:

Svein N. Remseth	*Department of Structural Engineering, Norwegian University of Science and Technology (NTNU)*
Anil K. Chopra	*Department of Civil and Environmental Engineering, University of California, Berkeley*

The thesis must be submitted to the Department of Structural Engineering at NTNU no later than July 23, 2013.

ABSTRACT

A two-stage procedure has been proposed for the elastic analysis phase of seismic design and safety evaluation of concrete gravity dams: (1) response spectrum analysis (RSA) in which the peak value of response is estimated directly from the earthquake design spectrum; and (2) response history analysis (RHA) of a finite element idealization of the dam monolith. Both analysis procedures include the effects of dam-water foundation interaction, known to be important in the earthquake response of dams.

Presented in this thesis are two important developments that have now been added to the computer program EAGD-84, implementing the RHA procedure: (1) a set of Matlab modules – including an easy-to-use graphical user interface (GUI) – has been developed, providing users with the capability of pre-processing input and post-processing analysis output from EAGD-84 in the Matlab scripting language; (2) a more complete set of compliance data that govern the interaction between the dam and the foundation region has been incorporated in the program. These developments greatly improve the accessibility and functionality of the EAGD-84 program, and provide users with sufficient control over the overall damping in the dam-water-foundation system to ensure consistency with recent research.

The above mentioned RSA procedure has likewise been modernized. A number of enhancements have been made to the procedure, the most significant being: (1) a more complete set of data for the parameters that characterize dam-foundation interaction has been computed and implemented; and (2) to enhance the accuracy of the procedure, a correction factor for computing beam stresses on the downstream face of the dam has been developed. In addition, a comprehensive evaluation of the accuracy of the RSA procedure has been conducted, demonstrating that it estimates stresses close enough to the "exact" results (determined by RHA) to be satisfactory for the preliminary phase in the design of new dams and in the safety evaluation of existing dams. The accuracy achieved by the procedure is noteworthy, especially considering the complicated effects of dam-water-foundation interaction and reservoir bottom absorption on the dynamics of the system, and the number of approximations necessary to develop the procedure.

The updated version of the computer program EAGD-84, the new Matlab modules and the GUI, as well as a new report presenting the updated RSA procedure, have all been made publicly available through the Pacific Earthquake Engineering Research (PEER) Center.

Keywords: Concrete gravity dams; earthquake analysis; dam-water-foundation interaction; response history analysis; response spectrum analysis.

SAMMENDRAG

En totrinnsprosedyre er tilgjengelig for lineær-elastisk jordskjelvanalyse av gravitasjonsdammer: (1) responsspektrumanalyse (RSA) der den maksimale responsen estimeres direkte ved bruk av et responsspektrum; og (2) responshistorieanalyse (RHA) av en elementmetodemodell av gravitasjonsdammen. Begge analysemetodene inkluderer interaksjonseffektene mellom dam, magasin og underliggende fjellfundament, som er vist å ha betydelig innvirkning på responsen av gravitasjonsdammer utsatt for jordskjelv.

Denne oppgaven presenterer to viktige utvidelser som nå er blitt implementert i programvaren EAGD-84 som tar i bruk RHA-metoden: (1) et sett Matlab-moduler – inkludert et brukervennlig grafisk brukergrensesnitt (GUI) – har blitt utviklet, og gir brukere av programmet muligheten til å preprosessere input-data og postprosessere resultater fra programmet i brukergrensesnittet til Matlab; og (2) et mer komplett datasett som beskriver interaksjonseffektene mellom dam og fundament har blitt implementert i programmet. Disse nyutviklingene byr på dramatisk forbedring av funksjonaliteten og brukervennligheten til EAGD-84, og sikrer brukere av programmet tilstrekkelig kontroll over den samlede energidissipasjonen (dempningen) i systemet til å være i overenstemmelse med resultater fra nyere forskning.

Den tidligere nevnte RHA-metoden har også blitt modernisert. Flere forbedringer og nyvinninger er blitt implementert, de mest betydningsfulle er: (1) et mer komplett datasett for parameterne som beskriver interaksjon mellom dam og fundament er blitt implementert i metoden; og (2) for å forbedre nøyaktigheten til analysemetoden har en korreksjonsfaktor for å beregne spenninger på nedstrøms side av gravitasjonsdammer blitt utviklet. I tillegg har en omfattende evaluering av nøyaktigheten til analysemetoden blitt gjennomført, resultatene demonstrerer at metoden estimerer spenninger som er tilstrekkelig nære de "eksakte" resultatene (beregnet ved bruk av RHA) til å bli brukt i en forprosjektfase ved design av nye dammer eller for sikkerhetsvurderinger av eksisterende dammer. Nøyaktigheten som oppnås i metoden er oppsiktsvekkende, spesielt med tanke på de kompliserte virkningene av interaksjon mellom dam, magasin og fundament, og de omfattende forenklingene som er nødvendig for å utvikle analysemetoden.

En ny versjon av programvaren EAGD-84, de nye Matlab-modulene, samt en selvstendig rapport som beskriver den oppdaterte RSA-metoden har alle blitt gjort tilgjengelig for brukere gjennom forskningssenteret Pacific Earthquake Engineering Research (PEER) Center.

Nøkkelord: Gravitasjonsdammer; jordskjelvanalyse; interaksjonseffekter; responshistorie-analyse; responsspektrumanalyse.

TABLE OF CONTENTS

PART B: RESPONSE SPECTRUM ANALYSIS OF CONCRETE GRAVITY DAMS

PREFACE

About This Thesis

This thesis was written in the spring of 2013 and submitted to the Department of Structural Engineering at the Norwegian University of Science and Technology (NTNU) as a requirement for the degree of Master of Science in Civil and Environmental Engineering, with a specialization in Computational Mechanics.

The research presented in this thesis was conducted during the author's six-month stay as a visiting student researcher at the University of California, Berkeley under the supervision of Professor Anil K. Chopra at the Department of Civil and Environmental Engineering.

Historical Background

The safety of dams during earthquakes is extremely important because failure of such a structure can have catastrophic consequences on life and property. It is therefore essential to have reliable analysis procedures to design earthquake resistant dams and evaluate the safety of existing dams. Traditional "static" design procedures have been widely used to design concrete dams – and are in some cases still being used – even though it has been shown repeatedly that they are based on unrealistic assumptions, and that dams designed according to these procedures have experienced widespread damage during earthquakes.

In 1978, a two-stage procedure was proposed for the elastic analysis phase of seismic design and safety evaluation of concrete gravity dams: (1) response spectrum analysis (RSA) in which the peak value, i.e., the maximum absolute value, of response is estimated directly from the earthquake design spectrum; and (2) response history analysis (RHA) of a finite element idealization of the dam monolith. The RSA procedure was recommended for the preliminary phase of design and safety evaluation of dams and the RHA procedure for accurately computing the dynamic response and checking the adequacy of the preliminary evaluation. In the mid 1980's, both procedures were extended to consider the full effects of dam-water interaction, dam-foundation interaction and reservoir bottom absorption, known to have profound influence on the response of a dam to earthquake ground motion. Both the RHA and RSA procedures have been implemented in computer software, which have been utilized extensively for research purposes and in actual projects.

Objectives

The objective of master's thesis has been to (1) review and evaluate the analysis procedures and software available for computing the earthquake response of concrete gravity dams, (2) enhance these analysis procedures to ensure consistency with recent research, and (3) modernize the available software to make it more accessible for today's users and consistent with current research. In particular, the objective has been to:

- Modernize the computer program EAGD-84 by computing and implementing a complete data set governing dam-foundation interaction, and developing a set of pre- and post-processing modules to improve the accessibility and user-friendliness of the program.
- Modernize the RSA procedure by generating new standard values for the parameters that characterize dam-foundation interaction, developing a correction factor to improve the accuracy of the procedure, and presenting new recommendations for input parameter selection.
- Evaluate the accuracy of the RSA procedure by comparing its results with those obtained from RHA of a finite element idealization of an actual dam.

Organization of This Report

This report is organized in two parts, in which Part A covers the work relating to the RHA procedure, and Part B the RSA procedure. This somewhat unconventional organization was motivated by the fact that the nature of the work with each of the RHA and RSA procedures has been substantially different, and furthermore, the partitioning came natural since Part B of this report (with certain editorial changes) also has been published as the PEER report:

> A. Løkke and A. K. Chopra, "Response spectrum analysis of concrete gravity dams including dam-water-foundation interaction," *Submitted for publication,* Pacific Earthquake Engineering Research Center, University of California, Berkeley, 2013.

Part A presents the theory and implementation of the RHA procedure, and summarizes the process of modernizing the computer program EAGD-84. In this part, Chapter 2 presents an outline of the RHA procedure implemented in EAGD-84. Chapter 3 describes the EAGD-84 program briefly, summarizes the two new developments that have been added to the program, and shows an example of using the newly developed pre- and post-processing modules. Presented in Chapter 4 is a summary of the large number of response history analyses of Pine Flat Dam done in order to obtain the benchmark to which the RSA procedure is compared in Part B of this report, and selected results are presented. This chapter also contains the details of the probabilistic seismic hazard analysis that was done to obtain the ensemble of 58 ground motions used in the analysis.

Part B contains a thorough review and evaluation of the RSA procedure. Chapter 7 outlines the analysis procedure, and Chapter 8 defines a set of standard vibration properties to facilitate its implementation. Presented in Chapter 9 are details of the implementation of the procedure, and a new correction factor to improve its accuracy is developed. Chapter 10 contains a comprehensive evaluation of the RSA procedure in estimating the response of an actual dam to a large ensemble of ground motions by comparing its results with the benchmark obtained in Part A of this report.

This report also contains five appendices: Appendix A presents the procedure for computing the new set of compliance data, and summarizes how to determine the dynamic stiffness matrix from this data set. Appendix B outlines the procedure for computing the Conditional Mean Spectrum utilized in the probabilistic seismic hazard analysis in Chapter 4. Appendix C provides the details of the computational steps involved in determining the response of Pine Flat Dam by the RSA procedure. Presented in Appendix D is a comprehensive user's manual for the new pre- and post-processing modules that was developed for the EAGD-84 program. Finally, Appendix E presents a complete set of standard values characterizing dam-water-foundation interaction to be used in the RSA procedure.

The majority of the theory and concepts utilized during the work with this master's thesis is outlined is this report, or relevant references are noted. However, it is assumed that the reader is familiar with numerical finite element analysis and general concepts within earthquake engineering and structural dynamics.

Berkeley, June 24th, 2013

_____

Arnkjell Løkke

ACKNOWLEDGMENTS

First and foremost I would like to express my deepest gratitude to my supervisor Professor Anil K. Chopra for sharing his extensive insight into the theory of earthquake analysis of concrete gravity dams, for facilitating my visit to the University of California, Berkeley, and for providing invaluable guidance during the preparation of this thesis. His contributions during our countless meetings and discussions have been integral to the follow-through and outcome of this master's thesis. Additionally, I would like to thank my supervisor at NTNU, Professor Svein N. Remseth, for making it possible for me to write this master's thesis for NTNU in collaboration with the University of California, Berkeley. I am also grateful to several other individuals who contributed to this research:

- Professor Gautam Dasgupta at Columbia University, New York provided the computer program to compute new compliance data for a viscoelastic half-plane.
- Professor Baris Binici at the Middle East Technical University (METU), Ankara, Turkey provided a set of Matlab scripts that were used as the starting point to develop the pre- and post-processing modules now provided with the EAGD-84 computer program.
- Professor Pierre Léger at École Polytechnique de Montréal, Canada incorporated the new data presented in Part B of this report into the "pseudo-dynamic procedure" in the widely used computer program CADAM.
- Doctoral student Neal Simon Kwong assisted with the probabilistic seismic hazard analysis and ground motion selection process, sharing his extensive knowledge on the subject.
- Bjørn Thomas Svendsen examined the final draft of this report, and provided valuable suggestions for improvement.

Finally, I would like to thank the Norwegian National Committee on Large Dams (NNCOLD) and the organization Norwegian Water for their financial support during my visit to the University of California, Berkeley in 2013 when this thesis was prepared.

PART A: RESPONSE HISTORY ANALYSIS OF CONCRETE GRAVITY DAMS

1 Introduction

In order to design earthquake resistant dams and evaluate the safety of existing dams that will be exposed to future earthquakes, it is essential to have accurate and reliable analysis procedures to predict the stresses and deformations in dams subjected to earthquake ground motion. For a dam-water-foundation system, the earthquake response is significantly influenced by the interaction of the dam with the impounded water and with the underlying foundation region, thus increasing the requirements for the analysis procedure to be used, and complicating what would otherwise have been considered a routine finite element analysis of a concrete cross-section.

A response history analysis (RHA) procedure, based on the substructure method, was presented in 1981 to determine the earthquake response of concrete gravity dams including the hydrodynamic effects of the impounded water and the effects of interaction between the dam and a flexible foundation [9]. In 1984, this RHA procedure was extended to also recognize absorption of hydrodynamic pressure waves into the alluvium and sediments invariably deposited at the bottom of reservoirs [13]. Through a comprehensive investigation it was shown that the effects of dam-water-foundation interaction and reservoir bottom absorption has a profound influence on the response of concrete gravity dams to horizontal and vertical ground motion.

The above-mentioned analysis procedure was implemented in the computer program EAGD-84 [15] to numerically evaluate the response of a two-dimensional dam-water-foundation system to earthquake ground motion. Although presented as early as in 1984, the program still represents state-of-the art of dynamic analysis of concrete gravity dams, and it has been (and still is) utilized extensively for research purposes and in seismic design and evaluation of concrete gravity dams. Since its development, no significant changes have been made to the program.

The first part of this report presents the development and implementation of two new additions to the EAGD-84 program: (1) to improve the accessibility and user-friendliness of EAGD-84, a set of Matlab modules – including an easy-to-use graphical user interface (GUI) – has been developed, providing users with the capability of pre-processing input and post-processing analysis output from EAGD-84 in the Matlab scripting language; (2) motivated by the realization that data currently provided with the program did not offer sufficient control over the overall damping in the dam-water-foundation system to ensure consistency with damping measured from motions of dams recorded during forced vibration tests and

earthquakes [10] [30] [31], a more complete set of compliance data that govern the interaction between the dam and the foundation region has now been computed.

Utilizing the new Matlab modules, the earthquake response of an actual dam to an ensemble of 58 ground motions is also computed in this part. These analyses were performed to obtain a benchmark to which the response spectrum analysis presented in Part B of this report can be evaluated.

2 Response History Analysis Procedure

In this chapter, the general response history analysis (RHA) procedure presented by Fenves and Chopra [13] for determining the earthquake response of concrete gravity dams including the effects of dam-water-foundation interaction and reservoir bottom absorption is outlined. The analysis procedure is based on the substructure method, wherein the dam, water and foundation region are modeled as three different substructures of the complete system.

2.1 System and Ground Motion

The system considered consists of a concrete gravity dam supported on the horizontal surface by underlying flexible foundation rock and impounding a reservoir of water (Figure 2.1.1). The response of the system to earthquake ground motion is computed considering the two dimensional vibration of individual dam monoliths, as the shear forces in the construction joints between the monoliths are likely to exceed their low shear capacity when subjected to intense ground motion [9] [31]. The system is analyzed assuming linear behavior for the concrete dam, the impounded water and the foundation rock.

The dam, water and foundation region are modeled as three different substructures of the complete system as shown in Figure 2.2.1. These substructures can be idealized independently of each other, and are only coupled through the interaction forces and appropriate compatibility conditions at the interaction surfaces, which together leads to the equations of motion for the coupled system. The dam cross-section is idealized as a two-dimensional finite element system in order to model arbitrary geometry and elastic material properties of the dam; the water impounded in the reservoir is idealized by a fluid domain of constant depth and infinite length in the upstream direction; and the foundation underlying the dam and reservoir bottom materials is idealized as a semi-infinite, homogeneous, isotropic, viscoelastic half-plane.

The bottom of the reservoir upstream of a dam is likely to consist of highly variable layers of exposed bedrock, alluvium, silt and other sedimentary material. These materials are not adequately modeled by the viscoelastic half-plane idealization of the foundation, they are instead approximately modeled by a boundary condition at the reservoir bottom that allows partial absorption of incident hydrodynamic pressure waves.

Earthquake excitation is defined by two components of free-field ground acceleration in a cross-sectional plane of the dam: the horizontal component $a_g^x(t)$ transverse to the dam axis, and the vertical component $a_g^y(t)$.

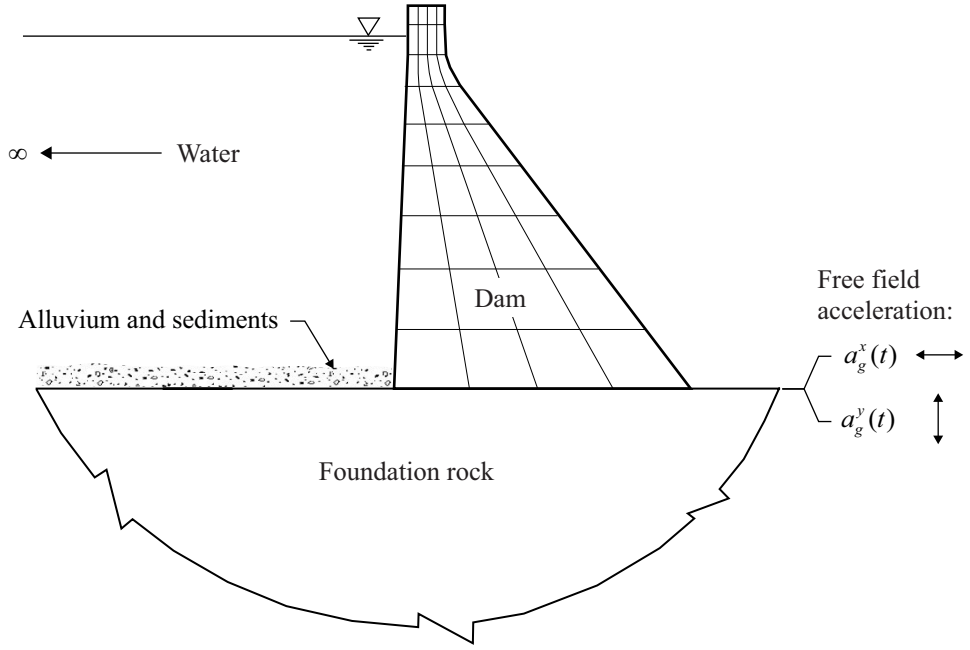

Figure 2.1.1 Dam-water-foundation rock system.

2.2 Frequency Domain Equations

2.2.1 Dam Substructure

The equations of motion for the concrete gravity dam shown in Figure 2.1.1, idealized as a planar, two-dimensional finite element system are

$$\mathbf{m}_c\ddot{\mathbf{r}}_c + \mathbf{c}_c\dot{\mathbf{r}}_c + \mathbf{k}_c\mathbf{r}_c = -\mathbf{m}_c\mathbf{1}_c^x a_g^x(t) - \mathbf{m}_c\mathbf{1}_c^y a_g^y(t) + \mathbf{R}_c(t) \tag{2.2.1}$$

where $\mathbf{m}_c$, $\mathbf{c}_c$ and $\mathbf{k}_c$ are the mass, damping and stiffness matrices for the finite element system; $\mathbf{r}_c$ is the vector containing the displacements of each nodal point relative to the free-field ground displacement (Figure 2.2.1):

$$\mathbf{r}_c^T = \left[r_1^x \quad r_1^y \quad r_2^x \quad r_2^y \quad \ldots \quad r_n^x \quad r_n^y \quad \ldots \quad r_{N+N_b}^x \quad r_{N+N_b}^y \right]$$

where r_n^x and r_n^y are the *x*- and *y*-components of the displacements at nodal point *n*; *N* is the number of nodal points above the base; N_b is the number of nodal points at the base; $a_g^x(t)$

and $a_g^y(t)$ are the *x*- and *y*-components of the free-field ground acceleration; and the influence vectors $\mathbf{1}_c^x$ and $\mathbf{1}_c^y$ are defined as

$$\left\{\mathbf{1}_c^x\right\}^T = \langle 1 \quad 0 \quad 1 \quad 0 \quad \ldots \quad 1 \quad 0 \rangle$$
$$\left\{\mathbf{1}_c^y\right\}^T = \langle 0 \quad 1 \quad 0 \quad 1 \quad \ldots \quad 0 \quad 1 \rangle$$

The force vector $\mathbf{R}_c(t)$ includes hydrodynamic forces $\mathbf{R}_h(t)$ at the upstream face of the dam and forces $\mathbf{R}_b(t)$ at the base of the dam due to dam-foundation interaction (Figure 2.2.1).

For harmonic acceleration, $a_g^l(t) = e^{i\omega t}$, $l = x, y$, the displacement and force vectors can be expressed in terms of their corresponding complex-valued frequency response functions: $\mathbf{r}_c(t) = \bar{\mathbf{r}}_c^l(\omega)e^{i\omega t}$, $\mathbf{R}_c(t) = \bar{\mathbf{R}}_c^l(\omega)e^{i\omega t}$, $\mathbf{R}_h(t) = \bar{\mathbf{R}}_h^l(\omega)e^{i\omega t}$ and $\mathbf{R}_b(t) = \bar{\mathbf{R}}_b^l(\omega)e^{i\omega t}$. The vector $\bar{\mathbf{r}}_c^l(\omega)$ contains the frequency responses for the displacement of all the nodal points in the finite element discretization due to the *l*-component of ground motion. If $\mathbf{r}_c$ is partitioned into $\mathbf{r}$ for nodal points above the base and $\mathbf{r}_b$ for nodal points at the base (Figure 2.2.1) and constant hysteretic damping is assumed for the dam, Equation (2.2.1) can be expressed in the frequency domain as [9]

$$\left(-\omega^2\begin{bmatrix}\mathbf{m} & \mathbf{0}\\ \mathbf{0} & \mathbf{m}_b\end{bmatrix} + (1+i\eta_s)\begin{bmatrix}\mathbf{k} & \mathbf{k}_b\\ \mathbf{k}_b^T & \mathbf{k}_{bb}\end{bmatrix}\right)\begin{Bmatrix}\bar{\mathbf{r}}^l(\omega)\\ \bar{\mathbf{r}}_b^l(\omega)\end{Bmatrix} = -\begin{Bmatrix}\mathbf{m}\mathbf{1}^l\\ \mathbf{m}_b\mathbf{1}_b^l\end{Bmatrix} + \begin{Bmatrix}\bar{\mathbf{R}}_h^l(\omega)\\ \bar{\mathbf{R}}_b^l(\omega)\end{Bmatrix} \qquad (2.2.2)$$

where η_s is the constant hysteretic damping factor for the dam concrete. The hydrodynamic interaction forces $\mathbf{R}_h$ acting on the upstream face of the dam is given by the solution of the corresponding boundary value problem for the fluid substructure. Additionally, the dam-foundation interaction forces $\mathbf{R}_b$ can be expressed in terms of the interaction displacements at the base by analysis of the foundation substructure; both expressions will be shown in the subsequent sections.

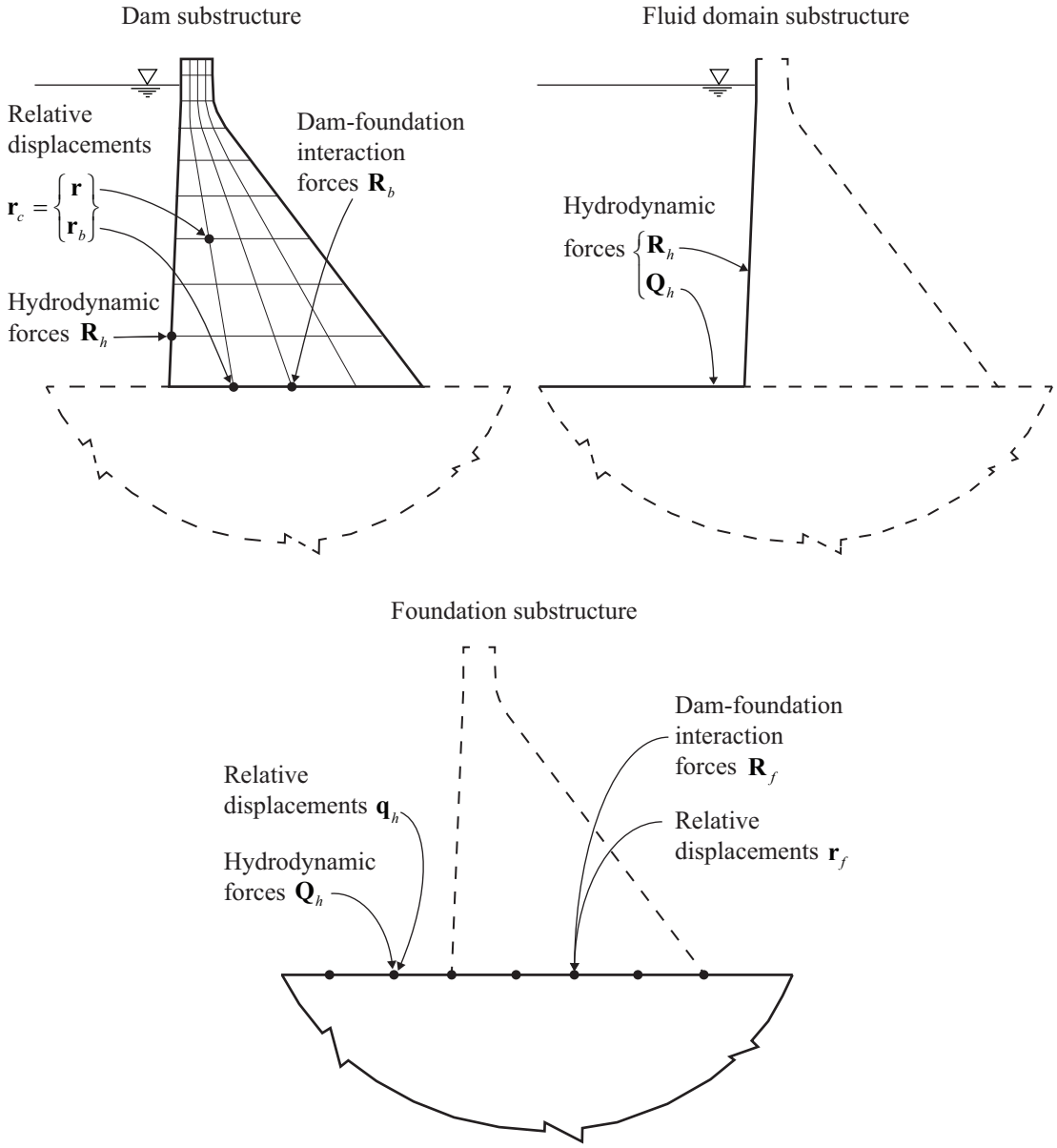

Figure 2.2.1 Substructure representation of the dam-water-foundation system.

2.2.2 Foundation Substructure

The complex-valued, frequency-dependent dynamic stiffness matrix $\underline{\mathbf{S}}(\omega)$ for the foundation substructure relates forces and displacements by [9]

$$\begin{bmatrix} \underline{\mathbf{S}}_{rr}(\omega) & \underline{\mathbf{S}}_{rq}(\omega) \\ \underline{\mathbf{S}}_{rq}^T(\omega) & \underline{\mathbf{S}}_{qq}(\omega) \end{bmatrix} \begin{Bmatrix} \overline{\mathbf{r}}_f(\omega) \\ \overline{\mathbf{q}}_h(\omega) \end{Bmatrix} = \begin{Bmatrix} \overline{\mathbf{R}}_f(\omega) \\ \overline{\mathbf{Q}}_h(\omega) \end{Bmatrix} \tag{2.2.3}$$

where the forces and displacements at the surface of the foundation region, relative to free-field ground acceleration, are expressed in terms of their complex-valued frequency response functions.

By the principles of static condensation, the first of the two matrix equations in Equation (2.2.3) can be expressed as

$$\mathbf{S}_f(\omega)\bar{\mathbf{r}}_f(\omega) = \bar{\mathbf{R}}_f(\omega) - \underline{\mathbf{S}}_{rq}(\omega)\underline{\mathbf{S}}_{qq}^{-1}(\omega)\bar{\mathbf{Q}}_h(\omega) \tag{2.2.4a}$$

where

$$\mathbf{S}_f(\omega) = \underline{\mathbf{S}}_{rr}(\omega) - \underline{\mathbf{S}}_{rq}(\omega)\underline{\mathbf{S}}_{qq}^{-1}(\omega)\underline{\mathbf{S}}_{rq}^{T}(\omega) \tag{2.2.4b}$$

The dynamic stiffness matrix $\mathbf{S}_f(\omega)$ of Equation (2.2.4b) contains all the effects of dam-foundation interaction. It can be conveniently computed from standard compliance data determined by a separate analysis of the foundation region idealized as a homogeneous, isotropic, viscoelastic half-plane using the methods developed in [11]; this procedure is summarized in Appendix A. The definition of element *ij* of this matrix, $\mathbf{S}_f(\omega)_{ij}$, is shown in Figure 2.2.2 where displacements have been imposed at nodal points within the base of the dam and tractions outside these nodal points are zero.

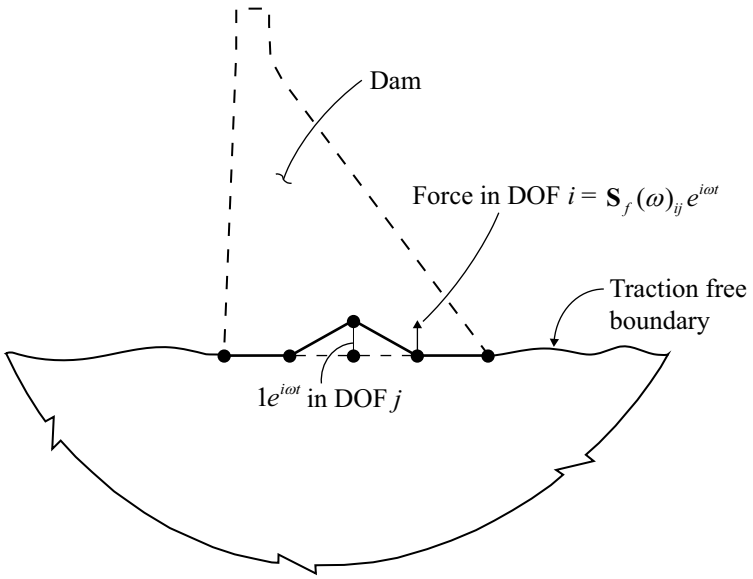

Figure 2.2.2 Definition of $\mathbf{S}_f(\omega)_{ij}$,i.e., element *ij* of the dynamic stiffness matrix $\mathbf{S}_f(\omega)$ for the foundation region.

2.2.3 Dam-Foundation System

The interaction forces between the dam and foundation substructure are required to be in equilibrium, which yields the relation:

$$\bar{\mathbf{R}}_b^l(\omega) + \bar{\mathbf{R}}_f(\omega) = \mathbf{0} \tag{2.2.5}$$

In addition, compatibility of the interaction displacements at the base requires that

$$\bar{\mathbf{r}}_b^l(\omega) + \bar{\mathbf{r}}_f(\omega) = \mathbf{0} \tag{2.2.6}$$

Combining Equations (2.2.4a), (2.2.5) and (2.2.6), with Equation (2.2.2) gives

$$\left(-\omega^2\begin{bmatrix}\mathbf{m} & \mathbf{0}\\ \mathbf{0} & \mathbf{m}_b\end{bmatrix} + (1+i\eta_s)\begin{bmatrix}\mathbf{k} & \mathbf{k}_b\\ \mathbf{k}_b^T & \mathbf{k}_{bb}\end{bmatrix} + \begin{bmatrix}\mathbf{0} & \mathbf{0}\\ \mathbf{0} & \mathbf{S}_f(\omega)\end{bmatrix}\right)\begin{Bmatrix}\bar{\mathbf{r}}^l(\omega)\\ \bar{\mathbf{r}}_b^l(\omega)\end{Bmatrix} = -\begin{Bmatrix}\mathbf{m}\mathbf{1}^l\\ \mathbf{m}_b\mathbf{1}_b^l\end{Bmatrix} + \begin{Bmatrix}\bar{\mathbf{R}}_h^l(\omega)\\ -\underline{\mathbf{S}}_{rq}\underline{\mathbf{S}}_{qq}^{-1}\bar{\mathbf{Q}}_h(\omega)\end{Bmatrix} \tag{2.2.7}$$

where the two vectors $\bar{\mathbf{R}}_h^l(\omega)$ and $\bar{\mathbf{Q}}_h(\omega)$ contains the frequency response functions for the hydrodynamic forces at the upstream face of the dam and at the reservoir bottom, respectively. These vectors can be expressed in terms of the acceleration at the upstream face of the dam and reservoir bottom by analysis of the fluid domain substructure, which is shown in Section 2.2.5.

2.2.4 Reduction of Degrees of Freedom by the Ritz Concept

Equation (2.2.7) represents a set of $2(N+N_b)$ complex-valued, frequency-dependent equations that would have to be solved simultaneously when written in their current form. Significant computational effort would be required for repeated solution of these equations for a range of excitation frequencies, even by modern computational standards.

Since linear elastic behavior was assumed for the dam, foundation region and impounded water, the principles of modal superposition is applicable when computing the dynamic response of this system. It has been shown [9] that an effective method of reducing the number of DOFs for interacting structural systems is the use of the Ritz concept ([6]: Sections 15.3 - 15.5). Here, the displacements relative to the free-field ground acceleration $\mathbf{r}_c$ are expressed as linear combinations of *J* Ritz vectors:

$$\mathbf{r}_c(t) = \sum_{j=1}^{J} Z_j(t)\boldsymbol{\psi}_j \tag{2.2.8}$$

where $Z_j(t)$ is the generalized coordinate corresponding to the j^{th} Ritz vector $\boldsymbol{\psi}_j$. For harmonic ground acceleration, Equation (2.2.8) can be written in terms of the corresponding complex-valued frequency response functions for the generalized coordinate as

$$\overline{\mathbf{r}}_c^l(\omega) = \sum_{j=1}^{J} \overline{Z}_j^l(\omega)\boldsymbol{\psi}_j \tag{2.2.9}$$

The required Ritz vectors are selected as the eigenmodes of the associated undamped dam-foundation system, where the frequency-dependent dynamic stiffness matrix $\mathbf{S}_f(\omega)$ is replaced by the static value $\mathbf{S}_f(0)$. The vibration frequencies λ_j and Ritz vectors $\boldsymbol{\psi}_j$ are thus solutions of the eigenvalue problem:

$$\left(\begin{bmatrix} \mathbf{k} & \mathbf{k}_b \\ \mathbf{k}_b^T & \mathbf{k}_{bb} \end{bmatrix} + \begin{bmatrix} \mathbf{0} & \mathbf{0} \\ \mathbf{0} & \mathbf{S}_f(0) \end{bmatrix} \right) \boldsymbol{\psi}_j = \lambda_j^2 \begin{bmatrix} \mathbf{m} & \mathbf{0} \\ \mathbf{0} & \mathbf{m}_b \end{bmatrix} \boldsymbol{\psi}_j \tag{2.2.10}$$

From the solution of Equation (2.2.10), the vector $\overline{\mathbf{q}}_h(\omega)$, containing the frequency response functions for the displacements at the reservoir bottom relative to free-field ground motion, can be expressed in terms of the generalized coordinates by manipulation of Equation (2.2.3):

$$\overline{\mathbf{q}}_h(\omega) = \underline{\mathbf{S}}_{qq}^{-1}(\omega)\overline{\mathbf{Q}}_h(\omega) + \sum_{j=1}^{J} \overline{Z}_j^l(\omega)\boldsymbol{\chi}_j \tag{2.2.11}$$

where the vector $\boldsymbol{\chi}_j$ is defined as

$$\boldsymbol{\chi}_j = \underline{\mathbf{S}}_{qq}^{-1}(0)\underline{\mathbf{S}}_{rq}^{T}(0)\boldsymbol{\psi}_{bj} \tag{2.2.12}$$

in which the zero-frequency terms have been used for $\underline{\mathbf{S}}_{qq}$ and $\underline{\mathbf{S}}_{rq}^T$ for consistency with how the Ritz vectors were obtained; and $\boldsymbol{\psi}_{bj}$ is a subvector of $\boldsymbol{\psi}_j$ corresponding to the nodal points at the base of the dam. The first term on the right side of Equation (2.2.11) represents the interaction between the fluid domain and the foundation region under the reservoir, i.e., it contains the effects of the reservoir bottom materials.

Substituting the transformation in Equation (2.2.9) into Equation (2.2.7) and using the orthogonality properties of the eigenvectors of the associated dam-foundation system leads to

$$\mathbf{S}(\omega)\overline{\mathbf{Z}}^l(\omega) = \mathbf{L}^l(\omega) \tag{2.2.13}$$

where each element of the matrix $\mathbf{S}$ and vector $\mathbf{L}^l$ are

$$S_{nj}(\omega) = \left[-\omega^2 + (1+i\eta_s)\lambda_n^2 \right]\delta_{nj} + \boldsymbol{\psi}_n^T \left[\tilde{\mathbf{S}}_f(\omega) - (1+i\eta_s)\tilde{\mathbf{S}}_f(0) \right] \boldsymbol{\psi}_j \tag{2.2.14a}$$

$$L_n^l(\omega) = -\boldsymbol{\psi}_n^T \mathbf{m}_c \mathbf{1}_c^l + \left\{ \boldsymbol{\psi}_n^f \right\}^T \overline{\mathbf{R}}_h^l(\omega) - \boldsymbol{\psi}_{bn}^T \underline{\mathbf{S}}_{rq}(\omega)\underline{\mathbf{S}}_{qq}^{-1}(\omega)\overline{\mathbf{Q}}_h(\omega) \tag{2.2.14b}$$

for $n, j = 1, 2, 3, ..., J$; $\bar{\mathbf{Z}}^l(\omega)$ is the vector of frequency response functions for the generalized coordinate; δ_{nj} is the Kronecker delta function†; $\boldsymbol{\psi}_n^f$ is a subvector of $\boldsymbol{\psi}_n$ containing only the elements corresponding to the nodal points at the upstream face of the dam; and $\tilde{\mathbf{S}}_f(\omega)$ is the dynamic stiffness matrix for the entire dam-foundation domain:

$$\tilde{\mathbf{S}}_f(\omega) = \begin{bmatrix} \mathbf{0} & \mathbf{0} \\ \mathbf{0} & \mathbf{S}_f(\omega) \end{bmatrix} \tag{2.2.15}$$

For a particular excitation frequency ω, Equations (2.2.13) and (2.2.14) represents J simultaneous, complex-valued equations in the generalized coordinates. The number of Ritz vectors that needs to be included to obtain accurate solution for the response of the dam is typically very small compared to the number of DOFs in the FE discretization of the dam substructure [9]. Thus will the evaluation of Equation (2.2.13) significantly reduce the computational effort required compared to a direct evaluation of Equation (2.2.7).

2.2.5 Fluid Domain Substructure

The vectors $\bar{\mathbf{R}}_h^l(\omega)$ and $\bar{\mathbf{Q}}_h(\omega)$ containing the frequency response functions of the unknown hydrodynamic forces can be expressed in terms of the hydrodynamic pressure at the upstream face of the dam and at the reservoir bottom. The frequency response function for the hydrodynamic pressure in the impounded water, $\bar{p}^l(x, y, \omega)$, can be expressed as

$$\bar{p}^l(x, y, \omega) = \bar{p}_0^l(x, y, \omega) + \sum_{j=1}^{J} \bar{\ddot{Z}}_j^l(\omega)\left[\bar{p}_j^f(x, y, \omega) + \bar{p}_j^b(x, y, \omega)\right] \tag{2.2.16}$$

where $\bar{p}_0^l(x, y, \omega)$, $l = x, y$ is the hydrodynamic pressure due to horizontal and vertical acceleration of a rigid dam; and $\bar{p}_j^f(x, y, \omega)$ is the hydrodynamic pressure due to horizontal acceleration of the upstream face of the dam in its j^{th} Ritz vector $\psi_j(y)$; both terms can be obtained using standard solution methods for boundary value problems. The last term entering Equation (2.2.16), $\bar{p}_j^b(x, y, \omega)$, has little influence on the response of the dam [9], and will be dropped from the equation in the following section. The boundary value problems corresponding to these hydrodynamic pressure functions are shown in Figure 2.2.3.

† The Kronecker delta function, $\delta_{nj} = \begin{cases} 0, & n \neq j \\ 1, & n = j \end{cases}$

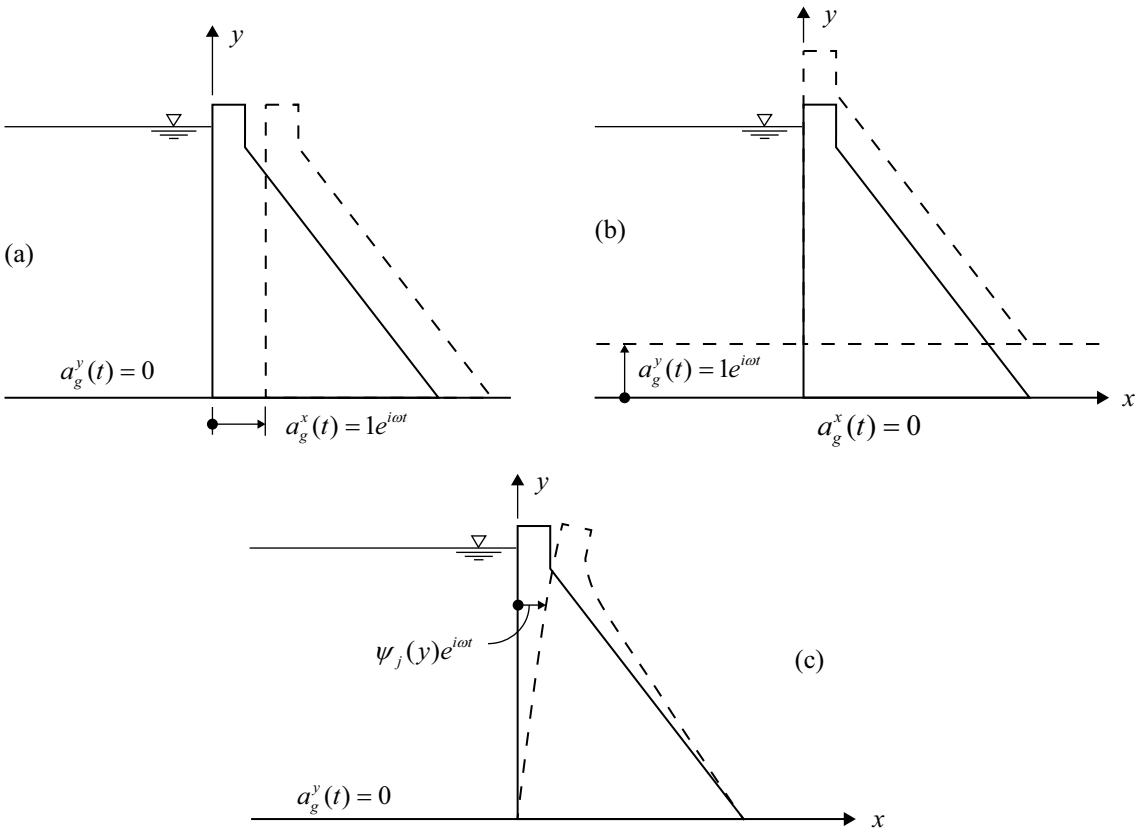

Figure 2.2.3 Acceleration excitations causing hydrodynamic pressures on the upstream face of the dam and at the reservoir bottom, defining the frequency response functions: (a) $\overline{p}_0^x(x, y, \omega)$, (b) $\overline{p}_0^y(x, y, \omega)$, and (c) $\overline{p}_j^f(x, y, \omega)$.

Considering an absorptive reservoir bottom and assuming a vertical upstream face of the dam, linearly compressible water and neglecting water viscosity, the boundary value problems shown were solved in Ref. [14], summarized here for the upstream face of the dam only:

$$\overline{p}_0^x(0, y, \omega) = -2\rho H \sum_{n=1}^{\infty} \frac{\mu_n^2(\omega)}{H\left[\mu_n^2(\omega) - (\omega q)^2\right] + i(\omega q)} \frac{I_{0n}(\omega)}{\sqrt{\mu_n^2(\omega) - \omega^2 / C^2}} \Upsilon_n(y, \omega) \tag{2.2.17a}$$

$$\overline{p}_0^y(0, y, \omega) = \frac{\rho C}{\omega} \frac{1}{\cos\frac{\omega H}{C} + iqC \sin\frac{\omega H}{C}} \sin\frac{\omega(H - y)}{C} \tag{2.2.17b}$$

$$\overline{p}_j^f(0, y, \omega) = -2\rho H \sum_{n=1}^{\infty} \frac{\mu_n^2(\omega)}{H\left[\mu_n^2(\omega) - (\omega q)^2\right] + i(\omega q)} \frac{I_{jn}(\omega)}{\sqrt{\mu_n^2(\omega) - \omega^2 / C^2}} \Upsilon_n(y, \omega) \tag{2.2.17c}$$

where $\mu_n(\omega)$ and $\Upsilon_n(y,\omega)$ are the complex-valued eigenvalues and eigenfunctions of the impounded water, respectively, equations governing these terms are presented in Ref. [14]; *H*, *C* and ρ are the depth, velocity of pressure waves, and density of the impounded water, respectively; *q* is the admittance coefficient at the reservoir bottom; and

$$I_{0n}(\omega) = \frac{1}{H}\int_0^H \Upsilon_n(y,\omega)dy \tag{2.2.18a}$$

$$I_{jn}(\omega) = \frac{1}{H}\int_0^H \psi_j(y)\Upsilon_n(y,\omega)dy \tag{2.2.18b}$$

where $\psi_j(y)$ is the continuous function analogue to the x-DOF elements of the j^{th} Ritz vector at the upstream face of the dam, $\boldsymbol{\psi}_n^f$.

The hydrodynamic force vectors $\bar{\mathbf{R}}_h^l(\omega)$ and $\bar{\mathbf{Q}}_h(\omega)$ entering Equation (2.2.14b) can be expressed in the same form as Equation (2.2.16) as

$$\bar{\mathbf{R}}_h^l(\omega) = \bar{\mathbf{R}}_0^l(\omega) + \sum_{j=1}^{J} \ddot{\bar{Z}}_j^l(\omega)\left[\bar{\mathbf{R}}_j^f(\omega) + \bar{\mathbf{R}}_j^b(\omega)\right] \tag{2.2.19a}$$

$$\bar{\mathbf{Q}}_h(\omega) = \bar{\mathbf{Q}}_0^l(\omega) + \sum_{j=1}^{J} \ddot{\bar{Z}}_j^l(\omega)\left[\bar{\mathbf{Q}}_j^f(\omega) + \bar{\mathbf{Q}}_j^b(\omega)\right] \tag{2.2.19b}$$

where the x-DOF elements of the vectors $\bar{\mathbf{R}}_0^l(\omega)$, $\bar{\mathbf{R}}_j^f(\omega)$ and $\bar{\mathbf{R}}_j^b(\omega)$ are the equivalent static nodal forces corresponding to the hydrodynamic pressure at the upstream face of the dam: $\bar{p}_0^l(0,y,\omega)$, $\bar{p}_j^f(0,y,\omega)$ and $\bar{p}_j^b(0,y,\omega)$, respectively; the y-DOF elements of the vectors $-\bar{\mathbf{Q}}_0^l(\omega)$, $-\bar{\mathbf{Q}}_j^f(\omega)$ and $-\bar{\mathbf{Q}}_j^b(\omega)$ are the equivalent static nodal forces corresponding to the hydrodynamic pressure at the reservoir bottom: $\bar{p}_0^l(x,0,\omega)$, $\bar{p}_j^f(x,0,\omega)$ and $\bar{p}_j^b(x,0,\omega)$, respectively. The y-DOF elements of $\bar{\mathbf{R}}_h^l(\omega)$ and x-DOF elements of $\bar{\mathbf{Q}}_h(\omega)$ are all zero.

2.2.6 Dam-Water-Foundation System

It can be shown that the terms $\bar{\mathbf{R}}_j^b$, $\bar{\mathbf{Q}}_0^l$, $\bar{\mathbf{Q}}_j^f$ and $\bar{\mathbf{Q}}_j^b$ in Equation (2.2.19) are all small in magnitude and can be dropped from the equation without introducing significant error [9]. Dropping these terms from Equation (2.2.19), combining it with the expression for the acceleration of the modal coordinate $\ddot{\bar{Z}}_j^l(\omega) = -\omega^2\bar{Z}_j^l(\omega)$, and inserting the result into Equation (2.2.14) gives the final form of the equations of motion for the modal coordinate of the dam-water-foundation system:

$$\tilde{\mathbf{S}}(\omega)\bar{\mathbf{Z}}^l(\omega) = \tilde{\mathbf{L}}^l(\omega) \tag{2.2.20}$$

where each element of the matrix $\tilde{\mathbf{S}}$ and vector $\tilde{\mathbf{L}}^l$ are given by

$$\tilde{S}_{nj}(\omega) = \left[-\omega^2 + (1+i\eta_s)\lambda_n^2\right]\delta_{nj} + \boldsymbol{\psi}_n^T\left[\tilde{\mathbf{S}}_f(\omega) - (1+i\eta_s)\tilde{\mathbf{S}}_f(0)\right]\boldsymbol{\psi}_j + \omega^2\left\{\boldsymbol{\psi}_n^f\right\}^T\bar{\mathbf{R}}_j^f(\omega) \tag{2.2.21a}$$

$$\tilde{L}_n^l(\omega) = -\boldsymbol{\psi}_n^T\mathbf{m}_c\mathbf{1}_c^l + \left\{\boldsymbol{\psi}_n^f\right\}^T\bar{\mathbf{R}}_0^l(\omega) \tag{2.2.21b}$$

These equations contain all the effects of dam-water interaction and dam-foundation interaction. The effects of reservoir bottom absorption are retained in the hydrodynamic terms $\bar{\mathbf{R}}_j^f(\omega)$ and $\bar{\mathbf{R}}_0^l(\omega)$, and the effects of dam-foundation interaction are retained in the second term of the right hand side of Equation (2.2.21a).

Repeated solution of Equation (2.2.20) for a range of excitation frequencies gives the complete vector of frequency response functions for the generalized coordinates of the dam-water-foundation system, which can be used to compute the total response due to earthquake ground motion following the procedure in the subsequent section.

2.3 Response to Arbitrary Ground Motion

Once the complex-valued frequency response functions $\bar{Z}_j^l(\omega)$, $l = x, y$, $j = 1, 2, ..., J$ have been computed from Equations (2.2.20) and (2.2.21) for the appropriate range of excitation frequencies ω, the response of the dam due to arbitrary ground motion can be computed as a superposition of responses due to individual harmonic components of ground motion. The generalized coordinates in the time domain are given by the Fourier integral

$$Z_j(t) = \frac{1}{2\pi}\int_{-\infty}^{\infty}\bar{Z}_j^l(\omega)A_g^l(\omega)e^{i\omega t}d\omega \tag{2.3.1}$$

where $A_g^l(\omega)$ is the Fourier transform of the *l*-component of the free-field ground acceleration $a_g^l(t)$:

$$A_g^l(\omega) = \int_0^d a_g^l(t)e^{-i\omega t}dt \tag{2.3.2}$$

where *d* is the duration of the ground acceleration. Evaluation of the integrals in Equations (2.3.1) and (2.3.2) is most efficiently computed in a discretized form using the Fast Fourier Transform (FFT) algorithm.

Repeating this procedure for all necessary values of *J*, the displacements of the dam due to the horizontal and vertical components of ground motion, separate or simultaneously, can be found by transforming the generalized coordinates back to nodal coordinates by the transformation in Equation (2.2.8):

$$\mathbf{r}_c(t) = \sum_{j=1}^{J} \left[Z_j^x(t) + Z_j^y(t) \right] \boldsymbol{\psi}_j \tag{2.3.3}$$

From the displacement response history, stresses in every element can be found at each time step by making use of the element stress-displacement transformation matrix, which is set up in the finite element discretization of the dam substructure.

3 Computer Program EAGD-84

EAGD-84 (Earthquake Analysis of Concrete Gravity Dams) [15] is a computer program for earthquake analysis of concrete gravity dam monoliths. Although developed as early as 1984, the program still represents state-of-the art of dynamic analysis of concrete gravity dams. This chapter presents a brief description of the program and summarizes the two new developments that have now been implemented in the program.

3.1 Description of Program

Published in 1984, EADG-84 provided an extension to the existing EAGD program [8], which was modified to include the full effects of dam-water-foundation interaction and reservoir bottom absorption. EAGD-84 implements the analysis procedure outlined in Chapter 2 to numerically evaluate the response of the two-dimensional dam-water-foundation system in Figure 2.1.1 subjected to horizontal and vertical earthquake ground acceleration. The dam monolith is idealized in the program using four node quadrilateral non-conforming elements, and the underlying foundation region is modeled as a viscoelastic half-plane using standard compliance data [11] to compute the required dynamic stiffness matrix $\mathbf{S}_f(\omega)$ entering Equation (2.2.21a); this procedure is summarized in Appendix A. The water impounded in the reservoir is idealized as a fluid domain of constant depth and infinite length in the upstream direction, and the dissipation of hydrodynamic pressure waves in the reservoir bottom materials is modeled approximately by a boundary condition that partially absorbs incident hydrodynamic pressure waves.

Input for the computer program consists of various control parameters, the finite element idealization and material properties of the dam monolith, material properties for the foundation, depth of the impounded water, the wave reflection coefficient for the reservoir bottom materials, and records for the horizontal and vertical components of free-field ground acceleration. The output consists of the displacement and stresses due to initial static loads, vibration frequencies and mode shapes for the dam, the complex-valued frequency response functions for the generalized coordinates, and complete response histories for displacements and stresses throughout the dam.

Detailed specifications of the program, in addition to a comprehensive description of its input and output, can be found in the EAGD-84 user manual [15].

3.2 Implementing New Compliance Data

When idealizing the foundation region as viscoelastic half-plane in the substructure method, the assumed constant hysteretic damping factor for the foundation rock, η_f, must be explicitly selected. This parameter has a significant influence on the overall response of the system, as it is reflects the energy dissipation that occurs through material damping in the foundation region.

Recent research has indicated that current practice of individually specifying a viscous damping ratio of 5% ($\eta = 0.10$) for the concrete dam alone and a similar value for the foundation rock should be abandoned because it is likely to lead to excessive damping in the overall dam-water-foundation system, and thus underestimate the response of the dam [7]. Assigning such values to the dam and foundation rock separately will lead to an overall damping in the system of 12-16% [14], whereas damping measured from motions of dams recorded during forced vibration tests and earthquakes is on the order of 2-4% for Pine Flat Dam in California [31], 2-3% for Mauvoisin and Emosson dams in Switzerland [10] [30], and 6% for Pacoima Dam in California [1].

Dynamic compliance coefficients for the viscoelastic half-plane model for rock used in EAGD-84 were originally developed for constant hysteretic damping factors, η_f = 0.01, 0.10, 0.25 and 0.50; these are equivalent to viscous damping ratios of 0.5, 5, 12.5 and 25%, respectively. In retrospect, it is apparent that these data does not provide sufficient control over the overall damping in the dam-water-foundation system to ensure consistency with the above mentioned results.

By using modern adaptive integration algorithms to handle singularities and ensure general numerical stability and accuracy, a complete set of compliance data has now been computed; this procedure is summarized in Appendix A. The new data was computed in the mathematical language Mathematica [24], and was compiled into a single data file to be supplied with EAGD-84. The new data set contains several important improvements compared to the existing data:

- The number of constant hysteretic damping factors for which data is available has been increased to η_f = 0.01, 0.02 0.03, 0.04, 0.05, 0.06, 0.07, 0.08, 0.09, 0.10, 0.12, 0.14, 0.16, 0.18, 0.20, 0.25, and 0.50, thus providing much better control of the overall damping in the dam-water-foundation system.
- The number of base nodal points for which data is available has been increased to NBASE = 16, allowing for a finer mesh to be used in the program.
- Data is now available for a finer spaced set of dimensionless frequencies a_0, thus improving the accuracy of the computed dynamic stiffness matrix for a given excitation frequency.
- The use of modern integration algorithms has in general improved the accuracy of the data set.

In addition to being implemented in EAGD-84, the new compliance data was used to generate a new set of parameters that characterize dam-foundation interaction in the response spectrum analysis procedure; this is described in Section 8.3.

3.3 Developing New Pre- and Post-Processing Modules

Direct use of EAGD-84 requires the user to enter all input data, including the entire finite element discretization and complete ground motion records, in a single file consisting of card sets divided into fields of fixed column widths according to the format specified in the EAGD-84 user manual [15]. Although this was the standard way of handling user input for computer programs at the time it was written, the complexity of generating a workable input file is now significantly limiting the accessibility and user-friendliness of the program. Additionally, because the output data is presented as plain text and raw binary data, it is essential for users of the program to have their own post-processors to interpret and plot analysis results. Such post-processors have previously not been supplied with the program.

Using the scripting language Matlab [25], widely used in research and professional practice, a set of modules have now been developed to perform pre-processing of the input and post-processing the analysis output from EAGD-84. These modules significantly reduce the complexity of using EAGD-84 to perform dynamic analysis of concrete gravity dams, and provide users with much easier access to the output from the program. Building on these modules, a self-explanatory graphical user interface (GUI) was also developed to provide users with an easy-to-use interface for performing analysis with EAGD-84.

Together, the GUI and the new modules meet a demand for easier access to rigorous and robust software for performing earthquake analysis of concrete gravity dams. The GUI is suitable for performing "standard" response history analyses, where only a few ground motions and/or analysis cases are of interest, and using the new modules directly in the Matlab scripting language, users now have the possibility of doing complex parameter studies or large statistical simulations for a number of parameters. An example of the latter is the response history analyses presented in Chapter 4 of this report. Here, the response of an actual dam was computed for an ensemble of 58 ground motions considering four different cases, i.e., 232 response history analyses, recognizing the full effects of dam-water-foundation interaction and reservoir bottom absorption were performed. Obviously, such an analysis would not have been possible had it not been for the capacity of the pre- and post-processing modules to efficiently sort and handle input and output data from the analysis.

The Matlab modules are not described here in further detail except for the example presented in the subsequent section. The reader is referred to the complete user manual included in Appendix D for a comprehensive description of the new modules and their organization, in addition to several examples showing the use of the modules and the GUI.

The new modules have been made available for download from the NISEE library website [27], a part of the Pacific Earthquake Engineering Research (PEER) Center. All code is provided open-source so that the user can tailor the code to be suitable for any particular application.

3.4 Example Analysis of Idealized Dam

The following example shows the use of the new modules directly in the Matlab scripting language (i.e. not by use of the GUI) to perform a dynamic analysis of an idealized concrete gravity dam cross-section. The input script necessary to run the analysis is shown, and examples of output such as mode shapes, displacements response histories and stress contours are plotted using the utility functions provided with the modules.

3.4.1 System and Ground Motion

An idealized cross-section with a vertical upstream slope, a downstream slope of 0.8:1, and a crest thickness of 10 ft. is chosen for the example analysis (Figure 3.4.2). The following properties are used: height of the dam, H_s = 300 ft.; modulus of elasticity of concrete, E_s = 4.0 million psi; unit weight of concrete, w_s = 155 pcf; constant hysteretic damping factor for the dam alone, η_s = 0.04 (corresponding to 2% viscous damping); modulus of elasticity of the foundation rock, E_f = 4.0 million psi; unit weight of rock, w_s = 165 pcf; constant hysteretic damping factor for the rock, η_f = 0.04; depth of water, H = 300 ft. (= at crest level); and wave reflection coefficient at the reservoir bottom, α = 0.75.

The dam is analyzed considering the horizontal and vertical components of the ground motion recorded at Taft Lincoln School Tunnel during the Kern County, California earthquake of July 21st 1952; both components are shown in Figure 3.4.1.

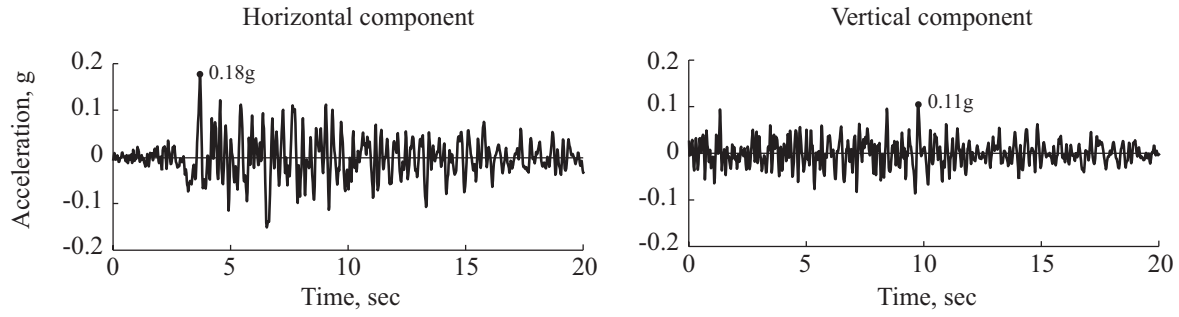

Figure 3.4.1 Horizontal (S69E) and vertical components of ground motion recorded at Taft Lincoln School Tunnel, during the Kern County, California, earthquake July 21st 1952.

3.4.2 Running the Program

The script used to create the EAGD-84 input file, execute the program, and load all output into the Matlab workspace is shown in Figure 3.4.3. This file contains all the necessary input for the program to run, and offers a *significant* reduction in complexity compared to the input file required to perform the analysis directly using EAGD-84 (examples of such files are presented in Ref. [15]). The ground motion records containing the horizontal and vertical components of Taft ground motion are stored in the two separate text files 'Taft_horz.txt' and 'Taft_vert.txt'. The automatic mesh generator provided with the modules is used to discretize the dam cross-section; the resulting mesh is shown in Figure 3.4.2.

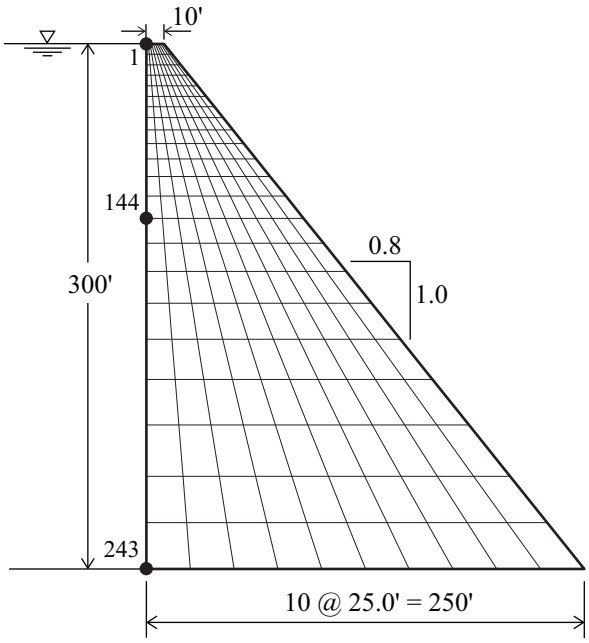

Figure 3.4.2 Mesh produced by the automatic mesh generator, consisting of 220 (22 x 10) quadrilateral four-node elements. Nodes 1, 144 and 243 are highlighted.

```
% EXAMPLE ANALYSIS OF IDEALIZED DAM CROSS SECTION
clc; clear all; close all

%% DEFINE INPUT

% 1. Define control parameters
IRES=0; ICOMB=1; IGRAV=1; IRIG=0; PSP=0.0;

% 2. Define material properties
EC=5.76e5; DENSC=4.8e-3; POISC=0.20; DAMPC=0.04; % Dam
EF=5.76e5; DENSF=5.1e-3;             DAMPF=0.04; % Foundation
ALPHA=0.75;                                      % Water

% 3. Define FE geometry using automatic mesh-generator
L1=250; L2=0; L3=10; L4=10;                        % lengths, in ft
elA=0; elB=300; elC=300; elD=300; elWL=300;        % elevations, in ft
NBASE=11;
ft=1.0;                                            % Conversion factor to ft

% 4 Define dynamic response parameters
NEV=12; NEXP=12; DT=0.01;

% 5. Define EQ ground motion data
IHV=2; NUMREC=3000; dt=0.01; SFAC=1;
hName='Taft_horz.txt'; hNumHead=1;
vName='Taft_vert.txt'; vNumHead=1;

%% CREATE INPUT FILE

% Create finite element idealization
[COORD Element WL Spacing NUMNP NUMEL NBASE, ...
 NPP WatNodes BaseNodes] = PRE_createMesh(L1,L2,L3,L4, ...
 elA,elB,elC,elD,elWL,NBASE,ft);

% Create earthquake array
[EQArrayH EQArrayV] = PRE_createEQArray(IHV, NUMREC, dt, SFAC, hName, ...
 hNumHead, vName, vNumHead);

% Create input file
PRE_writeInput(IRES,ICOMB,IGRAV,IRIG,PSP,EC,POISC,DENSC,DAMPC, ...
 EF,DENSF,DAMPF,ALPHA,NUMNP,NUMEL,NBASE,Spacing,WL,NPP,COORD,Element, ...
 WatNodes,BaseNodes,NEV,NEXP,DT,IHV,NUMREC,dt,EQArrayH,EQArrayV);

%% RUN EAGD-84
RUN_E1A

%% READ OUTPUT TO WORKSPACE
clear all;

% Read output file
[NUMNP NUMEL NBASE COORD Element Post] = POST_readOutput;

% Read fort.3 file
[NUMNP NUMEL Post] = POST_readFort3(Post);
```

Figure 3.4.3 Script to create input file, run EAGD-84, and read output data into the Matlab workspace.

3.4.3 Example of Output

Executing the script file shown in Figure 3.4.3 performs a complete response history analysis of the idealized dam and reads the analysis results into the Matlab workspace. The response of the dam is computed considering the reservoir to be at crest level, i.e., a full reservoir, and the foundation to be flexible. The response due to the horizontal and vertical components of Taft ground motion, simultaneously, is computed, and the dynamic response is combined with the response due to static loads (self-weight and hydrostatic pressure).

A few examples of post-processing of the output using the provided utility functions are presented below:

- The first four mode shapes of the associated dam-foundation system, including the corresponding vibration periods, are plotted in Figure 3.4.4.
- The horizontal and vertical displacements, relative to the free-field ground motion, at three levels on the upstream face of the dam (nodal points 1, 144 and 243) due to the horizontal and vertical components, simultaneously, of Taft ground motion are shown in Figure 3.4.5.
- The distribution of envelope values of the maximum principal stresses in the dam, including stresses due to static loads, is plotted in Figure 3.4.6a.
- The distribution of maximum principal stresses in the dam, including stresses due to static loads, at time t = 9.96 sec (the time when the peak value of maximum principal stress occurs on the upstream face of the dam) is plotted in Figure 3.4.6b.

By comparing the dynamic tensile capacity of concrete with values obtained from stress plots such as the ones shown in Figure 3.4.6, which includes stresses due to static loads, it is possible to identify the portions of the dam monolith that may crack during an earthquake. This is an important indicator of the level of damage expected to occur in the dam during earthquakes, and is therefore essential in evaluating the seismic safety of the dam.

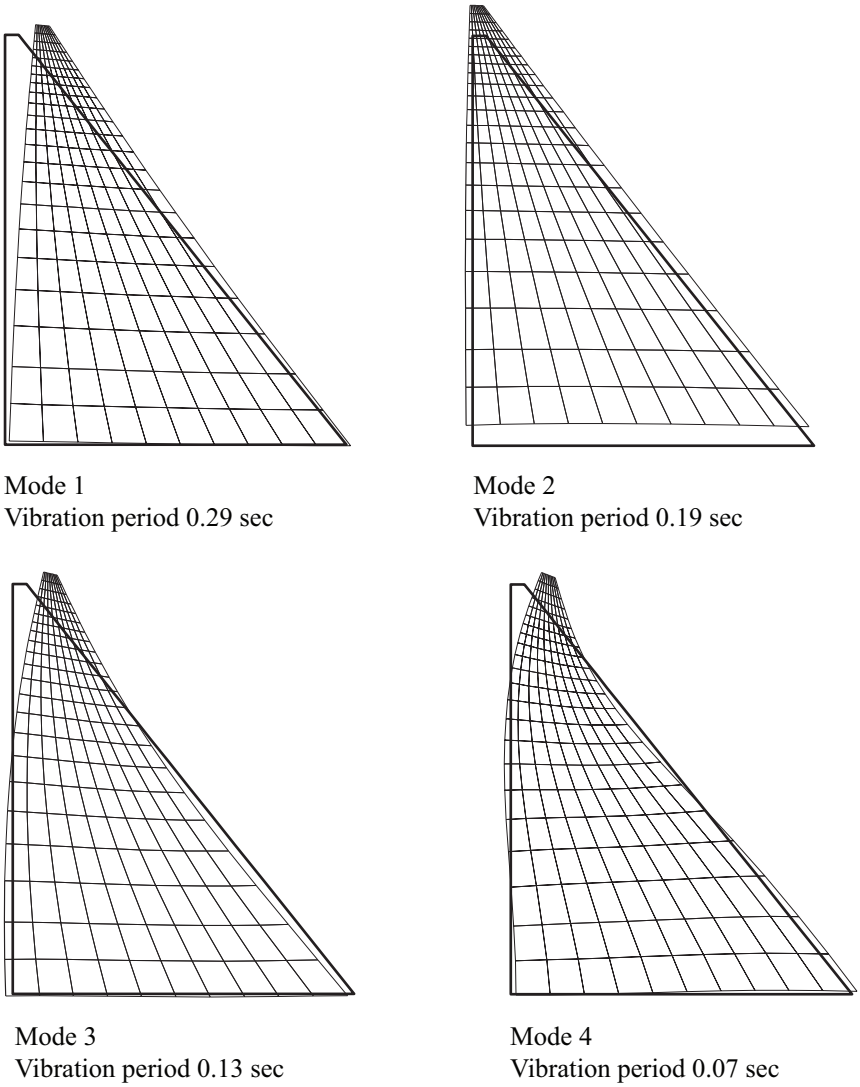

Figure 3.4.4 First four vibration modes and periods for the associated dam-foundation system.

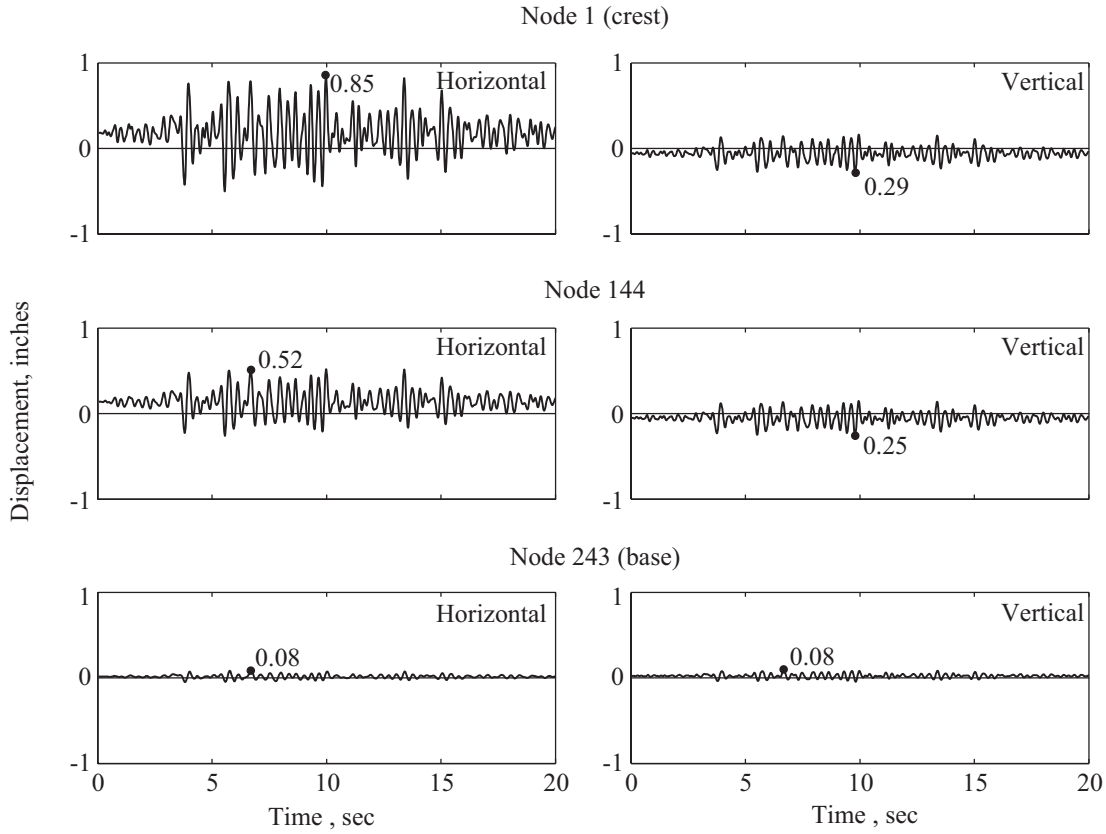

Figure 3.4.5 Displacement response of idealized dam due to horizontal and vertical components, simultaneously, of Taft ground motion; initial static displacements are included.

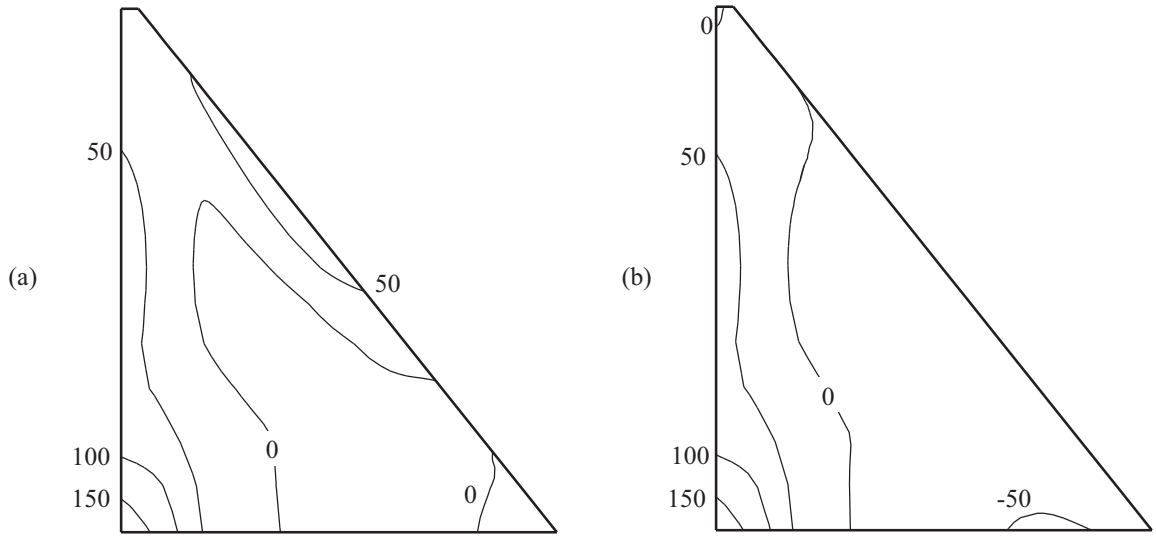

Figure 3.4.6 (a) Envelope values of maximum principal stresses, (b) Maximum principal stresses at time t=9.96 sec; initial static stresses are included.

4 Response History Analysis of Pine Flat Dam

In order to generate a basis for evaluating the accuracy of the response spectrum analysis (RSA) procedure presented in Part B of this report, response history analyses (RHA) of Pine Flat Dam were performed for an ensemble of 58 unique ground motions using the pre- and post-processing modules described in Section 3.3. The results obtained in these analyses provide the benchmark to which results obtained by the RSA procedure are compared in Chapter 10.

4.1 System Considered

Pine Flat Dam is a concrete gravity dam constructed of thirty-six monoliths and has a total crest length of 1840 ft. [31]. The tallest, non-overflow monolith shown in Figure 4.1.1 was selected for analysis. This cross-section has previously been analyzed in several publications, including investigations of its dynamic properties [31], and studies of the effects dam-water-foundation interaction [9] and reservoir bottom absorption [13]. The two-dimensional finite element idealization of the monolith (Figure 4.1.1) consists of 136 (17 x 8) quadrilateral elements with 162 nodal points.

The concrete in the dam is assumed to be a homogeneous, isotropic, linear elastic solid with the following properties: Young's modulus of elasticity, E_s = 3.25 million psi; unit weight 155 pcf; and Poisson's ratio = 0.2. Energy dissipation in the dam is represented by a constant hysteretic damping factor of 0.04 for the concrete, corresponding to a viscous damping ratio of 2% in all natural vibration modes of the dam (without impounded water) on rigid foundation; consistent with damping measured from forces vibration tests of the dam [31].

The foundation region supporting the dam is modeled with the following material properties: Young's modulus of elasticity, E_f = 3.25 million psi; unit weight = 165 pcf; Poisson's ratio = 1/3; and constant hysteretic damping factor η_f = 0.04 (corresponding to 2% viscous damping).

The impounded water has a constant depth of 381 ft., extends to infinity in the upstream direction, and is assumed compressible. For lack of data on the properties of the reservoir bottom materials upstream of Pine Flat Dam, a value for the wave reflection coefficient, α, describing the ratio of the amplitude of the reflected hydrodynamic pressure

wave to the amplitude of a vertically propagating pressure wave incident on the reservoir bottom, is arbitrarily selected as $\alpha = 0.75$.

The response of the dam is computed for the four different analysis cases listed in Table 4.1.1.

Table 4.1.1 Analysis cases for Pine Flat Dam.

Analysis Case	Foundation	Water
1	Rigid	Empty
2	Rigid	Full
3	Flexible	Empty
4	Flexible	Full

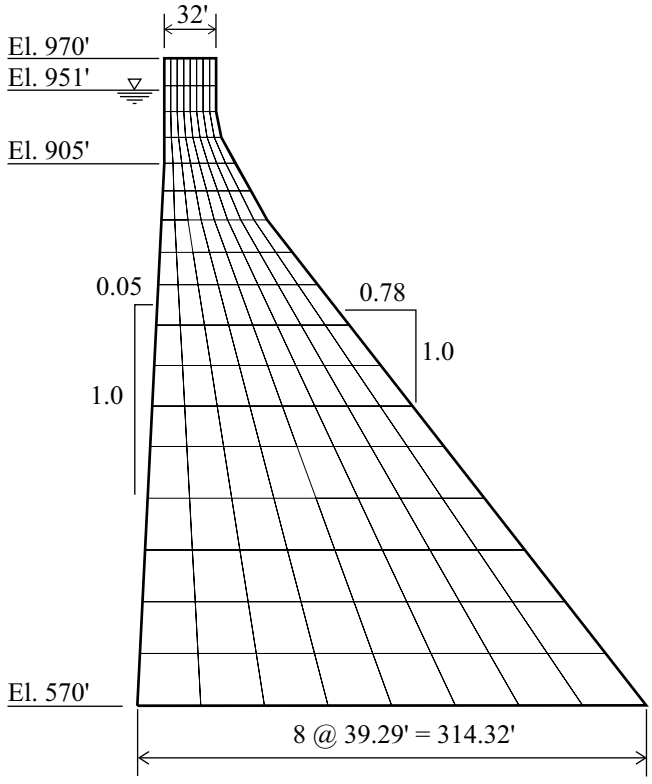

Figure 4.1.1 Tallest, non-overflow monolith of Pine Flat Dam.

4.2 Selection of Ground Motions: PSHA for Pine Flat Site

Based on a probabilistic seismic hazard analysis (PSHA) for the Pine Flat Dam site at the 1% in 100 years hazard level, a typical MCE (maximum considered earthquake) design level for dams, a target spectrum was developed. A total of 58 horizontal acceleration records were then selected and scaled to be consistent with this target spectrum, providing a broad ensemble of ground motions to be used in the analysis. This section presents a brief summary of the PSHA, as well as the procedure for selection and scaling of ground motion records. The reader is referred to the EERI monograph "Seismic hazard and risk analysis" by McGuire [26] for a broad discussion of PSHA in general.

4.2.1 Target Spectrum

Figure 4.2.1 shows two Conditional Mean Spectra (CMS) for the Pine Flat Dam site computed by the procedure summarized in Appendix B at the 1% in 100 years hazard level for the intensity measures $A(T_1)$ and $A(\tilde{T}_1)$. Here, $A(T)$ denotes the pseudo-acceleration of a SDF system with a natural vibration period T ([6]: Section 6.6.3); and $T_1 \approx 0.3$ sec and $\tilde{T}_1 \approx 0.5$ sec are the fundamental vibration periods of the dam alone on a rigid foundation and the dam with impounded water on flexible foundation, respectively. These values cover the range of periods for the four analysis cases listed in Table 4.1.1 (both periods are computed and presented in Table 4.3.1).

It was decided to perform the evaluation of the RSA procedure, and thus the response history analyses presented in this chapter, using the same ensemble of ground motions for all the four analysis cases considered. For this reason, ground motions need to be selected and scaled for a single target spectrum. Because the two CMS corresponding to the periods T_1 and $\tilde{T}_1$ are very similar – both in terms of spectral shape and in amplitude – the target spectrum is, for convenience, taken as the geometric mean of the two CMS, shown in Figure 4.2.1. Although more rigorous procedures exist for computing CMS for an intensity measure that averages spectral acceleration values over a range of periods (see Ref. [3] for a comprehensive description of such a procedure), the target spectrum selected is considered satisfactory for the limited objective of this analysis (also see Appendix B for a more thorough discussion of this simplification).

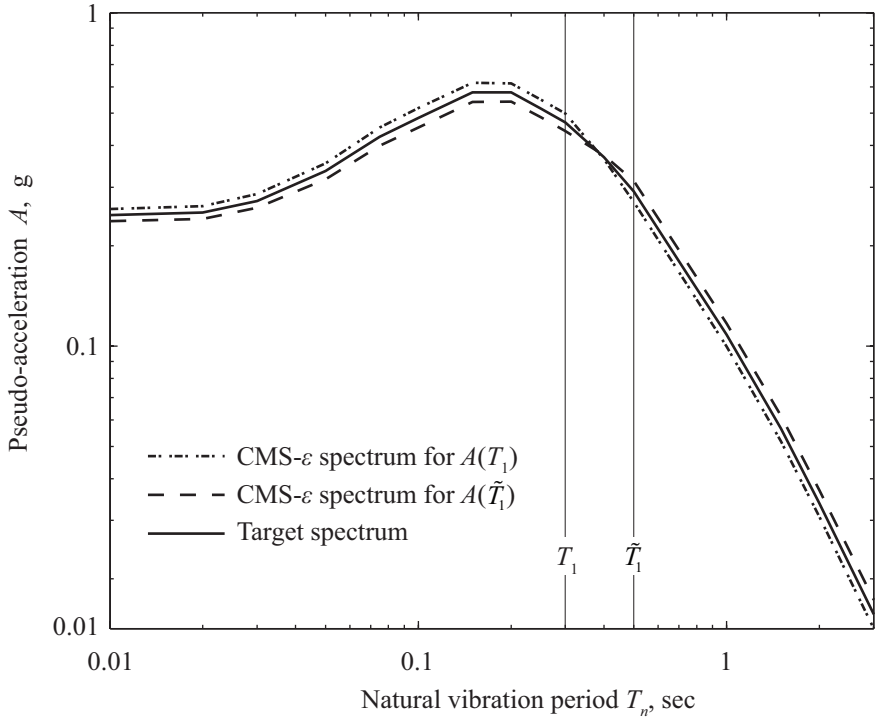

Figure 4.2.1 CMS-ε spectra for intensity measures $A(T_1)$ and $A(\tilde{T}_1)$ at the 1% in 100 years hazard level computed by the procedure summarized in Appendix B. Also plotted is the target spectrum; damping, ζ = 5%.

4.2.2 Selection and Scaling of Ground Motion Records

The 29 acceleration records listed in Table 4.2.1, each with two orthogonal horizontal components, were selected from the PEER Ground Motion Database [28] according to the following criteria:

- Fault distance, R = 0 - 50 km
- Magnitude, M_w = 5 - 7.5
- Shear wave velocity, $V_{s,30}$ > 183 m/s (corresponding to minimum NEHRP soil class D: stiff soil).

The range of M_w and R were selected to be consistent with the deaggregation of the seismic hazard at the Pine Flat Dam site – determined using the online USGS Seismic Deaggregation Tool [29] – where it was clear that the dominant events at the site for the main periods of interest were close distance earthquakes in magnitude range M_w = 5 - 7.5. The range of $V_{s,30}$ was chosen to discard ground motions recorded on very soft soils, which are clearly not representative for the rock site at Pine Flat Dam.

The selected records were amplitude-scaled by scaling each ground motion to minimize the mean square difference between the response spectrum for the individual

ground motion and the target spectrum over the period range of interest. A detailed description of this scaling procedure can be found in Ref. [28].

Figure 4.3.2 presents the response spectra for each of the scaled ground motions, the target spectrum, and the median (computed as the geometric mean) of the 58 response spectra. This median of the 58 response spectra will later be used to define the earthquake excitation in the RSA procedure (Chapter 10).

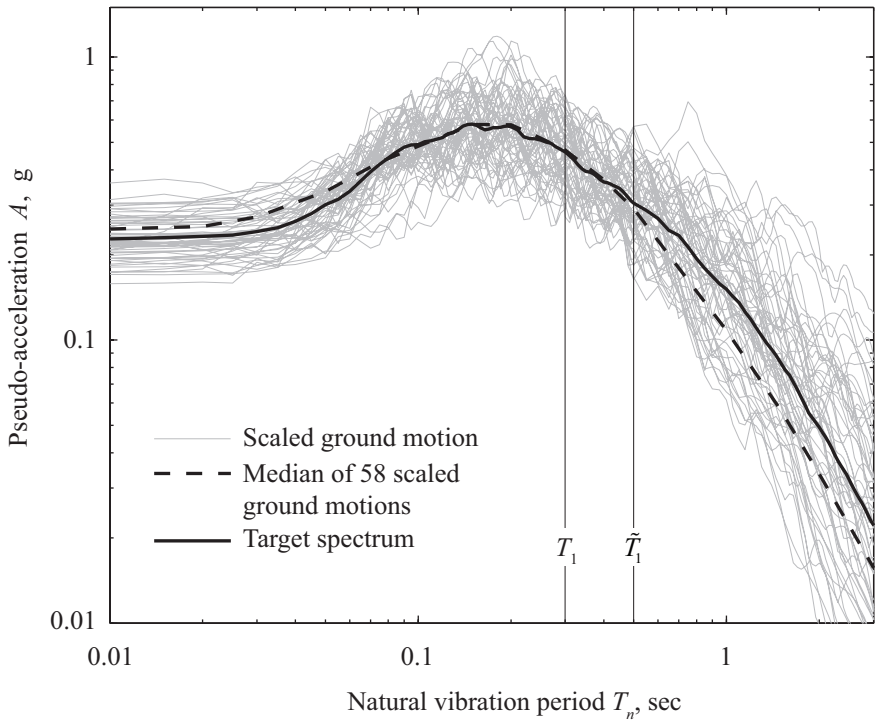

Figure 4.2.2 Response spectra for 58 scaled ground motion records, their median spectrum, and the target spectrum; damping, ζ = 5%.

Table 4.2.1 List of earthquake records. PGA values are for the scaled fault-normal and fault-parallel components of the ground motions.

#	Year	Event	Station	M_w	R, in km.	PGA, in g	
						FN comp.	FP comp.
1	1966	Parkfield	Cholame Shandon Array	6.19	17.6	0.232	0.246
2	1971	San Fernando	LA - Hollywood Stor FF	6.61	22.8	0.180	0.229
3	1971	San Fernando	Lake Hughes 4	6.61	25.1	0.256	0.319
4	1979	Imperial Valley	Victoria	6.53	31.9	0.179	0.306
5	1980	Mammoth Lakes	Mammoth Lakes H.S.	6.06	4.7	0.179	0.271
6	1980	Irpinia, Italy	Auletta	6.90	9.5	0.198	0.211
7	1980	Irpinia, Italy	Rionero In Vulture	6.90	30.1	0.226	0.210
8	1983	Mammoth Lakes	Convict Creek	5.31	7.1	0.191	0.313
9	1983	Coalinga 05	Oil Fields Fire Station FF	5.77	11.1	0.292	0.243
10	1984	Morgan Hill	Gilroy Array #2	6.19	13.7	0.278	0.228
11	1986	N. Palm Springs	San Jacinto - Valley Cemetary	6.06	31.0	0.253	0.219
12	1986	N. Palm Springs	Sunnymead	6.06	37.9	0.236	0.227
13	1986	Chalfant Valley	Benton	6.19	21.9	0.251	0.214
14	1987	Whittier Narrows	Glendale - Las Palmas	5.99	22.8	0.312	0.189
15	1987	Whittier Narrows	Glendora - N. Oakbank	5.99	22.1	0.282	0.205
16	1987	Whittier Narrows	LA - Century City CC North	5.99	29.9	0.188	0.275
17	1987	Whittier Narrows	Pomona - 4th&Locust FF	5.99	29.6	0.262	0.224
18	1987	Whittier Narrows	LA - Hollywood Stor FF	5.27	24.8	0.200	0.278
19	1992	Landers	Mission Creek Fault	7.28	27.0	0.223	0.231
20	1994	Northridge	Burbank - Howard Rd	6.69	16.9	0.134	0.171
21	1994	Northridge	LA - Centinela St	6.69	28.3	0.198	0.300
22	1994	Northridge	LA - Obregon Park	6.69	37.4	0.370	0.197
23	1994	Northridge	LA - Wonderland Ave	6.69	20.3	0.243	0.183
24	1994	Northridge	Santa Monica City Hall	6.69	26.4	0.216	0.324
25	1999	Hector Mine	Twentynine Palms	7.13	42.1	0.215	0.220
26	1999	Chi-Chi, Taiwan	TCU079	6.20	8.5	0.260	0.200
27	1999	Chi-Chi, Taiwan	TCU054	6.20	49.5	0.210	0.266
28	1999	Chi-Chi, Taiwan	TCU075	6.30	26.3	0.300	0.163
29	1999	Chi-Chi, Taiwan	TCU120	6.30	32.5	0.243	0.221

4.3 Response Results

From the data resulting from the large number of response history analyses performed, selected results are presented in this section. Given the purpose of the analysis (to obtain the benchmark used in Chapter 10), results are presented here without any discussion of the interaction effects that influence the results. The reader is referred to Ref. [9], [13], [16] and [17] for in-depth investigations of the important effects of dam-water interaction, dam-foundation interaction and reservoir bottom absorption. Additionally, the effects of interaction on the dynamic properties of an equivalent SDF system representing the dam-water-foundation system are discussed in detail in Chapters 8 and 9 of Part B of this report.

4.3.1 Fundamental Mode Properties

The fundamental mode properties of the dam-water-foundation system, i.e., the fundamental resonant period and the damping ratio at this period, are not explicitly needed in the RHA procedure. However, in order to evaluate the accuracy of the approximate vibration properties computed by the RSA procedure in Chapter 10, they are determined by the half-power bandwidth method ([6]:Section 3.2.6) applied to the frequency response function for the fundamental mode response of the dam-water-foundation system. This frequency response function, computed by repeated solution of Equation (2.2.20), is obtained from the EAGD-84 output. Results for the fundamental mode properties are presented in Table 4.3.1.

Table 4.3.1 Fundamental mode properties for Pine Flat Dam.

Case	Foundation	Water	Resonant period, in sec	Damping ratio, in percent
1	Rigid	Empty	0.318	2.0
2	Rigid	Full	0.395	3.2
3	Flexible	Empty	0.390	8.7
4	Flexible	Full	0.491	9.8

4.3.2 Peak Vertical Stresses

For a given element in the finite element discretization, the peak values of vertical stresses over the duration of each ground motion can be determined directly from the stress response histories. The median value of the peak vertical stress in any element is then computed as the geometric mean[†] of the stress values due to the 58 ground motions. By repeating this

[†] A statistical investigation of the peak stresses due to the 58 ground motions revealed that these showed the characteristics of a log-normal distribution. Using the statistical properties of a log-normal distribution, the median value of the peak stresses can therefore be computed as the geometric mean.

procedure for every element in the finite element discretization, contour plots showing the median values of the peak vertical stresses can be generated. Such results are presented in Figure 4.3.1 for each of the four analysis cases; note that stresses due to initial static loads are not included.

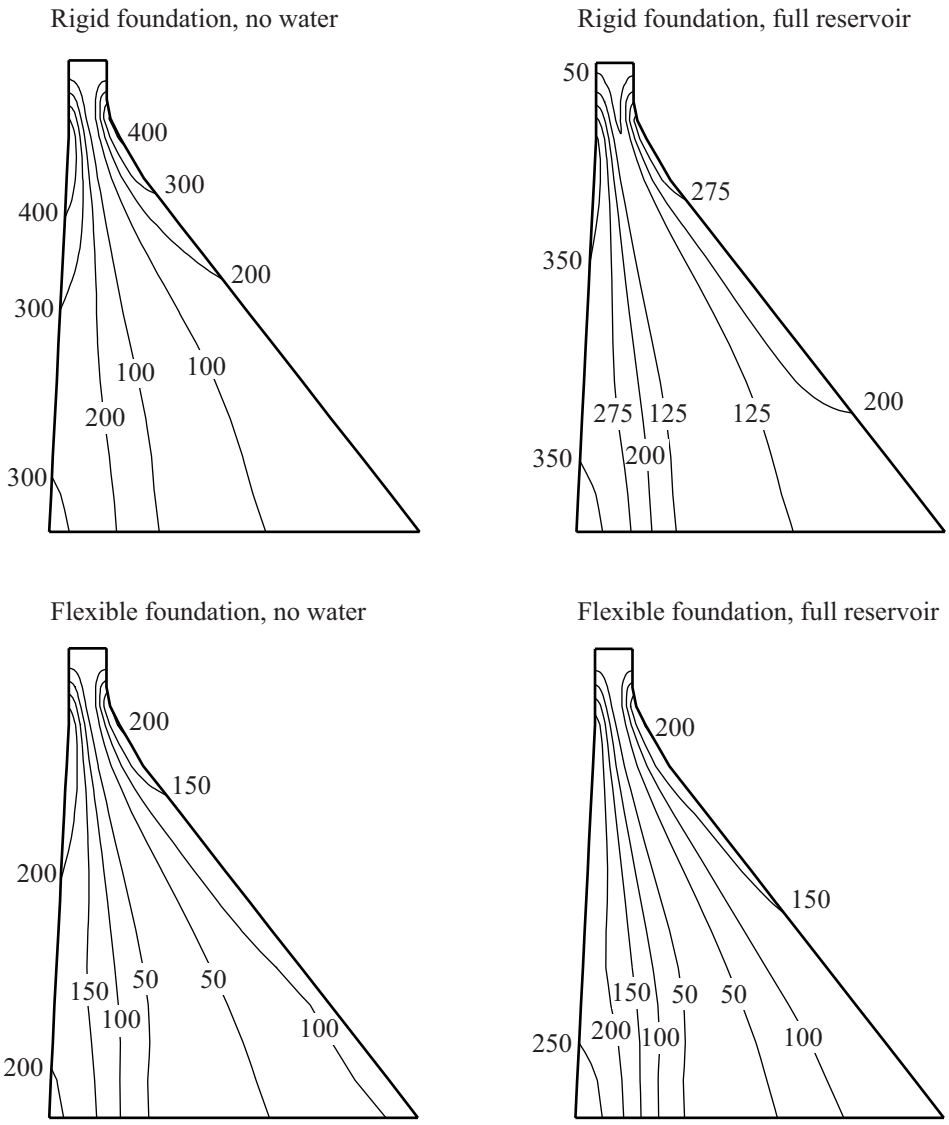

Figure 4.3.1 Median values of peak vertical stresses, in psi, in Pine Flat Dam due to 58 ground motions; initial static stresses are excluded.

It is apparent in Figure 4.3.1 that contributions from the higher modes to the total response are significant, especially for Case 1 (rigid foundation, no water) where steep stress gradients are evident in the upper part of the dam. This occurs mainly because of the low damping value assigned to the dam alone (2% viscous damping), which for the system in

Case 1 is the only mechanism for energy dissipation. For Case 4 however, where the reservoir is full and the foundation is considered flexible, the damping in the system is increased substantially by material and radiation damping in the foundation and dissipation of pressure waves in the reservoir bottom materials. Thus, the steep stress gradients in the upper part of the dam are absent. The implications of these observations are discussed further in Chapter 10.

4.3.3 Peak Principal Stresses: Benchmark Results

At the two faces of the dam, the principal stresses are essentially parallel to the faces if the upstream face is nearly vertical and the stresses due to tail-water at the downstream face are negligible [18]; these conditions are usually satisfied in practical problems. This implies that the direction of the peak value of maximum principal stress at locations on a dam face is essentially invariant among ground motions, therefore the peak values due to the 58 ground motions lend themselves to statistical analysis.

From the stress response histories, the peak values of the maximum principal stress over the duration of each ground motion are determined by the same procedure as for the vertical stresses. The median value at every nodal point on the two faces (not in the interior) is then computed as the geometric mean of the stress values due to the 58 ground motions.

Results for each of the 58 ground motions, in addition to the median values, are presented in Figure 4.3.2. The median results provide the benchmark to which the RSA procedure is evaluated in Chapter 10.

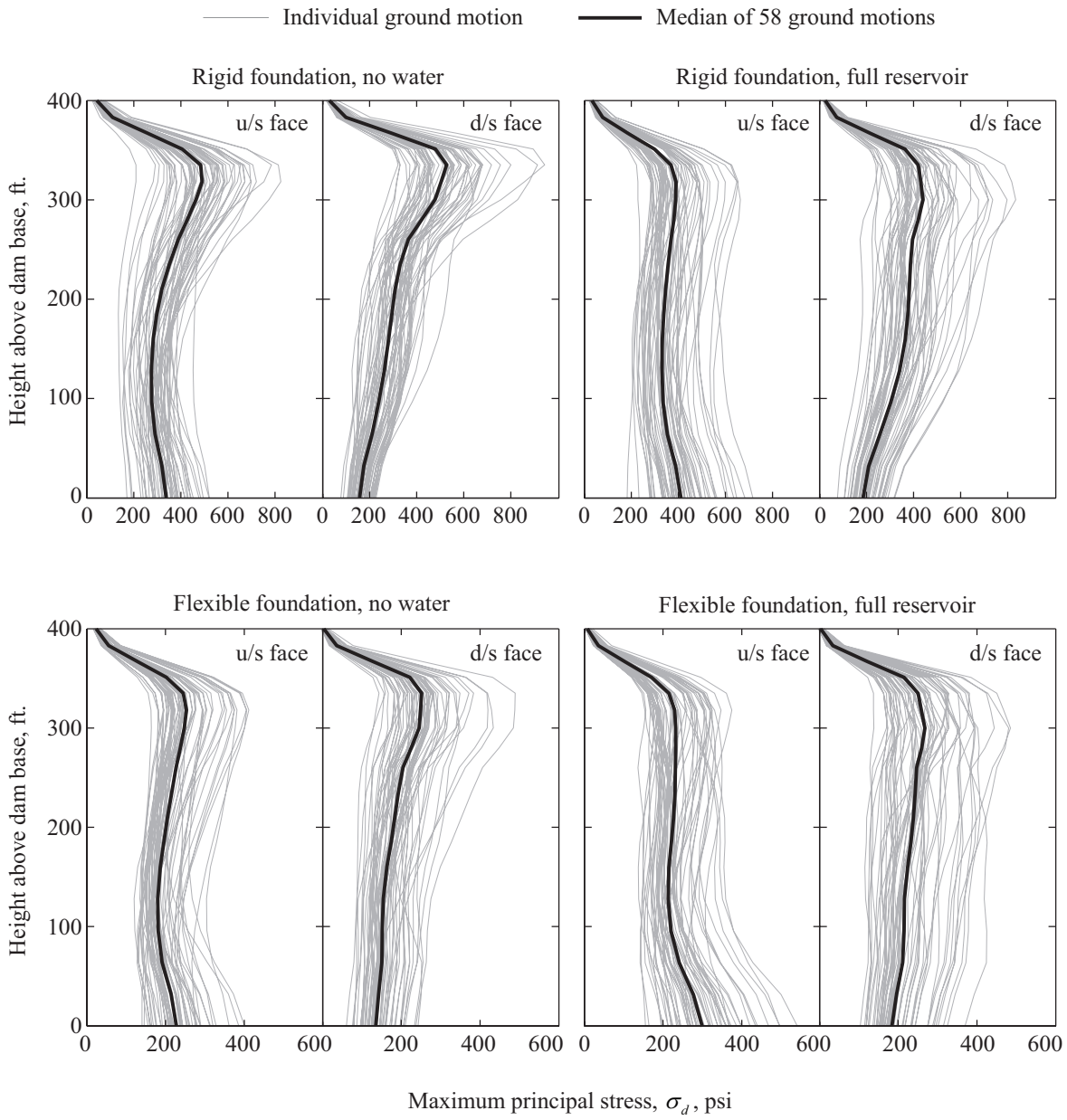

Figure 4.3.2 Peak values of maximum principal stresses at the two faces of Pine Flat Dam due to each of the 58 ground motions; initial static stresses are excluded. Also plotted are the median values.

5 Conclusions

The computer program EAGD-84, numerically evaluating the response of a dam-water-foundation system to earthquake ground motion, has been utilized extensively for research purposes and in seismic design and evaluation of concrete gravity dams. Two important developments have now been added to the program:

1. A set of Matlab modules and a GUI has been developed to perform pre-processing of the input and post-processing of the analysis results from EAGD-84 in the widely used Matlab scripting language. Together these represent a great improvement to the accessibility and user-friendliness of the EAGD-84 program, and enables users to perform complex parameter studies or large statistical simulations using EAGD-84, which has previously not been practical.
2. A more complete set of compliance data that govern the interaction between the dam and the foundation has been incorporated in the program, providing sufficient control of the overall damping in the dam-water-foundation system to ensure consistency with damping measured from motions of dams recorded during forced vibration tests and earthquakes.

An updated version of the EADG-84 program, including both of these developments, has been made available for download through the NISEE library web site [27].

Utilizing the new Matlab modules, the earthquake response of Pine Flat Dam to an ensemble of 58 ground motions was also computed. The median of the peak responses of the dam to these 58 ground motions provides a benchmark to which the response spectrum analysis procedure presented in Part B of this report is evaluated.

PART B: RESPONSE SPECTRUM ANALYSIS OF CONCRETE GRAVITY DAMS

6 Introduction

As mentioned earlier in this report, a response spectrum analysis (RSA) procedure, in which the peak value of response is estimated directly using the earthquake design spectrum, was presented in 1978 to be used in the preliminary phase of design of concrete gravity dams and for safety evaluation of existing dams [5]. This procedure considered the effects of dam-water interaction, known to have significant influence on the response of the dam to ground motion.

In 1986, the RSA procedure was extended to also consider absorption of hydrodynamic pressure waves into the alluvium and sediments invariably deposited at the bottom of reservoirs, and more importantly, interaction between the dam and the underlying foundation [19]. Recognizing that the cross-sectional geometry of concrete gravity dams does not vary widely, standard data for the vibration properties of dams and parameters characterizing dam-water-foundation interaction effects were presented to facilitate the implementation of the procedure [19]. This procedure has from the time of its publication been widely used for seismic design and safety evaluation of dams, and it is favored in several dam safety guidelines [33]. The procedure is also implemented in the much used computer program CADAM [21] for stability evaluations of concrete gravity dams.

The following chapters present a comprehensive evaluation of the accuracy of the RSA procedure, in contrast to the limited scope of the earlier investigation [19]. To enhance the accuracy of the procedure, the possibility of calculating stresses by finite element analysis versus the commonly used beam formulas is explored, and a correction factor for beam stresses on the downstream face of the dam is developed.

Also included is a more complete set of data for the parameters that characterize dam-foundation interaction, derived from the standard compliance data computed by the procedure described in Appendix A. This development was motivated by the realization that data presented earlier did not provide sufficient control of the overall damping in the dam-water-foundation system to ensure consistency with damping measured from motions of dams recorded during forced vibration tests and earthquakes [10] [30] [31], as was discussed in Chapter 3. Based on the results from recent research, updated recommendations for the selection of system parameters to be used in the procedure are presented.

For the sake of completeness, the RSA procedure is summarized and the standard values for parameters that characterize dam-water interaction and reservoir bottom absorption are also included, thus making this document self-contained.

The subsequent chapters, including Appendices C and E, have also been published – with certain editorial changes – as a separate report through the Pacific Earthquake Engineering Research Center [23].

7 Response Spectrum Analysis Procedure

The response spectrum analysis (RSA) procedure developed to estimate the earthquake-induced stresses in concrete gravity dams considers only the more significant aspects of the response. Although the dynamics of the system including dam-water-foundation interaction is considered in estimating the response due to the fundamental vibration mode, the less significant part of the response due to higher modes is estimated by the static correction method. Only the horizontal component of ground motion is considered because the response due to the vertical component is known to be much smaller [14].

Dam-water-foundation interaction introduces frequency-dependent, complex-valued hydrodynamic and foundation terms in the governing equations. Based on a clever series of approximations, frequency-independent values of these terms were defined and an equivalent SDF system developed to estimate the fundamental mode response of dams, leading to the RSA procedure summarized in the subsequent sections. This development was presented and approximations evaluated and justified in a series of publications [16] [17] [19].

The two-dimensional system considered consists of a concrete gravity dam monolith supported on a horizontal surface of underlying flexible foundation rock, idealized as a viscoelastic half-plane, and impounding a reservoir of water, possibly with alluvium and sediments at the bottom (Figure 7.1.1). A complete description of the dam-water-foundation system is presented in Ref. [13] and [16].

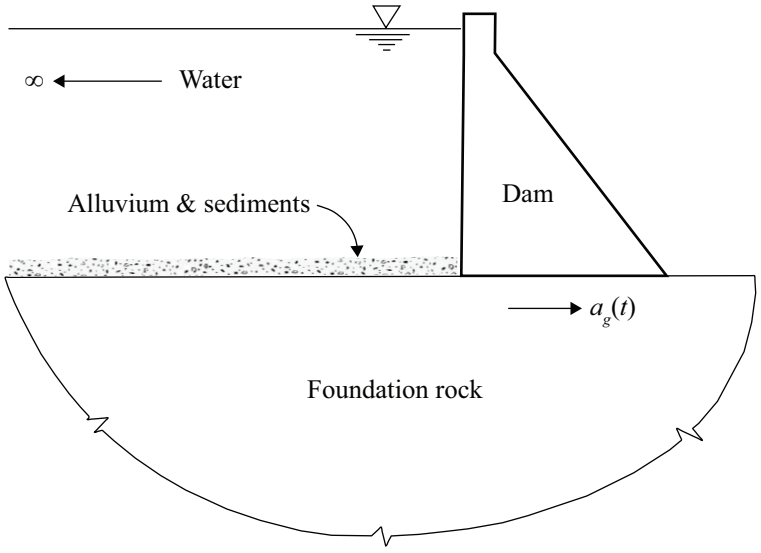

Figure 7.1.1 Dam-water-foundation system.

7.1 Equivalent Static Lateral Forces: Fundamental Mode

The peak response of the dam in its fundamental vibration mode including dam-water-foundation interaction effects can be estimated by static analysis of the dam alone subjected to equivalent static lateral forces acting on the upstream face of the dam:

$$f_1(y) = \tilde{\Gamma}_1 \frac{A\left(\tilde{T}_1, \tilde{\zeta}_1\right)}{g}\left[w_s(y)\phi_1(y) + gp\left(y, \tilde{T}_r\right)\right] \tag{7.1.1}$$

in which $\phi_1(y)$ is the horizontal component of displacement at the upstream face of the dam in the fundamental vibration mode shape of the dam supported on rigid foundation with empty reservoir; $w_s(y)$ is the weight per unit height of the dam; and $\tilde{\Gamma}_1 = \tilde{L}_1/\tilde{M}_1$, where $\tilde{M}_1$ and $\tilde{L}_1$ are given by

$$\tilde{M}_1 = M_1 + \int_0^H p\left(y, \tilde{T}_r\right)\phi_1(y)\,dy \tag{7.1.2}$$

$$\tilde{L}_1 = L_1 + \int_0^H p\left(y, \tilde{T}_r\right)dy \tag{7.1.3}$$

in which H is the depth of the impounded water; the generalized mass and earthquake force coefficient are given by

$$M_1 = \frac{1}{g}\int_0^{H_s} w_s(y)\phi_1^2(y)\,dy \tag{7.1.4}$$

$$L_1 = \frac{1}{g}\int_0^{H_s} w_s(y)\phi_1(y)\,dy \tag{7.1.5}$$

where H_s is the height of the dam; g is the acceleration due to gravity; and $A(\tilde{T}_1, \tilde{\zeta}_1)$ is the pseudo-acceleration ordinate of the earthquake design spectrum evaluated at vibration period $\tilde{T}_1$ and damping ratio $\tilde{\zeta}_1$ of the equivalent SDF system representing the dam-water-foundation system.

The function $p(y,\tilde{T}_r)$ is the real-valued component of the complex-valued function representing the hydrodynamic pressure on the upstream face due to harmonic acceleration at period $\tilde{T}_r$ in the shape of the fundamental mode; the corresponding boundary value problem is shown in Figure 7.1.2a. The natural vibration period of the equivalent SDF system representing the fundamental mode response of the dam (on rigid foundation) with impounded water is given by [16]

$$\tilde{T}_r = R_r T_1 \tag{7.1.6}$$

in which T_1 is the fundamental vibration period of the dam on rigid foundation with empty reservoir. Hydrodynamic effects lengthen the vibration period, i.e., the period-lengthening ratio, R_r, is greater than one, because of the frequency-dependent, added hydrodynamic mass arising from dam-water interaction. It depends on the properties of the dam, the depth of the water, and the absorptiveness of the reservoir bottom materials.

The natural vibration period of the equivalent SDF system representing the fundamental mode response of the dam (with empty reservoir) on flexible foundation is given by [16]

$$\tilde{T}_f = R_f T_1 \tag{7.1.7}$$

Dam-foundation interaction lengthens the vibration period, i.e., the period-lengthening ratio, R_f, is greater than one because of the frequency-dependent, added foundation flexibility arising from dam-foundation interaction. It depends on the properties of the dam and foundation, most importantly, on the ratio E_f / E_s of the elastic moduli of the foundation and the dam concrete.

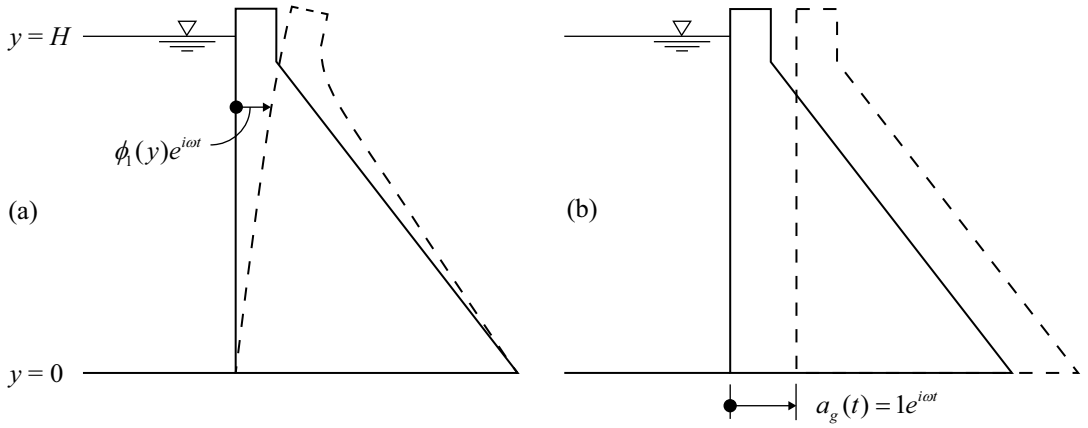

Figure 7.1.2 (a) Acceleration of a dam in its fundamental mode shape; (b) horizontal acceleration of a rigid dam.

The natural vibration period of the equivalent SDF system representing the fundamental mode response of the dam including dam-water-foundation interaction is given by [17]

$$\tilde{T}_1 = R_r R_f T_1 \tag{7.1.8}$$

The damping ratio of this equivalent SDF system can be expressed as [17]

$$\tilde{\zeta}_1 = \frac{1}{R_r}\frac{1}{\left(R_f\right)^3}\zeta_1 + \zeta_r + \zeta_f \tag{7.1.9}$$

in which ζ_1 is the damping ratio of the dam on rigid foundation with empty reservoir; ζ_r is the added damping due to dam-water interaction and reservoir bottom absorption; and ζ_f is the added radiation and material damping due to dam-foundation interaction. Considering that $R_r > 1$ and $R_f > 1$, Equation (7.1.9) shows that dam-water interaction and dam-foundation interaction reduce the effectiveness of structural (dam) damping. However, usually this reduction is more than compensated by the added damping due to reservoir bottom absorption and due to dam-foundation interaction, which leads to an increase in the overall damping of the dam.

Before closing this section, it is noted that the equivalent static lateral forces $f_1(x, y)$ vary over the cross-section of the dam monolith. These were integrated over the breadth of the monolith to obtain the forces per unit height of the dam, Equation (7.1.1). The variation of the fundamental mode shape $\phi_1^x(x, y)$ over the breadth of the dam is thus neglected, i.e., $\phi_1^x(x, y) \approx \phi_1^x(0, y)$, and the fundamental mode shape at the upstream face of the dam, $\phi_1(y) \equiv \phi_1^x(0, y)$, is used in all subsequent calculations. The implication of the one-

dimensional formulation of lateral forces to the estimation of stresses is discussed in Chapter 10.

7.2 Equivalent Static Lateral Forces: Higher Modes

Although the fundamental vibration mode is dominant in the response of the dam, the contributions of the higher modes are included by approximating them using the "static correction" concept ([6]: Sections 12.12 and 13.1.5). This implies that the ordinates of the pseudo-acceleration design spectrum at the higher mode periods are approximated by the zero-period ordinate, i.e., the peak ground acceleration. The quality of this approximation depends on dynamic amplification of the design spectrum at the higher mode periods, as will be discussed in Chapter 10.

Just as in the case of multistory buildings [34], soil-structure (dam-foundation) interaction effects may be neglected in a simplified procedure to compute the contributions of the higher vibration modes to the earthquake response of dams.

Utilizing the preceding concepts, the equivalent lateral earthquake forces associated with the higher vibration modes of dams, including the effects of the impounded water, are given by [19]

$$f_{sc}(y) = \frac{a_g}{g}\left\{ w_s(y)\left[1 - \frac{L_1}{M_1}\phi_1(y)\right] + \left[gp_0(y) - \frac{B_1}{M_1} w_s(y)\phi_1(y)\right]\right\} \tag{7.2.1}$$

In Equation (7.2.1), a_g is the peak ground acceleration; $p_0(y)$ is a real-valued frequency-independent function for hydrodynamic pressure on a rigid dam undergoing unit acceleration, with water compressibility neglected (Figure 7.1.2b); both assumptions being consistent with the “static correction” concept; and B_1 provides a measure of the portion of $p_0(y)$ that acts in the fundamental vibration mode:

$$B_1 = 0.20\frac{F_{st}}{g}\left(\frac{H}{H_s}\right)^2 \tag{7.2.2}$$

where F_{st} is the total hydrostatic force on the dam. The shape of only the fundamental vibration mode enters into Equation (7.2.1) and the higher mode shapes are not required, thus simplifying the analysis considerably.

7.3 Response Analysis

As shown in the preceding two sections, the maximum effects of earthquake ground motion in the fundamental vibration mode of the dam have been represented by equivalent static lateral

forces $f_1(y)$ and those due to all the higher modes by $f_{sc}(y)$, determined directly from the response (or design) spectrum without any response history analyses. Static analysis of the dam alone for these two sets of forces provide estimates of the peak modal responses r_1 and r_{sc} for any response quantity, r, e.g., the shear force or bending moment at any horizontal section, or the shear stress or vertical stress at any point. The total response is given by

$$r_{max} = r_{st} \pm \sqrt{(r_1)^2 + (r_{sc})^2} \tag{7.3.1}$$

where the initial value, r_{st}, of the response quantity prior to the earthquake is determined by standard static analysis procedures, including the effects of the self-weight of the dam, hydrostatic pressures, construction sequence, and thermal effects.

In Equation (7.3.1) the dynamic response is obtained by combining peak modal responses r_1 and r_{sc} in the fundamental and higher modes, respectively, by the SRSS rule, which is appropriate because the natural vibration frequencies of a concrete gravity dam are well separated. Because the directions of earthquake responses are reversible, both positive and negative signs are included in the dynamic response.

The SRSS combination rule is applicable to the computation of any response quantity that is proportional to the modal coordinates ([6]: Section 13.8). Thus, this rule is generally not valid to determine the principal stresses. However, the maximum principal stresses at the two faces of the dam can be determined by a simple transformation of the vertical stresses – determined by beam theory – if the upstream face is nearly vertical and the effects of tail-water at the downstream face are small ([18]: Appendix C). Under these restricted conditions, the resulting principal stresses at the two faces of a dam monolith (not in the interior) may be determined by the SRSS rule.

The preceding combination of static and dynamic responses is appropriate if r_{st}, r_1, and r_{sc} are oriented similarly. Such is obviously the case for the shear and vertical stresses at any point, but generally not for principal stresses except under the restricted conditions previously mentioned.

8 Standard System Properties for Fundamental Mode Response

The computations required to directly evaluate Equation (7.1.1) would be excessive in practical application. Recognizing that the cross-sectional geometry of concrete gravity dams does not vary widely, standard values for the vibration properties – vibration period and shape of the fundamental mode – of the dam, period lengthening ratios R_r and R_f due to dam-water and dam-foundation interaction, damping ratios ζ_r and ζ_f associated with the two interaction mechanisms, and the hydrodynamic pressure functions $p(y,\tilde{T}_r)$ and $p_0(y)$ are presented in this chapter. They represent an extension of the data first presented in Ref. [19].

8.1 Vibration Properties for the Dam

The fundamental vibration period, in seconds, for a "standard" cross-section (Figure 8.1.1a) for non-overflow monoliths of concrete gravity dams on rigid foundation with an empty reservoir can be approximated by [5]

$$T_1 = 1.4\frac{H_s}{\sqrt{E_s}} \tag{8.1.1}$$

where H_s is the height of the dam in feet and E_s is the modulus of elasticity of the dam concrete in psi. The fundamental vibration mode shape, $\phi_1(y)$, of the "standard" cross-section is shown in Figure 8.1.1b and presented in Table E.1. These standard vibration properties are compared in Figure 8.1.1b with the fundamental vibration periods and mode shapes determined by finite element analyses of six cross-sections – two actual dams and four idealized dams – chosen to cover the plausible range of shapes. It is apparent that the vibration properties of these cross-sections are very similar, demonstrating that it is appropriate to use the standard vibration period and mode shape for preliminary design and safety evaluation of concrete gravity dams.

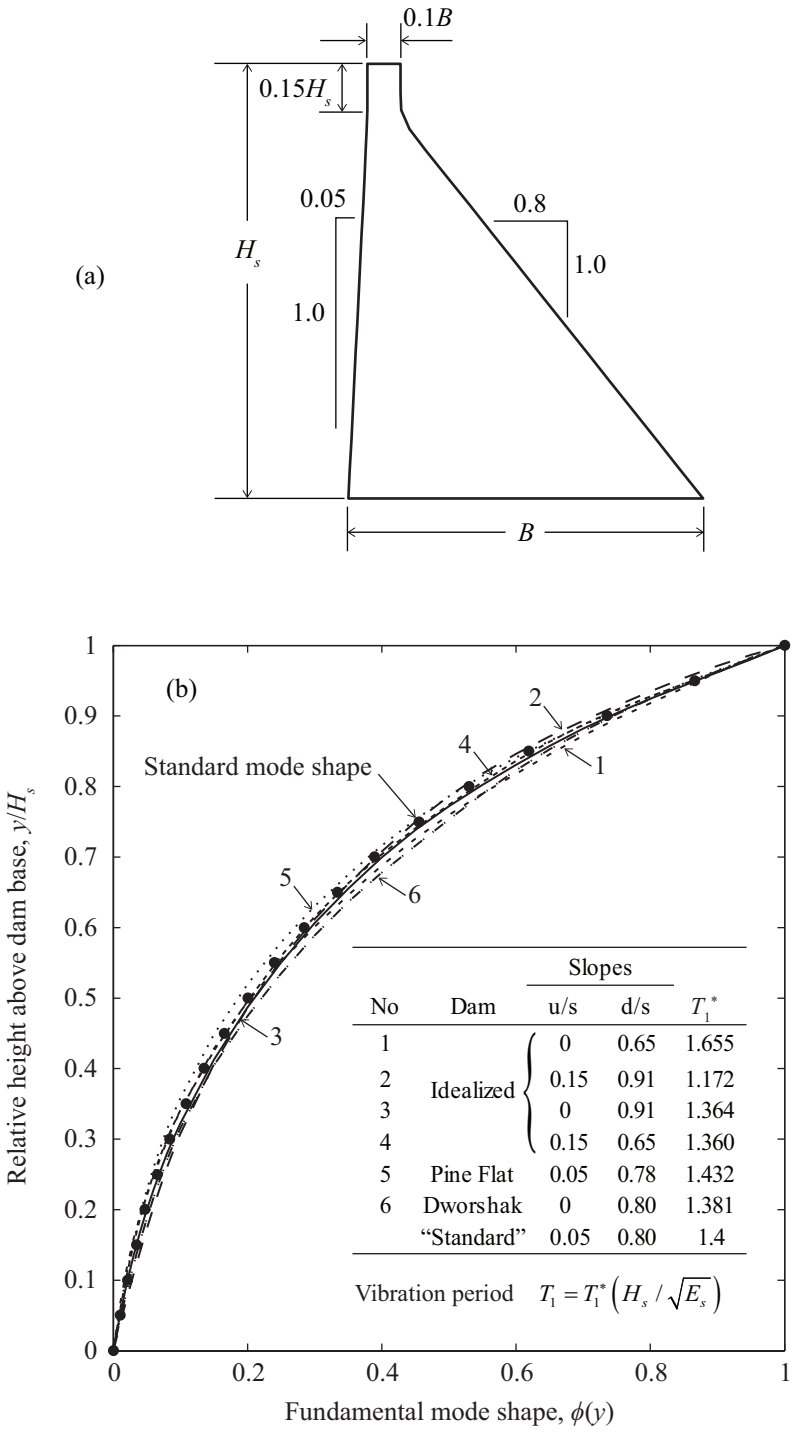

Figure 8.1.1 (a) "Standard" cross-section; (b) comparison of fundamental vibration period and mode shape for the "standard" cross-section and four idealized and two actual concrete gravity dam cross-sections. Data from Ref. [5].

8.2 Modification of Period and Damping due to Dam-Water Interaction

Dam-water interaction and reservoir bottom absorption modify the natural vibration period and damping ratio of the equivalent SDF system. For the "standard" dam cross-section, the period lengthening ratio R_r and added damping ζ_r are dependent on several parameters, the most significant being: modulus of elasticity E_s of the dam concrete, the ratio H/H_s of water depth to dam height, and the wave reflection coefficient α. This coefficient, α, is the ratio of the amplitude of the reflected hydrodynamic pressure wave to the amplitude of a vertically propagating pressure wave incident on the reservoir bottom [12] [13] [32], where $\alpha = 1$ indicates complete reflection of pressure waves, and smaller values of α indicate increasingly absorptive materials.

By performing many analyses of the "standard" dam cross-section using the procedures described in Ref. [14] and modified in Ref. [18] for dams with large values of modulus of elasticity E_s, the period lengthening ratio R_r and added damping ζ_r have been computed as a function of H/H_s for a range of values of E_s and α [18]; the results are summarized in Table E.2.

The mechanics of dam-water interaction and reservoir bottom absorption has been discussed elsewhere in detail [12] [13]. Here, it is simply noted that R_r increases and ζ_r generally – but not always – increases, with increasing water depth, absorptiveness of the reservoir bottom materials, and elastic modulus of concrete. The effects of dam-water interaction may be neglected in the analysis if the reservoir depth is less than half of the dam height, i.e., $H/H_s < 0.5$.

8.3 Modification of Period and Damping due to Dam-Foundation Interaction

Dam-foundation interaction modifies the natural vibration period and damping ratio of the equivalent SDF system. For the "standard" dam cross-section, the period lengthening ratio R_f and added damping ζ_f depend on several parameters, the most significant being: E_f/E_s, the ratio of the moduli of elasticity of the foundation rock to that of the dam concrete, and the constant hysteretic damping factor η_f for the foundation rock.

By performing many analyses of the "standard" dam cross-section using the procedures described in Ref. [14], the period lengthening ratio R_f and added damping ratio ζ_f were initially computed for a range of values of E_f/E_s and η_f = 0.01, 0.10, 0.25 and 0.50, which in retrospect turned out to be too coarse. The added damping ratio has now been recomputed for a closely spaced set of η_f values using the standard compliance data developed by the procedure in Appendix A; results are presented in Table E.3.

The mechanics of dam-foundation interaction has been discussed elsewhere in detail [13]. Here it is simply noted that for moduli ratios E_f/E_s that are representative of actual dam sites, the period ratio R_f varies little with η_f; therefore a single curve represents the variation of R_f with E_f/E_s, which may be used for any value of η_f. As expected, R_f increases as the moduli ratio E_f/E_s decreases, which for a fixed value of E_s implies that the foundation is increasingly flexible. The added damping ratio ζ_f increases with decreasing E_f/E_s and increasing constant hysteretic damping factor η_f. The foundation may be treated as rigid in the analysis if $E_f/E_s > 4$, as the effects of dam-foundation interaction are then negligible.

8.4 Hydrodynamic Pressure

In order to provide a convenient means for determining the hydrodynamic pressure function $p(y,\tilde{T}_r)$ in Equation (7.1.1), a non-dimensional form of this function, $gp(\hat{y})/wH$, where $\hat{y} = y/H$ and w is the unit weight of water, was computed in Ref. [18] for several values of α and a range of the period ratio

$$R_w = \frac{T_1^r}{\tilde{T}_r} \tag{8.4.1}$$

where T_1^r is the fundamental vibration period of the impounded water given by $T_1^r = 4H/C$, where C is the velocity of pressure waves in the water. Results for a full reservoir, $H/H_s = 1$, and a range of values of α and R_w are summarized in Table E.4. The function $gp(\hat{y})/wH$ for other values of H/H_s can be approximately computed as $(H/H_s)^2$ times the function for $H/H_s = 1$ [5].

8.5 Generalized Mass and Earthquake Force Coefficient

Instead of evaluating Equations (7.1.2) and (7.1.3), the generalized mass $\tilde{M}_1$, and generalized earthquake coefficient $\tilde{L}_1$ of the equivalent SDF system including hydrodynamic effects, can be conveniently computed from [18]

$$\tilde{M}_1 = (R_r)^2 M_1 \tag{8.5.1}$$

$$\tilde{L}_1 = L_1 + \frac{1}{g} F_{st} \left(\frac{H}{H_s} \right)^2 A_p \tag{8.5.2}$$

where $F_{st} = wH^2/2$ is the hydrostatic force, and the hydrodynamic force coefficient A_p is the integral over the depth of water of the pressure function $2gp(\hat{y})/wH$ for $H/H_s = 1$. The hydrodynamic force coefficient A_p, computed in Ref. [18] for a range of values for the period ratio R_w and wave reflection coefficient α, are summarized in Table E.5.

9 Implementation of Analysis Procedure

Presented in this section are recommendations for the selection of system parameters and a detailed outline of the computational steps required to determine the earthquake response of a dam by the RSA procedure. These are based on the recommendations first presented in Ref. [19], but a number of changes have been made to ensure consistency with results from recent research. To enhance the accuracy of the procedure, a correction factor for beam stresses on the downstream face of the dam is developed in Section 9.3.

9.1 Selection of System Parameters and Earthquake Design Spectrum

The response spectrum analysis (RSA) procedure requires only a few parameters to describe the dam-water-foundation system: E_s, ζ_1, H_s, E_f, η_f, H and α. In addition, a pseudo-acceleration design spectrum is required to represent the seismic hazard at the site. Based on the recommendations presented in Ref. [19], with a number of modifications, guidelines for selecting the system parameters to be used in the RSA procedure are presented in this section.

The Young's modulus of elasticity E_s for the dam concrete should be based on suitable test data in so as far as possible, or estimated from the design strength of concrete. The value of E_s may be modified to recognize the strain rates representative of those the concrete may experience during earthquake motions of the dam [5]. The dam-water interaction parameters R_r and ζ_r may be estimated for the selected E_s value by linearly interpolating, if necessary, between the nearest values for which data are available in Table E.2: E_s = 1.0, 2.0, 2.5, 3.0, 3.5, 4.0, 4.5, or 5.0 million psi. Correlation of recorded and computed motions of dams during earthquakes [1] [10], indicates that the viscous damping ratio ζ_1 for the dam alone is in the range of 1 to 3 percent. Assigning a value for ζ_1 in this range is recommended if no data specific to the dam is available. The height H_s of the dam is measured from the base to the crest.

The Young's modulus of elasticity E_f and constant hysteretic damping coefficient η_f of the foundation should be determined from a site investigation and appropriate tests. For the resulting value of E_f/E_s, the dam-foundation interaction parameters R_f and ζ_f can be estimated by linearly interpolating, if necessary, between the two nearest values for which data are available in Table E.3. In the absence of measured properties for the rock at the site, a

value of η_f in the range of 0.02 - 0.06 is recommended [10], corresponding to a viscous damping ratio of 1 - 3 percent.

The depth H of the impounded water is measured from the free surface to the reservoir bottom. In practical situations, the elevations of the reservoir bottom and dam base may differ. The standard values for unit weight of water and velocity of pressure waves in water are w = 62.4 pcf and C = 4720 feet/sec, respectively.

It may be impractical to determine reliably the wave reflection coefficient α because the reservoir bottom materials may consist of highly variable layers of exposed bedrock, alluvium, silt and other sediments, and appropriate site investigation techniques have not been developed. However, to be conservative, the estimated value of α should be rounded up to the nearest value for which the figures and tables are presented: α = 1.0, 0.90, 0.75, 0.50, 0.25, and 0; interpolation of data for intermediate values of α is not appropriate. For proposed new dams or recent dams where sediment deposits are meager, α = 0.90 or 1.0 is recommended and, lacking data, α = 0.75 or 0.90 is recommended for older dams where sediment deposits are substantial. In each case, the larger α value will generally give conservative results, which is appropriate at the preliminary design stage.

The horizontal earthquake ground acceleration is specified by a pseudo-acceleration design spectrum in the RSA procedure. This should be a smooth response spectrum – without the irregularities inherent in response spectra of individual ground motions – representative of the intensity and frequency characteristics of the earthquake events associated with the seismic hazard at the site.

9.2 Computational Steps

Computation of the earthquake response of the dam in the RSA procedure can be organized in three parts [19]:

Part I: Compute the earthquake forces and stresses due to response of the dam in its fundamental mode of vibration by the following computational steps:

l. Compute T_1, the fundamental vibration period of the dam, in seconds, on rigid foundation with an empty reservoir from Equation (8.1.1) in which H_s is the height of the dam in feet and E_s is the design value of the modulus of elasticity of dam concrete in psi.

2. Compute $\tilde{T}_r$, the fundamental vibration period of the dam, in seconds, including the influence of impounded water from Equation (7.1.6) in which T_1 was computed in Step 1; R_r is the period ratio determined from Table E.2 for the design values of E_s, the wave reflection coefficient α, and the depth ratio H/H_s, where H is the depth of the impounded water. If $H/H_s < 0.5$, computation of R_r may be avoided by using $R_r = 1$.

3. Compute the period ratio R_w from Equation (8.4.1) in which $\tilde{T}_r$ was computed in Step 2; and $T_1^r = 4H / C$ where $C = 4720$ feet per second.

4. Compute $\tilde{T}_1$, the fundamental vibration period of the dam in seconds, including the dam-water-foundation interaction, from Equation (7.1.8) in which R_r was determined in Step 2; R_f is the period ratio determined from Table E.3 for the design value of E_f / E_s; and E_f is the modulus of elasticity of the foundation. If $E_f / E_s > 4$, use $R_f \approx 1$.

5. Compute the damping ratio $\tilde{\zeta}_1$ of the dam from Equation (7.1.9) using the computed period ratios R_r and R_f; ζ_1 is the viscous damping ratio for the dam on rigid foundation with empty reservoir; ζ_r is the added damping ratio due to dam-water interaction and reservoir bottom absorption, obtained from Table E.2 for the selected values of E_s, α and H/H_s; ζ_f is the added damping ratio due to dam-foundation interaction, obtained from Table E.3 for the selected values of E_f / E_s, and η_f. If $H/H_s < 0.5$, use $\zeta_r = 0$; if $E_f / E_s > 4$, use $\zeta_f = 0$; and if the computed value of $\tilde{\zeta}_1 < \zeta_1$, use $\tilde{\zeta}_1 = \zeta_1$.

6. Determine $gp(y, \tilde{T}_r)$ from Table E.4 corresponding to the value of R_w computed in Step 3 (by interpolating, if necessary, between data for the two nearest available values of R_w), the design value of α, and for $H/H_s = 1$; the result is multiplied by $(H/H_s)^2$. If $H/H_s < 0.5$, computation of $p(y, \tilde{T}_r)$ may be avoided by using $p(y, \tilde{T}_r) \approx 0$.

7. Compute the generalized mass $\tilde{M}_1$ from Equation (8.5.1) in which R_r was computed in Step 2; and M_1 is computed from Equation (7.1.4) in which $w_s(y)$ is the weight of the dam per unit height; the fundamental vibration mode shape $\phi_1(y)$ is tabulated in Table E.1; and g is the acceleration due to gravity.

8. Compute the generalized earthquake force coefficient $\tilde{L}_1$ from Equation (8.5.2) in which L_1 is computed from Equation (7.1.5); $F_{\text{st}} = wH^2 / 2$; and A_p is given in Table E.5 for the values of R_w and α used in Step 6. If $H/H_s < 0.5$ computation of $\tilde{L}_1$ may be avoided by using $\tilde{L}_1 \approx L_1$.

9. Compute $f_1(y)$, the equivalent static lateral earthquake forces associated with the fundamental vibration mode from Equation (7.1.1) in which $A(\tilde{T}_1, \tilde{\zeta}_1)$ is the pseudo-acceleration ordinate of the earthquake design spectrum evaluated at the vibration period $\tilde{T}_1$ determined in Step 4 and damping ratio $\tilde{\zeta}_1$ determined in Step 5; $w_s(y)$ is the weight per unit height of the dam; $\phi_1(y)$ is the fundamental vibration mode shape of the dam from Table E.1; $\tilde{\Gamma}_1 = \tilde{L}_1 / \tilde{M}_1$ where $\tilde{L}_1$ and $\tilde{M}_1$ was determined in Steps 7 and 8, respectively; and the hydrodynamic pressure term $gp(y, \tilde{T}_r)$ was determined in Step 6.

10. Determine by static analysis of the dam subjected to the equivalent static lateral forces $f_1(y)$, from Step 9, applied to the upstream face of the dam, all the response quantities of interest, in particular the stresses throughout the dam. Traditional procedures for

design calculations may be used wherein the bending stresses across a horizontal section are computed by elementary formulas for stresses in beams. Alternatively, the finite element method may be used for a more accurate static stress analysis.

Note: If computed using beam theory, stresses at the sloping part of the downstream face should be multiplied by the correction factor of 0.75 developed in Section 9.3.

Part II: The earthquake forces and stresses due to the higher vibration modes can be determined approximately for purposes of preliminary design by the following computational steps:

11. Compute $f_{sc}(y)$, the equivalent static lateral earthquake forces associated with the higher vibration modes from Equation (7.2.1) in which M_1 and L_1 were determined in Steps 7 and 8, respectively; $gp_0(y)$ is determined from Table E.6; B_1 is computed from Equation (7.2.2); and a_g is the peak ground acceleration from the earthquake design spectrum. If $H/H_s < 0.5$ computation of $p_0(y)$ may be avoided by using $p_0(y) \approx 0$ and hence $B_1 \approx 0$.

12. Determine by static analysis of the dam subjected to the equivalent static lateral forces $f_{sc}(y)$, from Step 11, applied to the upstream face of the dam, all the response quantities of interest, in particular the stresses throughout the dam. The stress analysis may be carried out by the same procedures mentioned in Step 10.

Part III: The total bending moments, shear forces and stresses at any section in the dam are determined by the following computational step:

13. Compute the total value of any response quantity from Equation (7.3.1) in which r_1 and r_{sc} are values of the response quantity determined in Steps 10 and 12 associated with the fundamental and higher vibration modes, respectively; and r_{st} is its initial value prior to the earthquake due to various loads, including the self-weight of the dam, hydrostatic pressure, construction sequence, and thermal effects.

9.3 Correction Factor for Downstream Face Stresses

Formulas based on beam theory overestimate stresses at sloping faces, thus, stresses computed at the downstream face of concrete gravity dams should be multiplied by the correction factor developed in this section.

Figure 9.3.1 shows the vertical stresses, $\sigma_{y,1}$, at the upstream and downstream faces of Pine Flat Dam, which is typical of many dams, with empty reservoir on rigid foundation, due to the lateral forces of Equation (7.1.1). Stresses were computed by static analysis using beam

formulas and the finite element method; a detailed summary of these procedures are presented in Appendix C.

It is evident that beam theory provides results close to those from finite element analysis at the upstream face, but the stresses at the downstream face are considerably overestimated. As can be seen in Figure 9.3.1, multiplying the stress values at the sloping part of the downstream face by a correction factor of 0.75, leads to stresses that are much closer to the finite element values. However, the agreement is not as good near the toe of the dam or at the stress concentration where the downstream face changes slope. These discrepancies occur because of the inherent limitations in elementary beam theory, making it incapable of reproducing such abrupt changes in stresses.

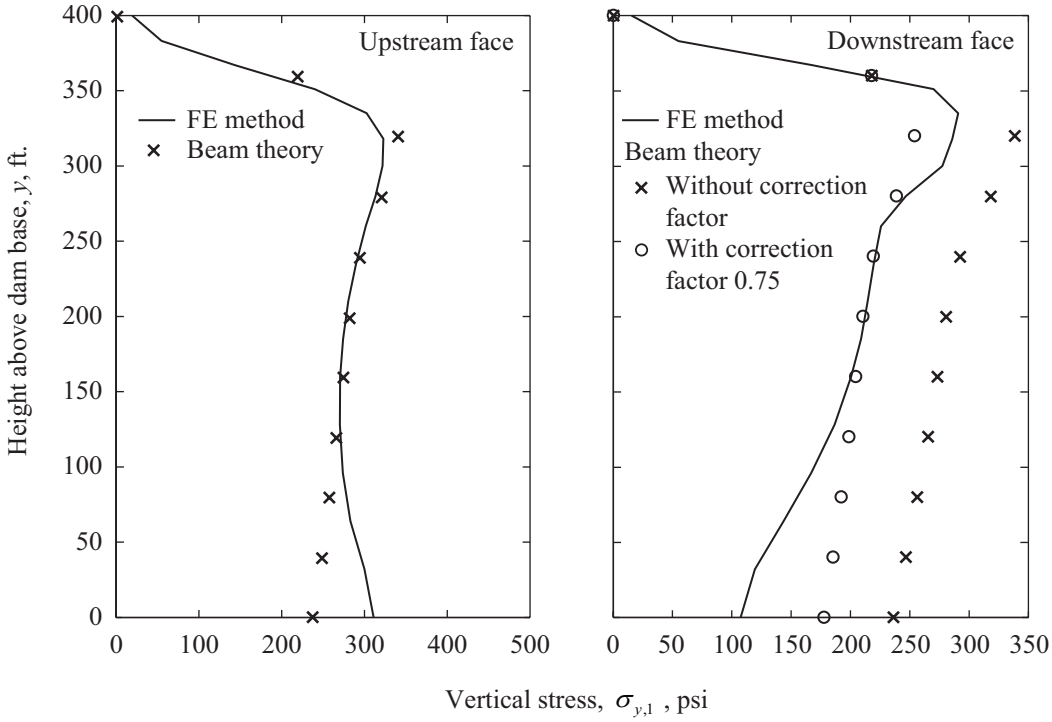

Figure 9.3.1 Vertical stresses, $\sigma_{y,1}$, at the upstream and downstream face of Pine Flat Dam with empty reservoir on rigid foundation due to the lateral forces of Equation (7.1.1).

The correction factor of 0.75 is applicable for modifying vertical stresses computed by beam theory if the slope of the downstream face is no steeper than 0.8:1; it will give conservative results for flatter slopes, but will underestimate the stresses if the slope is much steeper than 0.8:1. The same correction factor is applicable to the principal stresses computed by beam theory at the downstream face of the dam provided the stresses due to tail-water are negligible. With this restriction, the principal stresses are directly proportional to the vertical stresses [18].

Although the correction factor was determined from computed stresses due to the lateral forces associated with the fundamental mode only, it may also be applied to the higher

mode stresses, $\sigma_{y,sc}$. The effectiveness of the correction factor applied to both modal contributions is demonstrated in Section 10.2.

9.4 Use of S.I. Units

Because the standard values for most quantities required in the RSA procedure are presented in a non-dimensional form, implementation of the procedure using S.I. units is straightforward. The expressions and data requiring conversion to S.I. units are noted here:

1. The fundamental vibration period T_1 of the dam on rigid foundation with empty reservoir (Step l), in seconds, is given by:

$$T_1 = 0.38 \frac{H_s}{\sqrt{E_s}} \tag{9.4.1}$$

   where H_s is the height of the dam in meters; and E_s is the modulus of elasticity of the dam concrete in MPa.

2. The period ratio R_r and added damping ratio ζ_r due to dam-water interaction presented in Table E.2 is for specified values of E_s in psi, which should be converted to MPa as follows: 1 million psi $\approx$ 7 thousand MPa.

3. Where required in the calculations, the unit weight of water $w = 9.81$ kN/m^3, the acceleration due to gravity $g = 9.81$ m/s^2, and velocity of pressure waves in water $C = 1440$ m/s.

9.5 CADAM Computer Program

CADAM – Computer aided stability analysis of gravity dams – is a computer program, freely available, developed at the École Polytechnique de Montréal, Canada for static and seismic stability evaluations of concrete gravity dams [21]. Based on the gravity method, CADAM uses rigid body equilibrium and beam theory to perform stress analyses and compute crack lengths and safety factors for dams subjected to various static and seismic load cases. The program has since its release been widely used for educational purposes, R&D in dam engineering, and in actual projects.

CADAM implements the RSA procedure, referring to it as the "pseudo-dynamic method". Starting with user input, the program computes the equivalent static lateral forces associated with the response of the system in its fundamental mode and higher vibration modes by implementing the procedure as described in the previous sections. The earthquake induced bending moments, shear forces and stresses due to the two sets of forces are

computed and combined to determine the total dynamic response. Finally, the responses due to earthquake forces and initial static loads can be combined.

The program provides a fully integrated computing environment with output reports and graphical support to visualize input parameters and output performance indicators such as stresses, crack lengths, resultant positions and safety factors. In addition, the output can be exported to Microsoft Excel spreadsheets to allow users to perform further post-processing of the results. A complete description of the program and its capabilities can be found in Ref. [21].

The latest (2013) version of CADAM has been updated to implement the newly computed standard values for the parameters that characterize dam-foundation interaction, described in Section 8.3. The program is available for download from the web page of École Polytechnique de Montréal, Canada [22].

10 Evaluation of Response Spectrum Analysis Procedure

Although based on structural dynamics theory, the RSA procedure involves several approximations which have been checked individually [16] [17]. Presented in this chapter is an overall evaluation of the procedure, by comparing its results with those obtained from a series of response history analysis (RHA) of the dam modeled as a finite element system, including rigorously the effects of dam-water-foundation interaction and reservoir bottom absorption. These RHA results were computed and presented in Chapter 4.

10.1 System and Ground Motions

The properties for the tallest, non-overflow monolith of Pine Flat Dam are taken as the same as those assumed in the response history analysis in Chapter 4, repeated here for convenience: height of the dam, H_s = 400 ft.; modulus of elasticity of concrete, E_s = 3.25 million psi; unit weight of concrete, w_s = 155 pcf; damping ratio for the dam alone, ζ_1 = 2%; modulus of elasticity of the foundation, E_f = 3.25 million psi; constant hysteretic damping factor for the foundation, η_f = 0.04 (corresponding to 2% viscous damping); depth of water, H = 381 ft.; and wave reflection coefficient at the reservoir bottom, α = 0.75.

An ensemble of 58 ground motions were selected and scaled to be consistent with the probabilistic seismic hazard analysis (PSHA) performed for the Pine Flat Dam site at the 1% in 100 years hazard level presented in Section 4.2. In the RSA procedure, the horizontal earthquake excitation is defined by a single response spectrum. This is taken as the median – computed as the geometric mean[†] – of the response spectra for each of the 58 individual ground motions; the resulting spectrum is shown in Figure 10.1.1 for a range of damping values.

From Figure 10.1.1 it is apparent that this response spectrum is to a certain degree irregular, especially for low damping ratios, and is therefore in a strict sense inappropriate for use in the RSA procedure where a smooth design spectrum is recommended. However, the

[†] From investigating the distribution of the 58 response spectra, it was clear that they show the characteristics of a log-normal distribution, the median can therefore be computed as the geometric mean.

spectrum is used directly in the analysis in order to provide direct comparison with the results obtained from the RHA procedure.

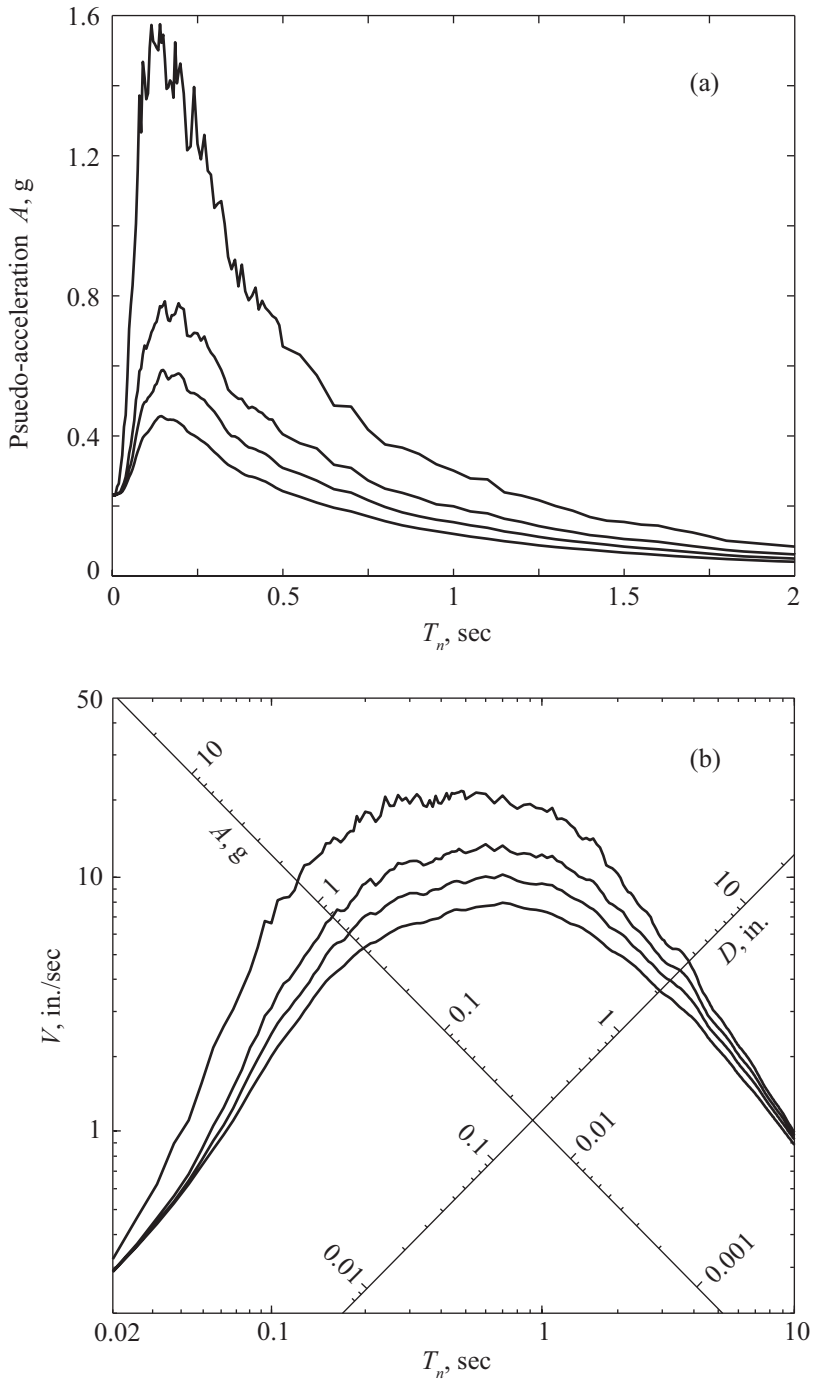

Figure 10.1.1 Median response spectra for 58 ground motions; damping, ζ = 0, 2, 5 and 10 percent; (a) linear plot; (b) four-way logarithmic plot.

10.2 Response Spectrum Analysis

With the earthquake excitation defined by the median response spectrum of Figure 10.1.1, the dam is analyzed by the RSA procedure for the same four analysis cases presented in Chapter 4; these are listed in Table 10.2.1. For the purpose of computing the equivalent static lateral forces in the RSA procedure, and subsequently determine the earthquake response of the dam, a new computer program implementing the step-by-step procedure described in Chapter 9 was developed. Presented in the next sections are selected results from the analysis, the reader is referred to Appendix C for a detailed summary of the computational procedure.

10.2.1 Equivalent Static Lateral Forces

The equivalent earthquake forces are computed by implementing Steps 1-9 and 11 in the step-by-step procedure. The vibration period and damping ratio of the equivalent SDF system, computed using Equations (7.1.6) - (7.1.9), are listed in Table 10.2.1 with the corresponding ordinates from the median response spectrum also presented. The equivalent static lateral forces $f_1(y)$ and $f_{sc}(y)$, representing the maximum earthquake effects of the fundamental and higher modes of vibration, respectively, are presented in Figure 10.2.1.

Table 10.2.1 Pine Flat Dam analysis cases, fundamental mode properties and corresponding pseudo-acceleration ordinates.

Analysis Case	Foundation	Water	$\tilde{T}_1$, in sec.	$\tilde{\zeta}_1$, in percent	$A(\tilde{T}_1, \tilde{\zeta}_1)$, in g
1	Rigid	Empty	0.311	2.0	0.606
2	Rigid	Full	0.387	3.9	0.409
3	Flexible	Empty	0.369	7.1	0.347
4	Flexible	Full	0.459	9.2	0.274

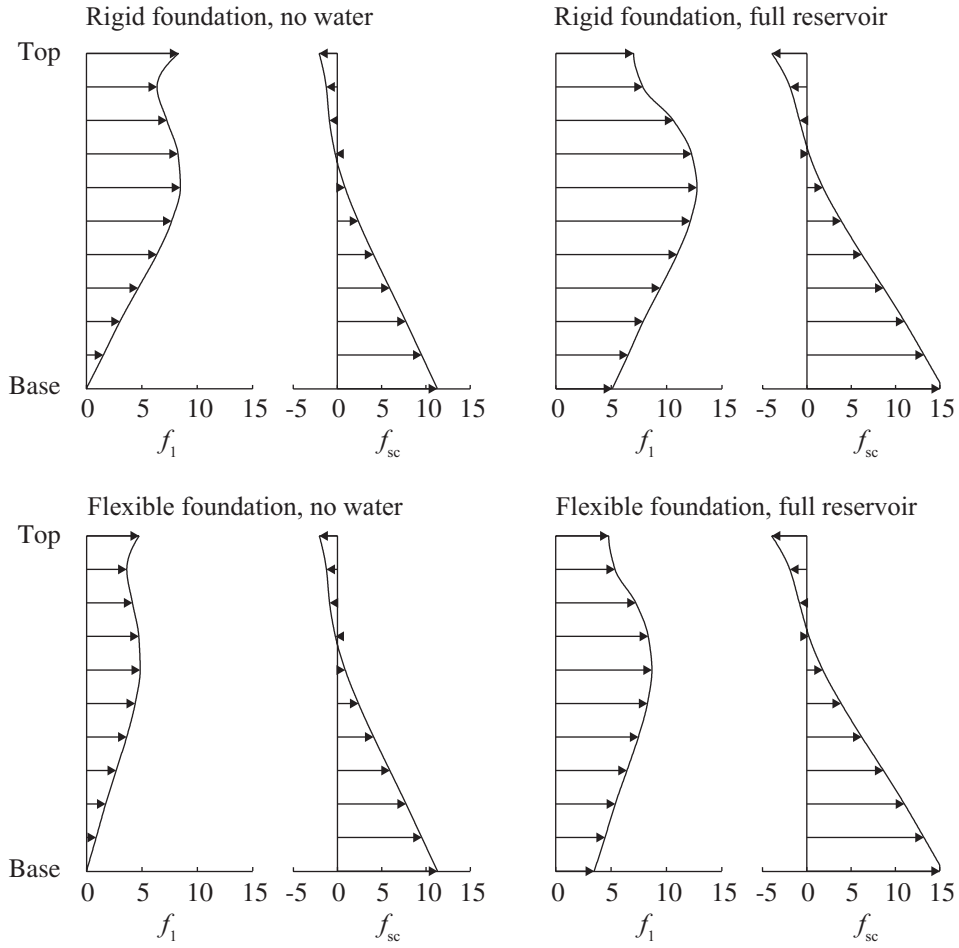

Figure 10.2.1 Equivalent static lateral forces, f_1 and f_{sc}, on Pine Flat Dam, in kips per foot height, computed by the RSA procedure for four analysis cases.

10.2.2 Computation of Stresses

The vertical stresses $\sigma_{y,1}$ and $\sigma_{y,sc}$ due to the two sets of forces f_1 and f_{sc} are computed by static stress analysis of the dam by two methods: (1) elementary formulas for stresses in beams; and (2) finite element analysis of the dam. Combining $\sigma_{y,1}$ and $\sigma_{y,sc}$ by the SRSS combination rule leads to the earthquake induced stresses, $\sigma_{y,d}$, presented in Figure 10.2.2; note that stresses due to initial static loads are not included. The stress values presented will occur as tensile stresses at the upstream face when the earthquake forces act in the downstream direction, and at the downstream face when the earthquake forces act in the upstream direction. A detailed description of the procedure for computing stresses by static analysis of the dam is included in Appendix C.

The results presented in Figure 10.2.2 confirm that the correction factor of 0.75 for stresses computed by beam theory at the sloping part of the downstream face is satisfactory for all four cases. The stresses determined by beam theory with the correction factor are very close to those determined by finite element analysis except near the stress concentrations in

the area near the heel and toe of the dam, and where the downstream face changes slope. It was discussed in Section 9.3 that this occurs because of the inherent limitations in elementary beam theory, thus making it incapable of representing these stress concentrations.

Since the results displayed in Figure 10.2.2 show such good agreement between stresses determined by beam theory and the finite element method, only the beam theory stresses are compared with the results from RHA in the following section.

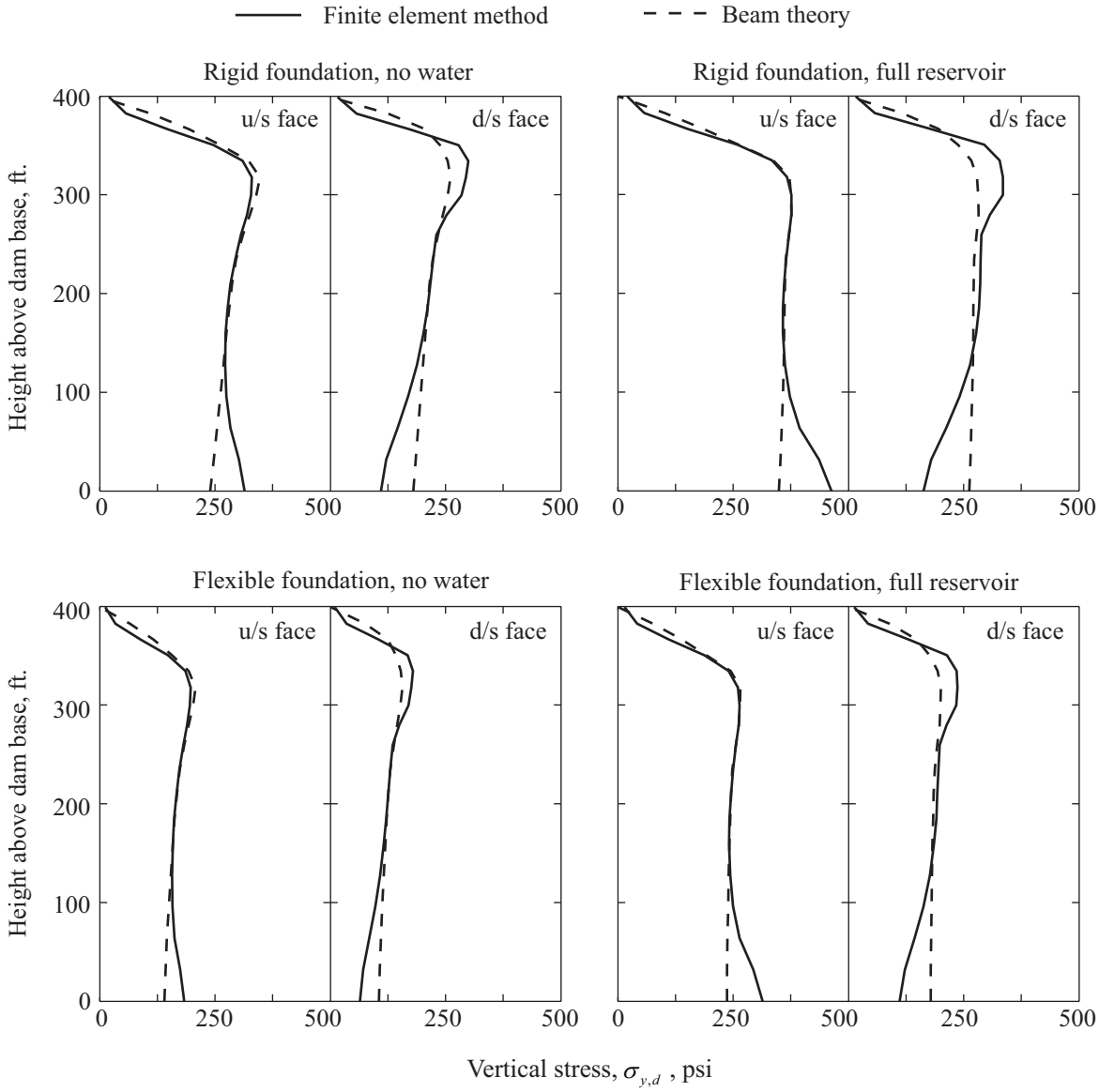

Figure 10.2.2 Earthquake induced vertical stresses, $\sigma_{y,d}$, in Pine Flat Dam computed in the RSA procedure by two methods: beam theory and the finite element method.

10.3 Comparison with Response History Analysis

Results from response history analyses of the dam monolith subjected to an ensemble of 58 ground motions were presented in Chapter 4. In the following subsections, results computed by the RSA and RHA procedures are compared.

10.3.1 Fundamental Mode Properties

The fundamental vibration period of the dam-water-foundation system, and the effective damping ratio at this period, were estimated in the RSA procedure and presented in Table 10.2.1. These vibration properties are not explicitly needed in the RHA procedure; however, for the purposes of evaluating the accuracy of the approximate results, they were determined by the half-power bandwidth method and presented in Chapter 4. These are referred to as the "exact" results in Table 10.3.1.

From this comparison it is apparent that the approximate procedure provides excellent estimates for the resonant period and effective damping ratio of the system in its fundamental mode for all four cases. This confirms that the equivalent SDF model for the dam-water-foundation system is able to represent the important effects of dam-water interaction, reservoir bottom absorption and dam-foundation interaction.

Table 10.3.1 "Exact" and approximate fundamental mode properties.

			Vibration Period, $\tilde{T}_1$, in sec		Damping Ratio, $\tilde{\zeta}_1$, in percent	
Case	Foundation	Water	Approx.	Exact	Approx.	Exact
1	Rigid	Empty	0.311	0.318	2.0	2.0
2	Rigid	Full	0.387	0.395	3.9	3.2
3	Flexible	Empty	0.369	0.390	7.1	8.7
4	Flexible	Full	0.459	0.491	9.2	9.8

10.3.2 Stresses

The peak values of the maximum principal stresses at every location in the dam were determined from the response histories due to the 58 ground motions computed and presented in Chapter 4. Recognizing that the peak stress values at each location on the two faces of the dam are suitable for statistical analysis, the median value was computed as the geometric mean of the data set. These median results are presented in Figure 10.3.1. Also plotted in Figure 10.3.1 are the peak values of the maximum principal stresses computed in the RSA procedure by a transformation of the vertical stresses determined by beam theory; see

Appendix C for details. By comparing these two sets of results, the accuracy of the RSA procedure used to compute peak values of earthquake induced stresses can be evaluated.

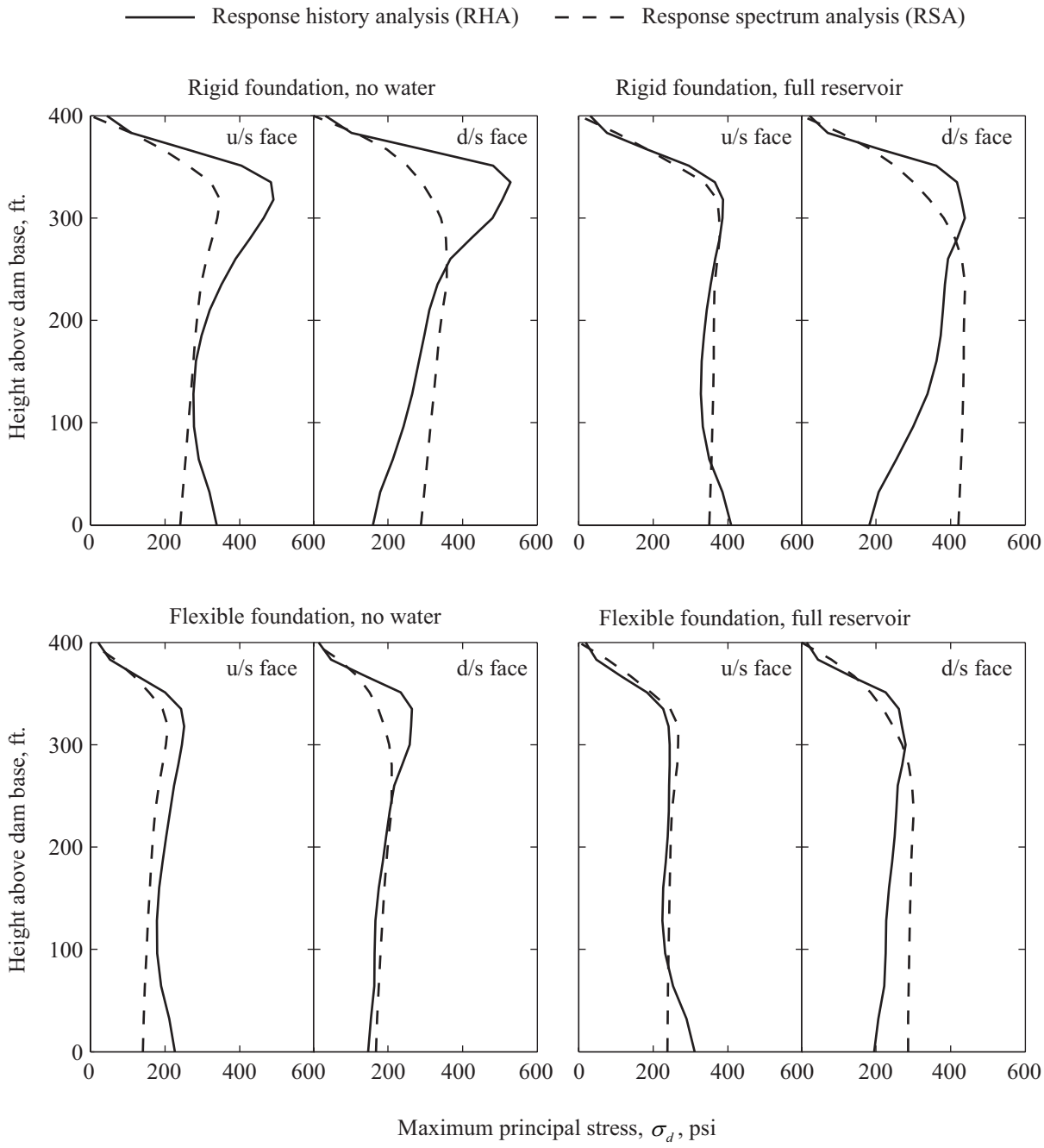

Figure 10.3.1 Comparison of peak values of maximum principal stresses in Pine Flat Dam computed by RSA and RHA procedures; initial static stresses are excluded.

As was discussed in Chapter 4, Case 1 (rigid foundation, empty reservoir) is an example where higher mode contributions are considerable, primarily in the upper part of the dam where the steep stress gradients are evident in the RHA results (Figure 10.3.1). The RSA procedure underestimates these higher mode contributions because the vibration periods are not short enough for the static correction approximation (Section 7.2) to be valid. As shown in Figure 10.3.2, the spectral accelerations at the 2nd and 3rd mode periods are more than two times the peak ground acceleration that is used instead in the static correction method, as a result, the static correction method grossly underestimates the higher mode stresses. For the response spectrum considered, such discrepancy would be much smaller in the case of a dam of lower height with shorter periods, thus bringing the spectral accelerations at the higher vibration periods closer to the PGA value. For Cases 2 – 4 however, the RSA procedure provides very good estimates of the maximum principal stresses.

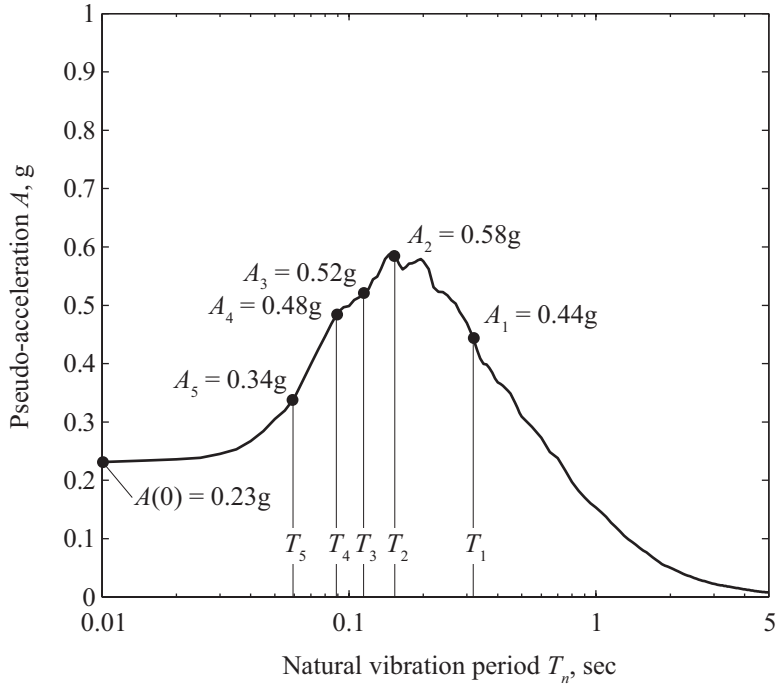

Figure 10.3.2 Spectral accelerations at the first five natural vibration periods of Pine Flat Dam on rigid foundation with empty reservoir; damping, ζ = 2%.

It can be seen in Figure 10.3.1 that the RSA procedure tends to be more conservative – relative to the RHA results – at the downstream face of the dam than at the upstream face. An investigation revealed that the underlying reason for this is the one-dimensional representation of the equivalent static lateral forces in Equation (7.1.1), wherein any variation of the fundamental mode shape over the breadth of the dam was neglected, thus ignoring the horizontal variation of the lateral forces.

The preceding results demonstrate that the RSA procedure estimates stresses to a degree of accuracy that is satisfactory for the preliminary phase in the design of new dams

and in the safety evaluation of existing dams. The level of accuracy achieved in the RSA procedure is noteworthy, especially considering the complicated effects of dam-water-foundation interaction and reservoir bottom absorption on the dynamics of the system, and the number of approximations necessary to develop the procedure. The accuracy of the computed results depends on several factors, including how well the fundamental resonant period and damping ratio are estimated in the RSA procedure, and how well the static correction method is able to account for the contributions from higher modes to the total response.

11 Conclusions

Two analysis procedures are available for earthquake analysis of concrete gravity dams including dam-water-foundation interaction: (1) response spectrum analysis (RSA) in which the peak response is estimated directly from the earthquake design spectrum; and (2) response history analysis (RHA) of a finite element idealization of the dam monolith. The investigation presented in Part B of this report has led to the following conclusions:

1. Analyses of an actual dam to an ensemble of 58 ground motions has demonstrated that the RSA procedure estimates dam response that is close enough to the "exact" response determined by the RHA procedure. Thus, the RSA procedure is satisfactory for the preliminary phase of the design of new dams and in the safety evaluation of existing dams.
2. To enhance the accuracy of this RSA procedure, the possibility of calculating stresses by finite element analysis versus the commonly used beam formulas was investigated, and a correction factor for beam stresses on the downstream face of the dam has been developed.
3. A more complete set of data for the parameters that characterize dam-foundation interaction in the RSA procedure has been developed. Availability of these data provides sufficient control over the overall damping in the dam-water-foundation system to ensure consistency with damping measured from motions of dams recorded during forced vibration tests and earthquakes.

REFERENCES

[1] S. W. Alves and J. F. Hall, "System identification of a concrete arch dam and the calibration of its finite element model," *Earthquake Engineering and Structural Dynamics,* vol. 35, no. 11, pp. 1321-1337, 2006.

[2] J. Baker, "Conditional mean spectrum: tool for ground motion selection," *Journal of Structural Engineering,* vol. 137, pp. 322-331, 2011.

[3] J. Baker and C. A. Cornell, "Spectral shape, epsilon and record selection," *Earthquake Engineering and Structural Dynamics,* vol. 35, pp. 1077-1095, 2006.

[4] P. Chakrabarti and A. K. Chopra, "Earthquake analysis of gravity dams including hydrodynamic interaction," *Earthquake Engineering and Structural Dynamics,* vol. 2, pp. 143-160, 1973.

[5] A. K. Chopra, "Earthquake resistant design of concrete gravity dams," *Journal of the Structural Division,* vol. 104, pp. 953-971, 1978.

[6] A. K. Chopra, *Dynamics of Structures: Theory and Applications to Earthquake Engineering,* 4th ed., Prentice Hall: Upper Saddle River, NJ, 2012.

[7] A. K. Chopra, "Comparison of recorded and computed responses of arch dams," *Proceedings,* International Symposium on Dams, Kyoto, Japan, 2012.

[8] A. K. Chopra, P. Chakrabarti and S. Gupta, "Earthquake response of concrete gravity dams including hydrodynamic and foundation interaction effects," *Report No. UCB/EERC-80/01,* Earthquake Engineering Research Center, University of California, Berkeley, 1980.

[9] A. K. Chopra and P. Chakrabarti, "Earthquake analysis of concrete gravity dams including dam-water-foundation rock interaction," *Earthquake Engineering and Structural Dynamics,* vol. 9, no. 4, pp. 363-383, 1981.

[10] A. K. Chopra and J.-T. Wang, "Linear analysis of concrete arch dams including dam–water–foundation rock interaction considering spatially varying ground motions," *Earthquake Engineering and Structural Dynamics,* vol. 39, no. 7, pp. 731-750, 2010.

[11] G. Dasgupta and A. K. Chopra, "Dynamic stiffness matrices for viscoelastic half planes," *Journal of the Engineering Mechanics Division,* vol. 105, no. EM5, pp. 729-745, October 1979.

[12] G. Fenves and A. K. Chopra, "Effects of reservoir bottom absorption on earthquake response of concrete gravity dams," *Earthquake Engineering and Structural Dynamics,* vol. 11, no. 6, pp. 809-829, 1983.

[13] G. Fenves and A. K. Chopra, "Earthquake analysis of concrete gravity dams including reservoir bottom absorption and dam-water-foundation rock interaction," *Earthquake Engineering and Structural Dynamics,* vol. 12, no. 5, pp. 663-680, 1984.

[14] G. Fenves and A. K. Chopra, "Earthquake analysis and response of concrete gravity dams," *Report No. UCB/EERC-84/10,* Earthquake Engineering Research Center, University of California, Berkeley, 1984.

[15] G. Fenves and A. K. Chopra, "EAGD-84: A computer program for earthquake response analysis of concrete gravity dams," *Report No. UCB/EERC-84/11,* Earthquake Engineering Research Center, University of California, Berkeley, 1984.

[16] G. Fenves and A. K. Chopra, "Simplified earthquake analysis of concrete gravity dams: Separate hydrodynamic and foundation interaction effects," *Journal of Engineering Mechanics,* vol. 111, no. 6, pp. 715-735, 1985.

[17] G. Fenves and A. K. Chopra, "Simplified earthquake analysis of concrete gravity dams: Combined hydrodynamic and foundation interaction effects," *Journal of Engineering Mechanics,* vol. 111, no. 6, pp. 736-756, 1985.

[18] G. Fenves and A. K. Chopra, "Simplified analysis for earthquake-resistant design of concrete gravity dams," *Report No. UCB/EERC-85/10,* Earthquake Engineering Research Center, University of California, Berkeley, 1986.

[19] G. Fenves and A. K. Chopra, "Simplified earthquake analysis of concrete gravity dams," *Journal of Structural Engineering,* vol. 113, no. 8, pp. 1688-1708, 1987.

[20] FEDEASLab , "A Matlab toolbox for nonlinear structural analysis," *version 3.1,* Filippou, F. C., 2005, software.

[21] M. Leclerc, P. Léger and R. Tinawi, "Computer aided stability analysis of gravity dams – CADAM," *Advances in Engineering Software,* vol. 34, no. 7, pp. 403-420, 2003.

[22] M. Leclerc, P. Léger and R. Tinawi, CADAM - (download), Polytechnique Montréal, [Online]. Available: http://www.polymtl.ca/structures/en/telecharg/cadam/telechargement.php.

[23] A. Løkke and A. K. Chopra, "Response spectrum analysis of concrete gravity dams including dam-water-foundation interaction," *Submitted for publication,* Earthquake Engineering Research Center, University of California, Berkeley, 2013.

[24] Mathematica®, *version 9.0.0.0,* Wolfram Research Inc., 2013, software.

[25] MATLAB®, *version 7.14.0.739 (R2012a),* The MathWorks Inc., 2012, software.

[26] R. K. McGuire, "Seismic hazard and risk analysis," Earthquake Engineering Research Institute, Monograph 10, 2004.

[27] NISEE Library, Pacific Earthquake Engineering Research Center, University of California, Berkeley, [Online]. Available: http://nisee2.berkeley.edu/.

[28] PEER Ground Motion Database, Pacific Earthquake Engineering Research Center, University of California, Berkeley, [Online]. Available: http://peer.berkeley.edu/peer_ground_motion_database/.

[29] PSHA Interactive Deaggregation Tool, U.S. Geological Survey, [Online]. Available: https://geohazards.usgs.gov/deaggint/2008/documentation.php.

[30] J. Proulx, et.al., "An experimental investigation of water level effects on the dynamic behavior of a large arch dam," *Earthquake Engineering and Structural Dynamics,* vol. 30, no. 8, pp. 1147-1166, 2001.

[31] D. Rea, C.-Y. Liaw and A. K. Chopra, "Mathematical models for the dynamic analysis of concrete gravity dams," *Earthquake Engineering and Structural Dynamics,* vol. 3, no. 3, pp. 249-258, 1975.

[32] E. Rosenblueth, "Presión hidrodynamica en presas debida a al acceleratión vertical con refracción en el fondo," in *2nd Congreso National de Ingenieriá Sismica*, Veracruz, Mexico, 1968.

[33] US Army Corps of Engineers, "Earthquake design and evaluation of concrete hydraulic structures," *Engineering Manual 1110-2-6053,* 2007.

[34] A. S. Veletsos, "Dynamics of structure-foundation systems," in *Structural and Geotechnical Mechanics*, W.J. Hall, Prentice-Hall, Clifton, New Jersey, 1977.

NOTATION

The following symbols have been used in this report:

PART A

$a_g^l(t)$	l-component of free field ground acceleration
$A(T)$	pseudo-acceleration ordinate at period T
$A_g^l(\omega)$	Fourier transform of $a_g^l(t)$, defined in Equation (2.3.2)
$\mathbf{c}_c$	damping matrix for the finite element system
C	velocity of pressure waves in water
d	duration of free-field ground motion
$E_f, E_s,$	Young's modulus of elasticity of foundation rock and dam concrete, respectively
g	acceleration due to gravity
H	depth of impounded water
H_s	height of upstream face of dam
$I_{0n}(\omega)$	integral defined in Equation (2.2.18a)
$I_{jn}(\omega)$	integral defined in Equation (2.2.18b)
J	number of generalized coordinates
$\tilde{M}_1$	integral defined in Equation (7.1.2)
$\mathbf{k}, \mathbf{k}_b, \mathbf{k}_{bb}$	submatrices of $\mathbf{k}_c$
$\mathbf{k}_c$	stiffness matrix for the finite element system
l	= x and y denotes horizontal and vertical components of ground motion
$\mathbf{m}, \mathbf{m}_b$	submatrices of $\mathbf{m}_c$
$\mathbf{m}_c$	mass matrix for the finite element system
M_w	moment magnitude of earthquake
N	number of nodal points above the base
N_b	number of nodal points at the base
$p(x, y, t)$	hydrodynamic pressure in the impounded water
$\overline{p}^l(x, y, \omega)$	frequency response function for $p(x, y, t)$ due to l-component of ground motion
$\overline{p}_0^l(x, y, \omega)$	frequency response function for hydrodynamic pressure with a rigid dam due to the l-component of ground motion
$\overline{p}_j^f(x, y, \omega)$	frequency response function defined in Equation (2.2.17c) for the upstream face of the dam
q	admittance (= damping) coefficient for the reservoir bottom materials
$\overline{\mathbf{q}}_h(\omega)$	vector of frequency response functions for displacement at the reservoir bottom
$\overline{\mathbf{Q}}_0^l(\omega)$	vector of nodal forces at the reservoir bottom statically equivalent to $-\overline{p}_0^l(x, 0, \omega)$
$\mathbf{Q}_h(t)$	vector of hydrodynamic forces at the reservoir bottom
$\overline{\mathbf{Q}}_h(\omega)$	vector of frequency response functions for $\mathbf{Q}_h(t)$
$\overline{\mathbf{Q}}_j^f(\omega)$	vector of nodal forces at the reservoir bottom statically equivalent to $-\overline{p}_j^f(x, 0, \omega)$
$\overline{\mathbf{r}}^l(\omega)$	vector of frequency response functions for displacements of nodal points above the base due to the l-component of ground motion
$\overline{\mathbf{r}}_b^l(\omega)$	vector of frequency response functions for displacements of nodal points at the base due to the l-component of ground motion

$\mathbf{r}_c(t)$	vector of nodal point displacements relative to free field ground displacements
$\bar{\mathbf{r}}_c^l(\omega)$	vector of frequency response functions for $\mathbf{r}_c(t)$ due to the *l*-component of ground motion
$\bar{\mathbf{r}}_f(\omega)$	vector of frequency response functions for displacements of nodal points at the surface of the foundation region underlying the dam
R	fault distance to earthquake
$\bar{\mathbf{R}}_0^l(\omega)$	vector of nodal forces at the upstream face of the dam statically equivalent to $\bar{p}_0^l(0, y, \omega)$
$\mathbf{R}_b(t)$	vector of forces at the base of the dam due to dam-foundation rock interaction
$\bar{\mathbf{R}}_b^l(\omega)$	vector of frequency response functions for $\mathbf{R}_b(t)$ due to the *l*-component of ground motion
$\mathbf{R}_c(t)$	vector containing hydrodynamic forces $\mathbf{R}_h(t)$ and dam-foundation interaction forces $\mathbf{R}_b(t)$
$\bar{\mathbf{R}}_c^l(\omega)$	vector of frequency response functions for $\mathbf{R}_c(t)$ due to the *l*-component of ground motion
$\bar{\mathbf{R}}_f(\omega)$	vector of frequency response functions for forces at the surface of the foundation region underlying the dam
$\mathbf{R}_h(t)$	vector of hydrodynamic forces at the upstream face of the dam
$\bar{\mathbf{R}}_h^l(\omega)$	vector of frequency response functions for $\mathbf{R}_h(t)$ due to the *l*-component of ground motion
$\bar{\mathbf{R}}_j^f(\omega)$	vector of nodal forces at the upstream face of the dam statically equivalent to $\bar{p}_j^f(0, y, \omega)$
$\underline{\mathbf{S}}(\omega)$	matrix defined in Equation (2.2.3)
$\mathbf{S}_f(\omega)$	dynamic stiffness matrix for the foundation region defined in Equation (2.2.4b)
$\tilde{\mathbf{S}}_f(\omega)$	matrix defined in Equation (2.2.15)
$\underline{\mathbf{S}}_{rr,rq,qq}$	submatrices of $\underline{\mathbf{S}}(\omega)$
$\mathbf{S}(\omega)$	matrix whose elements are defined in Equation (2.2.14a)
$\tilde{\mathbf{S}}(\omega)$	matrix whose elements are defined in Equation (2.2.21a)
t	time
$T_1, \tilde{T}_1$	fundamental vibration periods of the dam alone on a rigid foundation and the dam with impounded water on flexible foundation, respectively
$V_{s,30}$	shear wave velocity of upper 30 meters in soil at site
w_f, w_s	unit weight of concrete and foundation rock, respectively
x, y	coordinates along the breadth and height of the dam, respectively
$Z_j(t)$	generalized coordinate corresponding to the j^{th} Ritz vector
$\bar{Z}_j^l(\omega)$	frequency response function for $Z_j(t)$ due to the *l*-component of ground motion
$\bar{\mathbf{Z}}^l(\omega)$	vector whose elements are $\bar{Z}_j^l(\omega)$
α	$=(1-qC)/(1+qC)$, wave reflection coefficient for the reservoir bottom materials
δ_{nj}	Kronecker delta function
η_f, η_s	constant hysteretic damping factor for foundation rock and dam concrete, respectively
λ_n	vibration frequency for the n^{th} mode of the associated dam-foundation system
$\mu_n(\omega)$	eigenvalue for the n^{th} vibration mode for the impounded water
ρ	density of the impounded water
σ_d	peak value of maximum principal stress
$\Upsilon_n(y, \omega)$	eigenfunction for the n^{th} vibration mode for the impounded water
$\boldsymbol{\chi}_n$	vector defined in Equation (2.2.12)
$\psi_n(y)$	continuous function analogue to the x-DOF elements in $\boldsymbol{\psi}_n^f$
$\boldsymbol{\psi}_n$	n^{th} Ritz vector of the associated dam-foundation system
$\boldsymbol{\psi}_{bn}$	subvector of $\boldsymbol{\psi}_n$ corresponding to the nodal points at the base of the dam
$\boldsymbol{\psi}_n^f$	subvector of $\boldsymbol{\psi}_n$ corresponding to the nodal points at the upstream face of the dam
ω	harmonic excitation frequency

$\mathbf{1}_c^l$	influence vector for the *l*-component of ground motion
$\mathbf{1}^l, \mathbf{1}_b^l$	subvectors of $\mathbf{1}_c^l$ corresponding to nodal points above the base and at the base, respectively

PART B

$A\left(\tilde{T}_1, \tilde{\zeta}_1\right)$	pseudo-acceleration spectrum ordinate evaluated at natural period $\tilde{T}_1$ and damping ratio $\tilde{\zeta}_1$
A_p	integral of $2gp(\hat{y})/wH$ over depth of the impounded water for $H/H_s = 1$ as listed in Table E.5
a_g	peak ground acceleration
B_1	defined in Equation (7.2.2)
C	velocity of pressure waves in water
$E_f, E_s,$	Young's modulus of elasticity of foundation rock and dam concrete, respectively
F_{st}	$=½wH^2$, hydrostatic pressure
$f_1(y)$	equivalent static lateral forces acting on the upstream face of the dam due to the fundamental mode of vibration, as defined in Equation (7.1.1)
$f_{st}(y)$	equivalent static lateral forces acting on the upstream face of the dam due to higher modes of vibration, as defined in Equation (7.2.1)
g	acceleration due to gravity
H	depth of impounded water
H_s	height of upstream face of dam
L_1	generalized earthquake force coefficient, defined in Equation (7.1.5)
$\tilde{L}_1$	integral defined in Equation (7.1.3)
M_1	generalized mass of dam, defined in Equation (7.1.4)
$\tilde{M}_1$	integral defined in Equation (7.1.2)
$p\left(y, \tilde{T}_r\right)$	real-valued component of the complex-valued function representing the hydrodynamic pressure on the upstream face due to harmonic acceleration at period $\tilde{T}_r$ in the shape of the fundamental mode
$p_0(y)$	hydrodynamic pressure on a rigid dam with water compressibility neglected
R_f	period lengthening ratio due to dam-foundation interaction
R_r	period lengthening ratio due to dam-water interaction
R_w	$=T_1^r / \tilde{T}_r$
r_1	response due to earthquake forces associated with the fundamental mode of vibration
r_{max}	peak earthquake response of the dam including initial static effects
r_{sc}	response due to earthquake forces associated with the higher modes of vibration
r_{st}	response due to initial static effects
T_1	fundamental vibration period of dam on rigid foundation with empty reservoir given by Equation (8.1.1)
$\tilde{T}_1$	fundamental resonant period of dam on flexible foundation with impounded water given by Equation (7.1.8)
T_1^r	$=4H/C$, fundamental vibration period of impounded water
$\tilde{T}_f$	fundamental resonant period of dam on flexible foundation with empty reservoir given by Equation (7.1.7)
$\tilde{T}_r$	fundamental resonant period of dam on rigid foundation with impounded water given by Equation (7.1.6)
t	time
w	unit weight of water
$w_s(y)$	weight of dam per unit height

x, y	coordinates along the breadth and height of the dam, respectively
$\hat{y}$	$= y / H$
α	wave reflection coefficient for reservoir bottom materials
$\tilde{\Gamma}_1$	$= \tilde{L}_1 / \tilde{M}_1$
$\phi_1(y)$	fundamental vibration mode shape of dam at upstream face
η_f	constant hysteretic damping factor for foundation rock
ζ_1	damping ratio of dam on rigid foundation with empty reservoir
$\tilde{\zeta}_1$	damping ratio for dam on flexible foundation with impounded water
$\tilde{\zeta}_f$	added damping due to dam-foundation interaction
$\tilde{\zeta}_r$	added damping due to dam-water interaction
$\sigma_{y,1}$	vertical stress due to earthquake forces associated with the fundamental mode of vibration
$\sigma_{y,d}$	earthquake induced vertical stress
$\sigma_{y,sc}$	vertical stress due to earthquake forces associated with the higher modes of vibration
σ_d	peak value of maximum principal stress

APPENDIX

Appendix A Generation of New Compliance Data

It was shown in Section 2.2.2 that dam-foundation interaction introduces a complex-valued, frequency-dependent dynamic stiffness matrix, $\mathbf{S}_f(\omega)$, for the foundation region in the governing equations of motion. This matrix can be computed from a set of dynamic compliance coefficients determined from solutions of the appropriate boundary value problems for the foundation region.

Presented in this appendix is the procedure for generating the new set of dynamic compliance coefficients that have been implemented in EAGD-84, and was used to generate the new set of standard values characterizing dam-foundation interaction in the RSA procedure. The expressions for computing these compliance coefficients are presented, and for completeness, the procedure for computing the dynamic stiffness matrix from the tabulated compliance data is outlined.

Standard Compliance Data

Analytical expressions and numerical results for the frequency-dependent dynamic flexibility coefficients for a homogeneous, isotropic, linearly viscoelastic half-plane in plane strain or generalized plane stress were presented in Ref. [11]. The dynamic flexibility coefficients were obtained from solutions of two boundary value problems associated with harmonically time-varying stresses that were applied uniformly distributed between two adjacent nodal points of a discretized interaction surface.

The definition of the dynamic flexibility coefficient for a nodal point *m*, at a discretized interaction surface, F_m^{ij}, $i, j = x, y$, is shown in Figure A.1b. For a constant hysteretic solid, the analytical expressions for these coefficients are [11]

$$F_m^{xx}(a_0) = \frac{2a_0^2\zeta^2}{\pi\mu}\int_0^\infty \frac{\sqrt{\beta^2-\zeta a_0^2}\ \sin(\beta/2)\ \cos\left(\left[m-1/2\right]\beta\right)}{\beta\left[4\beta^2\sqrt{(\beta^2-\chi\zeta a_0^2)(\beta^2-\zeta a_0^2)}-(2\beta^2-\zeta a_0^2)^2\right]}d\beta \tag{A.1a}$$

$$F_m^{yy}(a_0) = \frac{2a_0^2\zeta^2}{\pi\mu}\int_0^\infty \frac{\sqrt{\beta^2-\chi\zeta a_0^2}\ \sin(\beta/2)\ \cos\left(\left[m-1/2\right]\beta\right)}{\beta\left[4\beta^2\sqrt{(\beta^2-\chi\zeta a_0^2)(\beta^2-\zeta a_0^2)}-(2\beta^2-\zeta a_0^2)^2\right]}d\beta \tag{A.1b}$$

$$F_m^{xy}(a_0) = \frac{2\zeta}{\pi\mu}\int_0^{\infty} \frac{\left[-2\sqrt{(\beta^2-\chi\zeta a_0^2)(\beta^2-\zeta a_0^2)}+2\beta^2-\zeta a_0^2\right]\ \sin(\beta/2)\ \sin\left([m-1/2]\beta\right)}{4\beta^2\sqrt{(\beta^2-\chi\zeta a_0^2)(\beta^2-\zeta a_0^2)}-(2\beta^2-\zeta a_0^2)^2} d\beta \tag{A.1c}$$

$$F_m^{yx}(a_0) = -F_m^{xy}(a_0) \tag{A.1d}$$

where β is a dimensionless Fourier parameter; μ is the shear modulus for the foundation rock; $\zeta = (1+i\eta_f)^{-1}$, where η_f is the constant hysteretic damping factor for the foundation rock; a_0 is a dimensionless frequency parameter:

$$a_0 = \frac{\omega b}{C_s} \tag{A.2}$$

where b is the spacing between the nodal points and C_s is the velocity of shear waves in the rock; and χ is

$$\chi = \frac{(1-2\nu)}{2(1-\nu)} \tag{A.3}$$

where ν is the Poisson's ratio for the foundation rock.

The coefficients F_m^{ij} in Equation A.1 can be expressed in terms of the two real-valued coefficients f_m^{ij} and g_m^{ij} as

$$F_m^{ij}(a_0) = \frac{1}{\mu}\left[f_m^{ij}(a_0) + i g_m^{ij}(a_0)\right] \tag{A.4}$$

For a constant hysteretic solid in plane stress or plane strain, the coefficients f_m^{ij} and g_m^{ij} are only dependent on the Poisson's ratio ν and constant hysteretic damping factor η_f for the foundation rock, and the dimensionless frequency parameter a_0. They can therefore be conveniently tabulated for general cases, as was done in Ref. [11] for a limited number of η_f values.

From the expressions in Equation A.1, a complete set of compliance data, expressed in terms of the coefficients f_m^{ij} and g_m^{ij}, has now been computed using modern integration algorithms for a closely spaced set of η_f values, in particular η_f = 0.01, 0.02 0.03, 0.04, 0.05, 0.06, 0.07, 0.08, 0.09, 0.10, 0.12, 0.14, 0.16, 0.18, 0.20, 0.25, and 0.50. From these dynamic compliance coefficients, the dynamic stiffness matrix $\mathbf{S}_f(\omega)$ can easily be computed for any given excitation frequency ω by the procedure described in the next section.

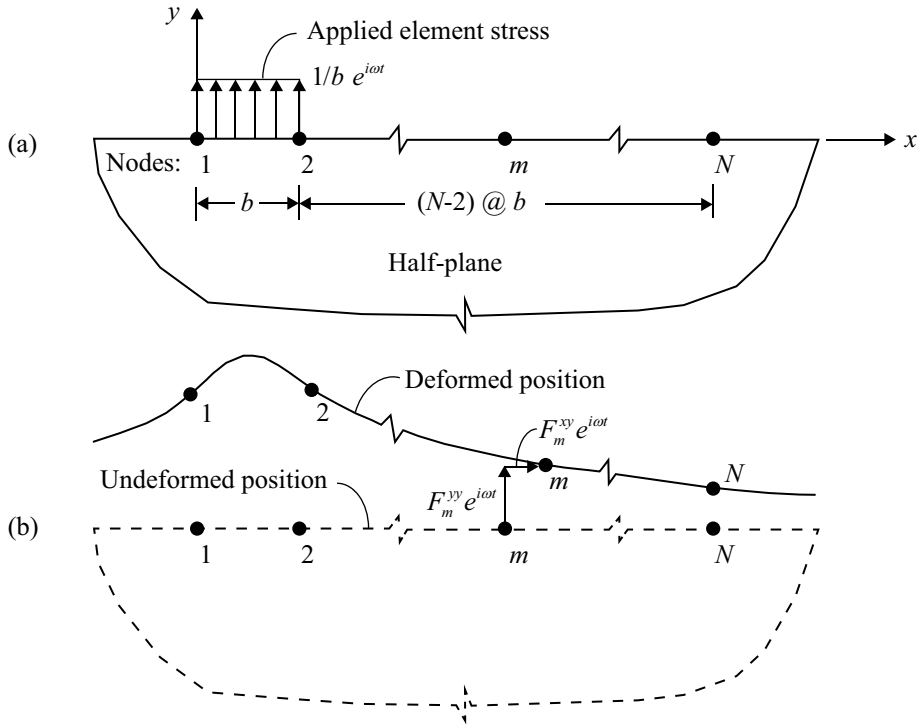

Figure A.1 (a) Vertically applied element load; (b) definition of the dynamic flexibility coefficient F_m^{ij}.

The new set of compliance data was compiled and implemented in the computer program EAGD-84. It was also used to compute the new set of standard values characterizing dam-foundation interaction in the RSA procedure, which has been implemented in the computer program CADAM.

Computing the Dynamic Stiffness Matrix

The dynamic flexibility matrix $\mathbf{F}(\omega)$, relating the complex amplitude of the interaction forces $\overline{\mathbf{P}}_l = e^{i\omega t}$ on each element l to the corresponding complex amplitude displacements $\overline{\mathbf{r}}_m$ [†] at every nodal point m along the interaction surface, can be expressed as

$$\begin{Bmatrix} \overline{\mathbf{r}}_1 \\ \overline{\mathbf{r}}_2 \\ \overline{\mathbf{r}}_3 \\ \dots \\ \dots \\ \overline{\mathbf{r}}_N \end{Bmatrix} = \begin{bmatrix} \mathbf{F}_1 & \mathbf{F}_3^T & \mathbf{F}_4^T & \dots & \mathbf{F}_N^T \\ \mathbf{F}_2 & \mathbf{F}_1 & \mathbf{F}_3^T & \dots & \mathbf{F}_{N-1}^T \\ \dots & \dots & \dots & \dots & \dots \\ \mathbf{F}_{N-1} & \mathbf{F}_{N-2} & \mathbf{F}_{N-3} & \dots & \mathbf{F}_1 \\ \mathbf{F}_N & \mathbf{F}_{N-1} & \mathbf{F}_{N-2} & \dots & \mathbf{F}_2 \end{bmatrix} \begin{Bmatrix} \overline{\mathbf{P}}_1 \\ \overline{\mathbf{P}}_2 \\ \overline{\mathbf{P}}_3 \\ \dots \\ \overline{\mathbf{P}}_{N-1} \end{Bmatrix} \tag{A.5}$$

where $\overline{\mathbf{r}}_m$ and $\overline{\mathbf{P}}_l$ are 2x1 vectors containing the components along the x and y axis; and

$$\mathbf{F}_m = \begin{bmatrix} F_m^{xx} & F_m^{xy} \\ F_m^{yx} & F_m^{yy} \end{bmatrix} \tag{A.6}$$

where m denotes the nodal number relative to the element with prescribed stresses (Figure A.1).

The symmetry of the system implies that the nodal displacements due to prescribed stresses at element l are symmetric about the center of the element, i.e., $\mathbf{F}_{-m} = \mathbf{F}_m^T$. This identity was utilized when setting up the matrix $\mathbf{F}(\omega)$ in Equation (A.5), resulting in the sub-matrices above the main diagonal being transposed matrices.

The precise relationship between the displacements at midpoint of an element to the displacements at the two nodes at its ends will vary with the excitation frequency ω. However, a reasonable approximation can be made by assuming linear variation of the displacements over each element along the base of the structure, leading to the relationship

$$\overline{\mathbf{p}}_l = \frac{1}{2}\left(\overline{\mathbf{r}}_l + \overline{\mathbf{r}}_{l+1}\right) \tag{A.7}$$

where $\overline{\mathbf{p}}_l$ is the 2x1 complex-valued displacement vector at the center of element l. Combining this relationship for all the elements at the interaction surface yields the definition of the transformation matrix **D**:

$$\overline{\mathbf{p}} = \mathbf{D}\overline{\mathbf{r}} \tag{A.8}$$

[†] Note that the subscript *f*, used in Chapter 2 to denote the displacements $\mathbf{r}_f$ along the base of the dam, has been dropped in this section for convenience.

By the definition of the dynamic stiffness matrix and the principal of virtual work, it can be shown [11] that the dynamic stiffness matrix can then be determined from

$$\mathbf{S}_f(\omega) = \mathbf{D}^T \left[\mathbf{D} \cdot \mathbf{F}(\omega)\right]^{-1} \mathbf{D} \tag{A.9}$$

Recalling that $\mathbf{F}(\omega)$ is known in terms of the dynamic flexibility coefficients, and **D** is a simple displacement transformation matrix, Equation (A.9) provides a convenient means for determining $\mathbf{S}_f(\omega)$ from the dynamic flexibility coefficients f_m^{ij} and g_m^{ij}, which were computed for a wide range of damping parameters in the previous section.

Appendix B Conditional Mean Spectrum

Probabilistic seismic hazard analysis (PSHA) has become a widely used framework for determining the seismic hazard at a given site. Contrary to taking a deterministic approach, PSHA considers a multitude of earthquake occurrences and ground motions, and produces an integrated description of seismic hazard representing all events [26]. From this hazard description a target spectrum can be generated, and predictions of structural response can be obtained by selecting records to be consistent with the target, and using those ground motions as input to a dynamic analysis.

The Conditional Mean Spectrum (CMS) has been presented as an appropriate tool for selecting ground motions as input to dynamic analysis [2]. The CMS provides the expected response spectrum, conditioned on occurrence of a target spectral acceleration value at a certain period of interest, i.e., it answers the question: "what is the expected response spectrum associated with a target $A(T)$?" Conveniently, the CMS can be computed using parameters easily be obtained from PSHA.

Computing the CMS can be summarized in four steps [2]:

Step 1: Determine the target $A(T^*)$ at a given period, and the associated M, R and ε

A target pseudo-acceleration value A at a period of interest T^* must first be defined. It is also necessary to determine the magnitude, M, distance R, and $\varepsilon(T^*)$ values associated with $A(T^*)$, where $\varepsilon(T)$ denotes the number of standard deviations from the median predicted $\ln A$:

$$\varepsilon(T) = \frac{\ln A(T) - \mu_{\ln A}(M, R, T)}{\sigma_{\ln A}(T)} \tag{B.1}$$

where $\mu_{\ln A}(M, R, T)$ and $\sigma_{\ln A}(T)$ are the predicted mean and standard deviation, respectively, of $\ln A$ at a given period.

If the target $A(T^*)$ value is obtained from PSHA, these values can be taken as the mean M, R and $\varepsilon(T^*)$ from the deagreggation of the seismic hazard at the site; such information is available from online tools [29].

Step 2: Compute the mean and standard deviation of the response spectrum, given M and R.

The mean and standard deviation of $\ln A$ at all periods, for the target M, R, etc. is determined using existing ground motion models; several online calculation tools exist to aid in obtaining these values.

Step 3: Compute ε at other periods, given $\varepsilon(T^*)$

The conditional mean ε at other periods can be shown to be equal to $\varepsilon(T^*)$, multiplied by the correlation coefficient between the ε values at the two periods:

$$\mu_{\varepsilon(T_i)|\varepsilon(T^*)} = \rho(T_i, T^*)\varepsilon(T^*) \tag{B.2}$$

where $\mu_{\varepsilon(T_i)|\varepsilon(T^*)}$ denotes the mean value of $\varepsilon(T_i)$ given $\varepsilon(T^*)$. Predictions of the required correlation coefficient, $\rho(T_i, T^*)$, have been pre-calculated in previous studies, so users of this procedure can obtain the needed correlations using a simple predictive equation.

Step 4: Compute the Conditional Mean Spectrum

The CMS can now be computed using the mean and standard deviation from Step 2 and the conditional mean ε values from Step 3. Substituting the mean value of $\varepsilon(T_i)$ from Equation (B.2) into Equation (B.1) and solving for $\ln A(T)$ produces the corresponding conditional mean value of $\ln A(T_i)$, given $\ln A(T^*)$:

$$\mu_{\ln A(T_i)|\ln A(T^*)} = \mu_{\ln A}(M, R, T) + \rho(T_i, T^*)\varepsilon(T^*)\sigma_{\ln A}(T_i) \tag{B.3}$$

Taking the exponential of Equation (B.3) for many periods gives the final CMS.

It is apparent that the CMS can be computed using relatively simple formulas and available statistical correlation coefficients, but it requires ground motion predictions (Step 2) which are cumbersome to compute by hand. As mentioned however, several ground motion prediction models have been incorporated into online tools, and some of these tools have been extended to also perform the complete calculation of the CMS. The two CMS that are shown in Figure 4.2.1 of this report was computed by the USGS Seismic Deaggregation Tool [29], implementing the procedure described above.

Once the CMS is computed, it can be used to select ground motions for use in dynamic analysis. The CMS provides the mean spectral shape associated with the target $A(T^*)$, so ground motions that match that target spectral shape can be treated as representative of ground motions that naturally have the target $A(T^*)$ value. This was utilized in the selection and scaling process for the ground motions used in the analysis in Chapter 4.

It is assumed in the above procedure that the earthquake intensity is measured by $A(T^*)$, i.e., spectral acceleration at a single period. This intensity measure (IM) is a perfect predictor of structural response for elastic single-degree-of-freedom systems with natural period T, and for multi-degree-of-freedom systems the period T is often chosen as the

fundamental period of vibration. On the other hand, for systems where the structural response (and thus the spectral acceleration) at several periods are of special interest, the IM can be extended to average spectral acceleration values over a range of periods; such a procedure has been presented in Ref. [3].

For the analysis of the coupled dam-water-foundation system in Chapter 4, the fundamental resonant period changes depending on which interaction effects are included in the analysis. Based on the above discussion, the single target CMS used to select ground motions for the analysis should therefore, in a strict sense, have been computed for an intensity measure that averages spectral acceleration values over the period range of interest. However, since the two periods who bound the period range for the analyses in Chapter 4 are very close, it is apparent that implementing this procedure will provide little extra value, especially considering that a CMS computed by this procedure will be bounded by the two CMS in Figure 4.2.1, shown to be very similar. It was therefore decided to compute the target spectrum as the geometric mean of the two CMS shown in Figure 4.2.1.

Appendix C Detailed Calculations for Pine Flat Dam

This appendix presents details of the calculations required in the RSA procedure to determine the equivalent lateral earthquake forces and earthquake induced stresses in Pine Flat Dam that were presented in Chapter 10.

Simplified Block Model of Dam Monolith

The simplified model of the tallest, non-overflow cross-section of Pine Flat Dam is shown in Figure C.1.1. The cross-section is divided into 10 blocks of equal height of 40 ft.; the properties of each of the blocks are presented in Table C.1.1. The total weight of the dam in the simplified block model is 9486 kips, and the modal parameters L_1 and M_1 are computed by replacing the integrals in Equations (7.1.4) and (7.1.5) by their respective summations over all the blocks, which yields L_1 = (1390 kips) / g and M_1 = (500 kips) / g.

Table C.1 Properties of each block in the simplified model.

Block	Weight, w, kips	Elevation of centroid, ft.	ϕ_1 at centroid	$w\phi_1$, kips	$w\phi_1^2$, kips
1	202.8	379.9	0.865	175.4	151.8
2	267.3	338.5	0.612	163.7	100.2
3	417.7	298.6	0.450	188.1	84.7
4	610.8	258.9	0.331	202.3	67.0
5	816.7	219.2	0.238	194.6	46.4
6	1022.5	179.3	0.164	167.7	27.5
7	1228.3	139.4	0.107	131.8	14.2
8	1434.2	99.5	0.065	92.6	6.0
9	1640.0	59.6	0.034	55.3	1.9
10	1845.9	19.6	0.010	18.1	0.2
Total	9486			1390	500

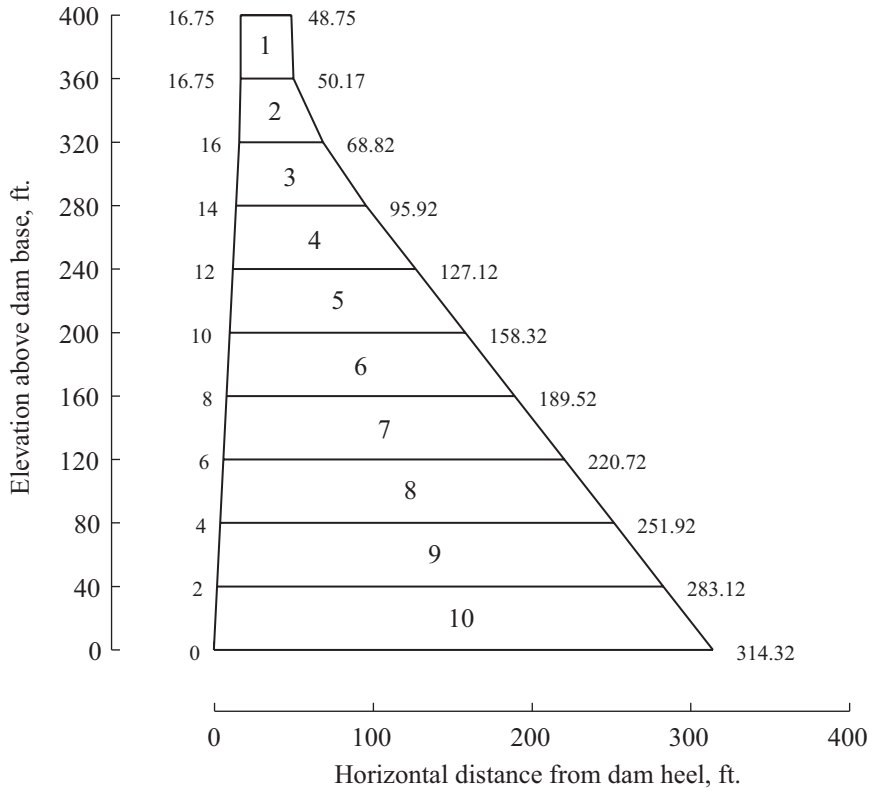

Figure C.1 Coordinates of simplified block model.

Computation of Equivalent Static Lateral Forces

The equivalent static lateral forces associated with the fundamental mode, f_1, and higher modes, f_{sc}, are computed by implementing the step-by-step procedure described in Chapter 9. The details of the computational steps are summarized in this section.

1. For $E_s = 3.25$ million psi and $H_s = 400$ ft., T_1 is computed from Equation (8.1.1) as $T_1 = (1.4)(400)/\sqrt{3.25 \cdot 10^6} = 0.311$ sec.

2. For $E_s = 3.25$ million psi, $\alpha = 0.75$ and $H / H_s = 381/400 = 0.95$, Table E.2(b) gives $R_r = 1.246$ (linearly interpolated between values for $E_s = 3.0$ million psi and $E_s = 3.5$ million psi), so $\tilde{T}_r = (1.240)(0.311) = 0.387$ sec.

3. The fundamental vibration period for the impounded water is $T_1^r = 4H/C = 4(381)/4720 = 0.323$ sec, Equation (8.4.1) then gives $R_w = 0.323/0.387 = 0.83$.

4. For $E_f / E_s = 1$, Table E.3 gives $R_f = 1.187$, leading to $\tilde{T}_1 = (1.187)(0.311) = 0.369$ sec for Case 3, and $\tilde{T}_1 = (1.187)(0.387) = 0.459$ sec for Case 4.

5. For Cases 2 and 4, Table E.2(b) gives $\zeta_r = 0.023$ for $E_s = 3.25$ million psi (interpolated), $\alpha = 0.75$, and $H / H_s = 0.95$. For Cases 3 and 4, $\zeta_f = 0.059$ from Table E.3 for $E_f / E_s = 1$ and $\eta_f = 0.04$. With $\zeta_1 = 0.02$, Equation (7.1.9) then gives:

$\tilde{\zeta}_1 = 0.02/1.246 + 0.023 = 0.039$ for Case 2; $\tilde{\zeta}_1 = 0.02/(1.187)^3 + 0.059 = 0.071$ for Case 3; and $\tilde{\zeta}_1 = 0.02/[(1.24)(1.187)^3] + 0.023 + 0.059 = 0.092$ for Case 4.

6. The values of $gp(y)$ presented in Table C.1.3 at eleven equally spaced levels were obtained from Table E.4(c) for $R_w = 0.83$ (by linearly interpolating between the data for the two closest values for which data are available, $R_w = 0.80$ and $R_w = 0.90$) and $\alpha = 0.75$, and multiplied by $(0.0624)(381)(.95)^2 = 21.6$ k/ft.

7. Evaluating Equation (7.1.4) in discrete form gives $M_1 = (500\,\text{kip})/g$. From Equation (8.5.1), $\tilde{M}_1 = (1.246)^2(1/g)(500) = (776\,\text{kip})/g$.

8. Evaluating equation (7.1.5) in discrete form gives $L_1 = (1390\,\text{kip})/g$. From Table E.5(b), $A_p = 0.327$ for $\alpha = 0.75$ and $R_w = 0.83$ (interpolated). Equation (8.5.2) then gives $\tilde{L}_1 = 1390/g + (1/g)(4529)(0.95)^2(0.327) = (2732\,\text{kip})/g$. Consequently, for Cases 1 and 3, $\tilde{\Gamma}_1 = L_1/M_1 = 1390/500 = 2.78$, and for Cases 2 and 4, $\tilde{\Gamma}_1 = \tilde{L}_1/\tilde{M}_1 = 2732/776 = 3.52$.

9. For each of the four cases listed in Table C.1.2, Equation (7.1.1) was evaluated at eleven equally spaced intervals along the height of the dam, including the top and bottom, by substituting values for $\tilde{\Gamma}_1 = \tilde{L}_1/\tilde{M}_1$ and $gp(y)$ computed in the preceding steps; computing the weight of the dam per unit height $w_s(y)$ from the monolith dimensions shown in Figure C.1.1 and the unit weight of concrete; and substituting $\phi_1(y)$ from Table E.1 and the pseudo-acceleration ordinate $A(\tilde{T}_1, \tilde{\zeta}_1)$ from the median pseudo-acceleration response spectrum in Figure 6.2.1 corresponding to the $\tilde{T}_1$ and $\tilde{\zeta}_1$ computed in Steps 4 and 5. The resulting equivalent static lateral forces $f_1(y)$ are presented in Table C.1.4 for each case, with intermediate values shown in Table C.1.3.

10. The vertical stresses $\sigma_{y,1}$ due to the response of the dam in its fundamental mode are computed by a static stress analysis of the dam subjected to the equivalent static lateral forces $f_1(y)$ from Step 9 applied to the upstream face of the dam. A summary of the static stress analysis is presented in the next subsection.

11. For each of the four cases, Equation (7.2.1) was evaluated at eleven equally spaced intervals along the height of the dam, including the top and bottom, by substituting numerical values for the quantities computed in the preceding steps; obtaining $gp_0(y)$ from Table E.6; using Equation (7.2.2) to compute $B_1 = (0.20)(4529/g)(0.95)^2 = (817.5\text{kip})/g$, which yields $B_1/M_1 = 817.5/500 = 1.64$; and substituting $a_g = 0.232$ g. The resulting equivalent static lateral forces $f_{sc}(y)$ are presented in Table C.1.4 for each case, with intermediate values shown in Table C.1.3.

12. The vertical stresses $\sigma_{y,sc}$ due to the response of the dam in all higher modes are computed by a static stress analysis of the dam subjected to the equivalent static lateral forces $f_{sc}(y)$ from Step 11 applied to the upstream face of the dam. A summary of the static stress analysis is presented in the next subsection.

13. Computation of the earthquake induced vertical stresses $\sigma_{y,d}$ is done by combining the response quantities $\sigma_{y,1}$ and $\sigma_{y,sc}$ computed in Steps 10 and 12 by the SRSS combination rule; this is described in a later subsection.

Table C.2 Analysis cases, fundamental mode properties and pseudo-acceleration values.

Analysis Case	Foundation	Water	$\tilde{\Gamma}_1 = \tilde{L}_1/\tilde{M}_1$	$\tilde{T}_1$, in sec	$\tilde{\xi}_1$, in percent	$A(\tilde{T}_1, \tilde{\xi}_1)$, in g
1	Rigid	Empty	2.78	0.311	2.0	0.606
2	Rigid	Full	3.52	0.387	3.9	0.409
3	Flexible	Empty	2.78	0.369	7.1	0.347
4	Flexible	Full	3.52	0.459	9.2	0.274

Table C.3 Intermediate values for calculation of equivalent static lateral forces.

y, ft.	w_s, k/ft.	ϕ_1	$w_s\phi_1$, k/ft.	$w_s[1-(L_1/M_1)\phi_1]$, k/ft.	gp, k/ft.	gp_0 k/ft.	$gp_0-(B_1/M_1)w_s\phi_1$, k/ft.
400	4.96	1.000	4.96	-8.83	0	0	-8.16
360	5.18	0.735	3.81	-5.41	1.75	3.47	-2.79
320	8.19	0.530	4.34	-3.88	3.16	7.45	0.31
280	12.7	0.389	4.94	-1.04	3.73	10.3	2.15
240	17.8	0.284	5.07	3.75	3.94	12.5	4.12
200	23.0	0.200	4.60	10.20	3.99	14.1	6.59
160	28.1	0.135	3.80	17.57	3.94	15.6	9.21
120	33.3	0.084	2.80	25.51	3.87	16.4	11.8
80	38.4	0.047	1.81	33.41	3.76	17.1	14.1
40	43.6	0.021	0.92	41.03	3.69	17.5	16.0
0	48.7	0	0	48.72	3.60	17.6	17.6

Table C.4 Equivalent static lateral forces, in kips/ft., on Pine Flat Dam.

y, ft.	Case 1		Case 2		Case 3		Case 4	
	f_1	f_{sc}	f_1	f_{sc}	f_1	f_{sc}	f_1	f_{sc}
400	8.31	- 2.05	7.02	- 3.94	4.74	- 2.05	4.78	- 3.94
360	6.38	- 1.25	7.86	- 1.90	3.64	- 1.25	5.36	- 1.90
320	7.27	- 0.90	10.6	- 0.83	4.15	- 0.90	7.24	- 0.83
280	8.28	- 0.24	12.3	0.26	4.72	- 0.24	8.36	0.26
240	8.49	0.87	12.8	1.83	4.85	0.87	8.69	1.83
200	7.71	2.37	12.2	3.90	4.40	2.37	8.28	3.90
160	6.37	4.08	11.0	6.21	3.63	4.08	7.47	6.21
120	4.69	5.92	9.44	8.66	2.67	5.92	6.43	8.66
80	3.03	7.75	7.88	11.0	1.73	7.75	5.37	11.0
40	1.53	9.52	6.52	13.2	0.88	9.52	4.44	13.2
0	0.00	11.3	5.10	15.4	0.00	11.3	3.47	15.4

Computation of Vertical Stresses

The vertical stresses $\sigma_{y,1}$ and $\sigma_{y,sc}$ due to each set of equivalent static lateral forces $f_1(y)$ and $f_{sc}(y)$, respectively, are computed by static stress analysis of the dam monolith by two different methods: (1) stresses at both faces of the dam are computed by elementary formulas for stresses in beams; and (2) stresses are computed by a finite element analysis.

Selected results are presented in this section for analysis case 4 only, as the computational steps are identical for all the four analysis cases.

Beam Theory

The inertia forces associated with the mass – given by the first term of Equations (7.1.1) and (7.2.1) – are applied at the centroid of each of the 10 blocks shown in Figure C.1.1, and the forces associated with hydrodynamic pressure – given by the second term of the same equations – are applied as a linearly distributed load on the upstream face of each block. The resulting bending moments in the dam monolith are computed at each level from the equilibrium equations, and the normal bending stresses at two faces are computed by elementary beam theory as $\sigma_y = M / S$, where M and S are the bending moment and section modulus, respectively, at the horizontal section considered; these stresses act in the vertical direction. The procedure is implemented in a newly developed computer program similar to the computer program SIMPL described in Appendix D of Ref. [18]. The vertical stresses computed at the two faces of Pine Flat Dam are listed in Table C.1.5 for analysis case 4.

The stresses with their algebraic signs shown in Table C.1.5 will occur on the upstream face of the dam when the earthquake forces act in the downstream direction, and on the downstream face of the dam when the earthquake forces act in the upstream direction. The

stresses on the sloping part of the downstream face are subsequently multiplied by the correction factor of 0.75 developed in Section 9.3.

Table C.5 Vertical stresses $\sigma_{y,1}$ and $\sigma_{y,sc}$ for analysis case 4 computed by elementary beam theory.

		Fundamental mode		Higher modes	
y, ft.	Section modulus, $S = 1/6b^2$, ft^3	Bending moment, k-ft.	Vertical stress at faces, psi	Bending moment, k-ft.	Vertical stress at faces, psi
400	171	0	0	0	0
360	186	3,479	130	-2,579	-96
320	465	15,577	233	-8,632	-129
280	1,118	39,103	243	-16,060	-100
240	2,208	75,854	239	-23,020	-72
200	3,665	126,35	239	-26,978	-51
160	5,490	190,037	240	-24,673	-31
120	7,683	265,64	240	-12,398	-11
80	10,242	351,517	238	13,675	9
40	13,170	446,139	235	57,289	30
0	16,464	547,841	231	122,028	51

Finite Element Method

The forces $f_1(y)$ and $f_{sc}(y)$ are applied as linearly distributed forces to the upstream face of a finite element discretization of the dam, chosen for convenience to be identical to the idealization shown in Figure 4.1.1. Static analysis of the finite element model leads to stresses at the centroid of each element, and a stress recovery procedure is applied in order to obtain stresses at the nodal points. All finite element analyses in the RSA procedure were implemented using the Matlab toolbox FEDEASLab [20].

The resulting vertical stresses $\sigma_{y,1}$ and $\sigma_{y,sc}$, at the nodal points on the two faces of the dam due to earthquake forces applied in the downstream direction are listed in Table C.1.6 for analysis case 4. Applying the forces in the upstream direction reverses the algebraic signs of the stresses; numerical values remain unchanged.

Table C.6 Vertical stresses $\sigma_{y,1}$ and $\sigma_{y,sc}$, in psi, for analysis case 4 computed by finite element analysis.

	Fundamental mode		Higher modes	
Height, *y*, ft.	Vertical stress at u/s face	Vertical stress at d/s face	Vertical stress at u/s face	Vertical stress at d/s face
400	12	-9	-9	7
383	34	-34	-24	25
367	92	-108	-61	71
351	160	-183	-98	110
335	209	-207	-118	111
318	232	-214	-119	100
300	240	-216	-110	88
280	243	-200	-98	69
260	241	-190	-86	54
235	239	-190	-73	42
210	237	-190	-62	30
185	237	-190	-52	18
160	238	-185	-43	4
128	241	-176	-32	-9
96	249	-161	-19	-19
64	264	-140	3	-26
32	290	-118	44	-27
0	306	-107	71	-27

Response Combination

The vertical stress at a location due to earthquake excitation is computed by combining $\sigma_{y,1}$ and $\sigma_{y,sc}$ by the SRSS formula:

$$\sigma_{y,d} = \pm\sqrt{\sigma_{y,1}^2 + \sigma_{y,sc}^2} \tag{C.1}$$

Because the direction of the applied earthquake forces is reversible, these stresses can be either positive (tensile stresses) or negative (compressive stresses).

The earthquake induced vertical stresses for Pine Flat Dam computed by beam theory and the finite element method are shown in Figure 10.2.2, where stresses computed by beam theory on the sloping part of the downstream face have been modified by the correction factor of 0.75.

Principal Stresses: Beam Theory

At the upstream and downstream faces of the dam, principal stresses due to each of the force distributions f_1 and f_{sc} can be determined by a simple transformation of the corresponding vertical stresses determined by beam theory. If the upstream face of the dam is nearly vertical and the effects of tail-water are negligible, this transformation can be written as [18]:

$$\sigma_1 = \sigma_{y,1} \sec^2 \theta \tag{C.2a}$$

$$\sigma_{sc} = \sigma_{y,sc} \sec^2 \theta \tag{C.2b}$$

where θ is the angle of the face with respect to the vertical. Under these restricted conditions the principal stresses are directly proportional to the vertical stresses, and hence also to the modal coordinate, therefore modal combination rules are applicable.

The maximum principal stresses on the two faces of the dam computed by combining σ_1 and σ_{sc} using the SRSS formula are shown in Figure 10.3.1, where the vertical stresses entering the Equation (C.2) are computed by beam theory.

Appendix D User Manual for Pre- and Post-Processing Modules

USER MANUAL

PRE- AND POST-PROCESSING MODULES TO FACILITATE ANALYSIS WITH EAGD-84

Arnkjell Løkke,
Department of Structural Engineering
Norwegian University of Science and Technology

June 2013

PURPOSE

The modules described in this document are meant to be used as an addition to the original EAGD-84 program, providing users with the capabilities of pre-processing input and post-processing output from the program in the Matlab scripting language. They do not offer any new functionality to the computational part of the program EAGD-84.

It is assumed that the user is familiar with the use of EAGD-84. Additionally, the user should be familiar with the Matlab scripting language, in particular with numeric arrays and array operations, and with data structures and cell arrays.

All scripts are provided open-source, so the user can make modifications and/or additions to the code as required.

RUNNING THE PROGRAM

1. To run the GUI: Type GUI_EAGD in the Matlab command window, or open and run the script file GUI_EAGD.m. The use of the GUI should be self-explanatory.
2. To run modules in a script interface, see example files Example1.m or Example2.m.

SYSTEM REQUIREMENTS

All the modules and scripts described in this report have been written and tested in a Windows environment using Matlab release 2012a. The scripts should be compatible with older (and newer) versions of Matlab, but modifications to the code might be necessary for use in other environments. Because the scripts make use of basic Windows functionality, they cannot be used on systems running OS X, Linux or any other non-Windows operating systems.

LIMITATIONS

The application of these modules is first and foremost limited by the extent to which EAGD-84 can be used. For practical reasons, a few additional restrictions have been imposed on the possible user input. These should have little influence on a typical use of the program and are described further in the input data description.

EAGD-84 COMPUTER PROGRAM

EAGD-84 [Fenves and Chopra 1984] is a self-contained computer program that numerically evaluates the response of concrete gravity dams to earthquakes, including the effects of dam-water-foundation interaction, water compressibility and reservoir bottom absorption.

The dam monolith is idealized as a two-dimensional assemblage of planar, four-node non-conforming finite elements. Energy dissipation in the dam concrete is represented by constant hysteretic damping. The water impounded in the reservoir is idealized as a fluid domain of constant depth and infinite length in the upstream direction, and at the reservoir bottom, the absorptiveness of the reservoir bottom materials is characterized by a wave reflection coefficient. If the effects of dam-foundation interaction are to be included, the frequency-dependent dynamic stiffness matrix for the foundation region is defined with respect to the degrees-of-freedom of the nodal points at the dam base, computed from standard compliance data provided with the program. Earthquake excitation is defined by two components of free-field ground acceleration in a cross-sectional plane of the dam: the horizontal component transverse to the dam axis, and the vertical component.

Outputs from the program include hydrostatic loads; nodal point displacements and element stresses due to static loads; natural vibration frequencies and mode shapes of the dam (if the foundation is assumed to be rigid) or of an associated dam-foundation system (if dam-foundation interaction is included); complete response histories for stresses and displacements for each finite element; and the peak maximum and minimum principal stress in each finite element and the times at which they occur. The user is referred to the EAGD-84 user manual [Fenves and Chopra 1984] for additional details regarding the system idealization or description of input/output.

Recently, compliance data for the foundation region have been recomputed for an increased number of base nodal points, a finer range of dimensionless frequencies and a closely spaced set of constant hysteretic damping factors [Løkke and Chopra 2013], in particular η_f = 0.01, 0.02 0.03, 0.04, 0.05, 0.06, 0.07, 0.08, 0.09, 0.10, 0.12, 0.14, 0.16, 0.18, 0.20, 0.25, and 0.50; and NBASE ≤ 16. The new data is now provided with the program, and the source code has been updated to allow for the implementation of the extended data set.

Additionally, the EAGD-84 source code has been compiled to a running Windows executable; this file should work on most Windows computers, including 64-bit versions. The updated source code and the Windows executable can be run independently of the pre-and post-processor modules described in this user manual.

ORGANIZATION OF PRE- AND POST-PROCESSING MODULES

Pre-Processing and Program Execution

Use of the pre-processor scripts is organized in the three steps shown in Figure 1: (1) the user defines all the necessary input parameters; (2) the scripts pre-process the user input to compile a correctly formatted EAGD-84 input file; and (3) EAGD-84 is executed and the output is saved. The input parameters required to run an analysis are described in a later chapter.

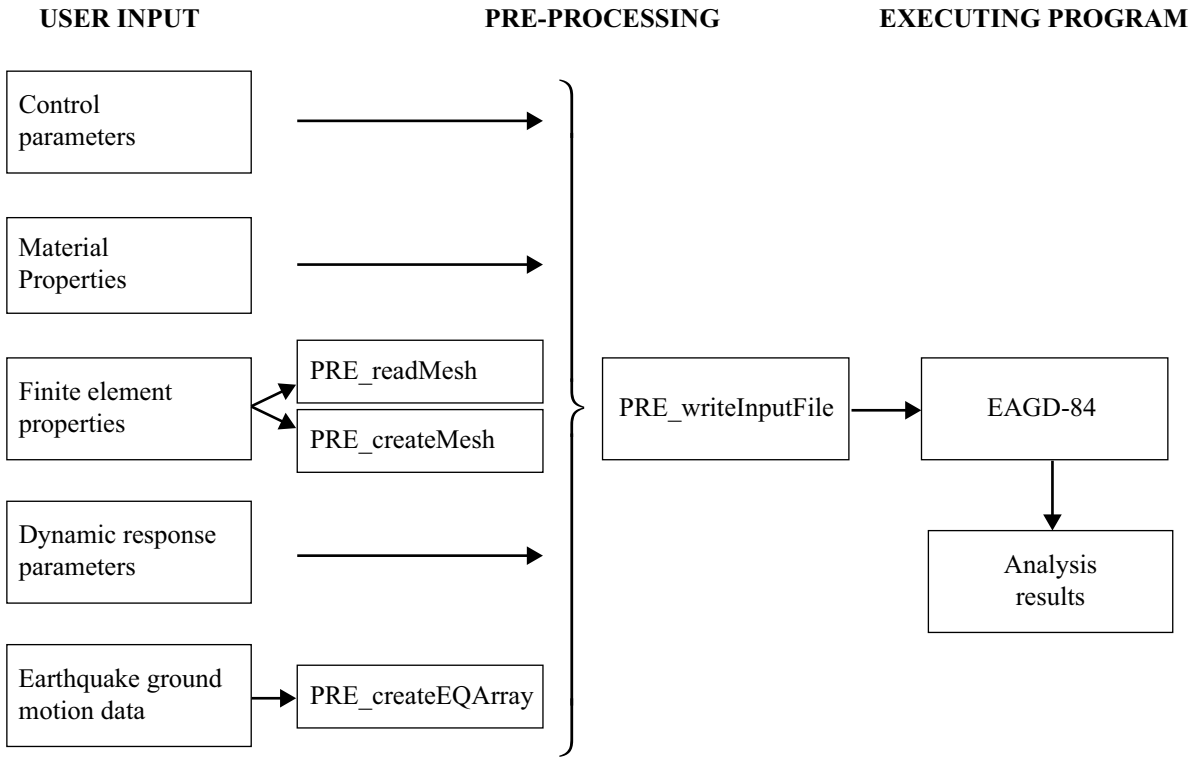

Figure 1 Organization of pre-processing and program execution.

Post-Processing

The output from EAGD-84 is organized in two files: (1) the file 'output', a formatted text file containing the majority of the output; and (2) 'fort.3', an unformatted binary file containing displacements and stresses for every time step in the analysis. This output is read into Matlab workspace by the two functions POST_readOutput and POST_readFort3, and can subsequently be easily accessed for the user to perform post-processing of the results. Figure 2 shows a schematic overview of the post-processing. Note that post-processing can be done independently of the pre-processor; its only requirement is that the two output files from EAGD-84 are present.

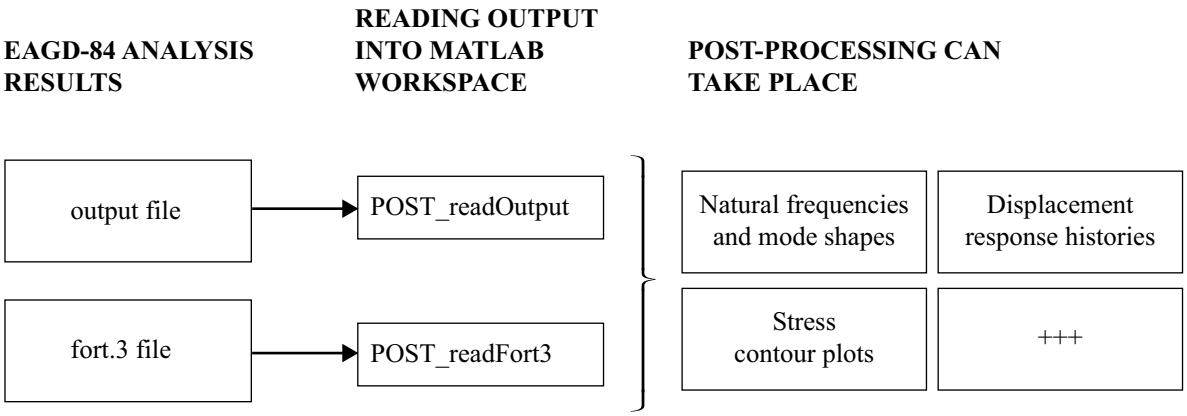

Figure 2 Organization of post-processing.

The majority of the analysis output is stored in the data structure 'Post', the fields comprising this data structure are described in Table 1.

Table 1 Description of fields in data structure 'Post'.

Post.Static	Contains displacements and stresses due to initial static loads, and the hydrostatic load vector.
Post.Vibration	Contains the vibration properties of the system, such as frequencies, mode shapes and frequency response functions.
Post.PrinStrOA	Contains the peak values of the maximum and minimum principal stresses, as well as their time of occurrence.
Post.Stress	Contains the stresses $\sigma_{xx}, \sigma_{yy}, \sigma_{xy}$, as well as the principal stresses σ_1 and σ_2, in each element at every time step of the computed response.
Post.Displacement	Contains the horizontal and vertical displacements of each nodal point at every time step of the computed response.

A set of functions that address basic post-processing tasks are also provided, all the plots presented in the examples in this user manual are generated by these functions.

Table 2 Basic plot functions

Plot_Mesh	Plots the finite element idealization of the dam.
Plot_Disp	Plots the displacement response history for a given DOF.
Plot_Modeshape	Plots the mode shape for a given mode number.
Plot_Contour	Plots stress contours for a given stress distribution. Users can choose between filled contour plot in colors or contour lines in B/W.

Graphical User Interface

To further ease the accessibility of EAGD-84, a self-explanatory graphical user interface (GUI) has been developed (Figure 3). The GUI makes use of the functions described in the previous sections to create an EAGD-84 input file, execute EAGD-84, and perform basic post-processing of the results. An example showing the use of the GUI is presented later.

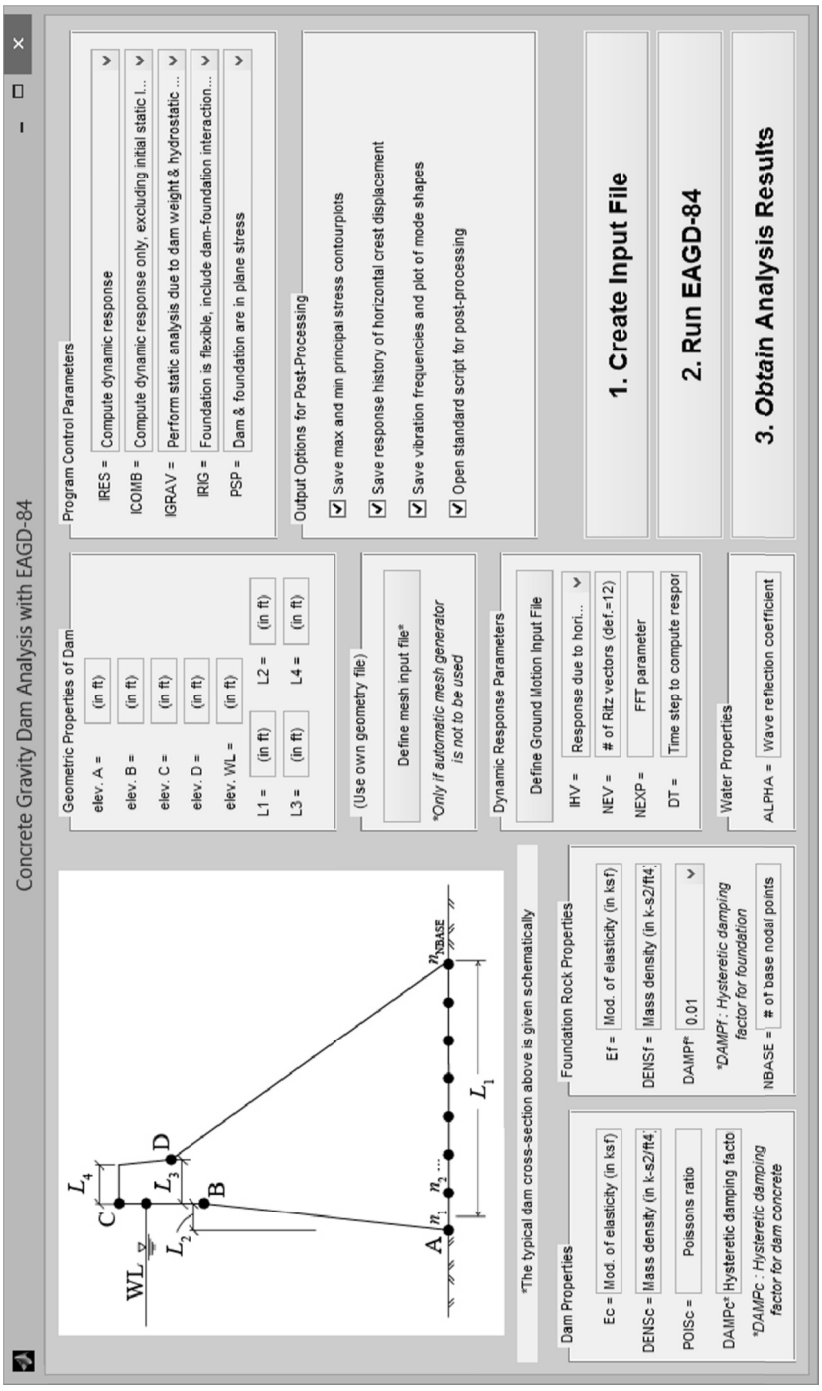

Figure 3 Graphical user interface.

DESCRIPTION OF INPUT DATA

The input data necessary to run the pre-processor scripts are organized in the five categories described in this section. The user is referred to the EAGD-84 user manual for a more thorough description of the input parameters.

Control Parameters

The following input parameters for the control of program execution must be specified:

Table 3 Program control parameters.

IRES	= 0, compute the dynamic response due to earthquake ground motion. = 1, only perform static analysis and compute vibration properties.
ICOMB	= 0, Compute only dynamic response. = 1, Compute dynamic response and combine with response due to the static loads. This will automatically set IGRAV=1.
IGRAV	= 0, do not perform static analysis. = 1, perform static analysis due to weight of the dam and hydrostatic pressure of the impounded water.
IRIG	= 0, foundation rock is flexible, include dam-foundation rock interaction effects. = 1, foundation rock is rigid, exclude dam-foundation rock interaction effects.
PSP	= 0.0, dam and foundation are in generalized plane stress. = 1.0, dam and foundation are in plane strain.

Additionally, a set of control parameters will keep their default value unless they are changed directly in the code for the function PRE_writeInput: IOPR=0; IOPP=1; IGEN=1; ISEL=1; NUMMAT=1; NPRINT=100. The most important implication of this is that only a single material is allowed in the dam discretization.

Material Properties

The following material properties must be specified for the dam, foundation, and water. The user is referred to the EAGD-84 user manual for guidelines on the selection of material input parameters.

Table 4 Material input parameters.

Dam	EC	Young's modulus of elasticity, in ksf, of the dam concrete.
	POISC	Poisson's ratio of the dam concrete.
	DENSC	Mass density, in k-s^2/ft^4, of the dam concrete.
	DAMPC	Constant hysteretic damping factor for the dam concrete.
Foundation	EF	Young's modulus of elasticity, in ksf, of the foundation rock.
	DENSF	Mass density, in k-s^2/ft^4, of the foundation rock.
	DAMPF	Constant hysteretic damping factor for the foundation rock.
Water	ALPHA	Wave reflection coefficient α for the reservoir bottom materials, such as alluvium and sediments.

Finite Element Properties

The user can choose between two options for defining the finite element properties: (1) use the automatic mesh generator PRE_createMesh that idealizes the dam using straight-line segments; or (2) provide a complete definition of the finite element idealization in a separate text file which is read by the function PRE_readMesh.

NOTE: The maximum number of nodal points at the base of the dam, NBASE, that can be selected in the program (if the foundation is assumed flexible) is limited by the maximum number of nodal points for which compliance data is available. With the current data set this is limited to NBASE ≤ 16, selecting a higher value for NBASE may give significantly erroneous results.

(1) Using PRE_createMesh

The function PRE_createMesh automatically generates a finite element idealization of the dam cross section defined by five straight line segments as shown in Figure 4a. The mesh is created top-down, using a constant number of elements along the breadth of the dam. Three examples of finite elements idealizations produced by PRE_createMesh are shown in Figure 4b-d.

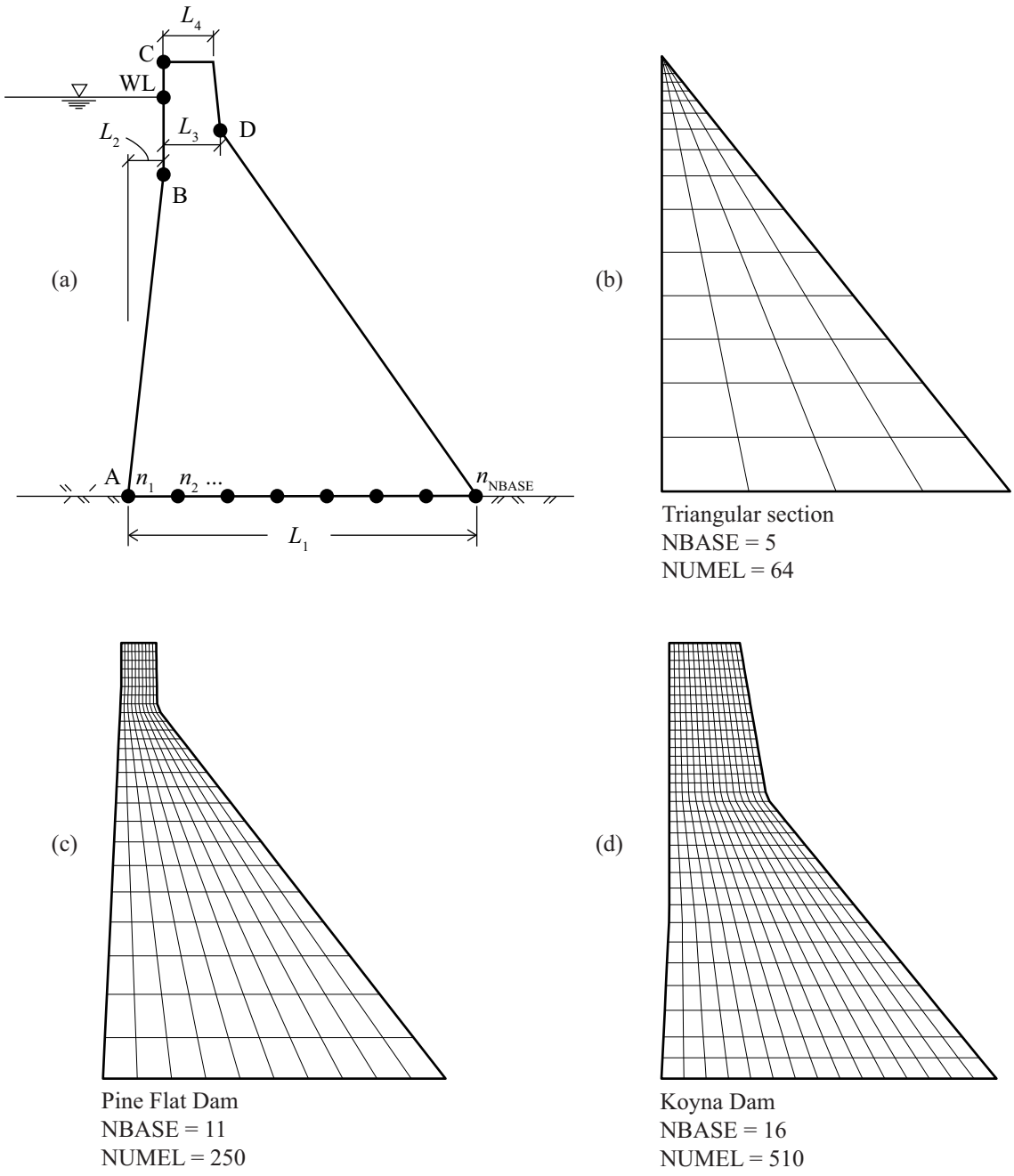

Figure 4 (a) Idealization of dam-cross section using straight-line segments; (b) - (d) examples of finite element idealizations for three different cross sections created by PRE_createMesh.

(2) Using PRE_readMesh

The use of an arbitrary, user-specified, finite element discretization of the dam is administered by the function PRE_readMesh. The following finite element parameters must be specified:

Table 5 Input for function PRE_readMesh.

NUMNP	Number of nodal points in the finite element idealization.
NUMEL	Number of elements in the finite element idealization.
NBASE	Number of nodal points at the dam base, in contact with the foundation. Available compliance data limits NBASE ≤ 16.
Spacing	Spacing, in ft., between the nodal points at the dam base.
WL	Elevation, in ft., of the free-surface of the impounded water.
NPP	Number of nodal points at the upstream face of the dam affected by the impounded water. NPP = 0 indicates an empty reservoir.
fName	File name, including extension, of the text file containing the finite element idealization. Example is 'Meshfile.txt'.

Nodal point coordinates, element definition, water nodal points and base nodal points of the finite element idealization are defined in a separate text file, see Table 6. This file must contain the equivalents of Card Sets E, F, G and H in the EAGD-84 card input (see EAGD-84 user manual). An example of a correct mesh input file is shown in App. A.

Table 6 Contents of mesh input file.

Nodal point coordinates	Defines the boundary condition and the *x*-, and *y*-coordinates, in ft., of every nodal point in the finite element idealization.
Element definition	Defines the element connectivity. Nodal points at each element must be numbered in counterclockwise direction
Water nodal points	Specifies the nodal points at the upstream face of the dam affected by the impounded water. If the free-surface water level is between two nodal points, both nodal points must be included.
Base nodal points	Specifies the nodal points at the base of the dam in contact with the flexible foundation. These nodal points must be equally spaced.

Dynamic Response Parameters

Since EAGD-84 computes dynamic response by use of Fourier transformations, a set of dynamic response parameters must be (carefully) selected:

Table 7 Dynamic response parameters.

NEV	Number of generalized coordinates (i.e. modes) included in the response computation. A general rule is to include all vibration modes that significantly contribute to the dynamic response.
NEXP	Compute the complex frequency response function for the generalized coordinates at N = 2^{NEXP} harmonic excitation frequencies; the response history of the dam is computed at N time intervals.
DT	Time interval, in seconds, for which the response history is computed. Also determines the maximum excitation frequency represented in the response.

The parameter DT determines the maximum excitation frequency F, in Hz, represented in the response:

$$F = \frac{1}{2\mathrm{DT}} \tag{1}$$

To ensure that the program computes accurate dynamic response, this frequency should be (i) greater than the frequencies of all the significant harmonics represented in the ground motion, and (ii) large enough to include the range of frequencies over which the dam has significant dynamic response; the latter criterion is met if $F > f_{\mathrm{NEV}}$, where f_{NEV} is the vibration frequency, in Hz, of the highest vibration mode included in the analysis. The parameters DT and NEXP also need to satisfy the two conditions:

$$\mathrm{DT} \cdot 2^{\mathrm{NEXP}} \geq \frac{1}{f_1} \max\left\{25, \frac{1.5}{\eta_s}\right\} \tag{2}$$

$$\mathrm{DT} \cdot 2^{\mathrm{NEXP}} \geq \mathrm{DUR} \tag{3}$$

where f_1 is the fundamental vibration period, in Hz, of the dam-foundation rock system; η_s is the constant hysteretic damping factor of the dam concrete; and DUR is the duration of response history computation determined by the earthquake ground motion data (see Table 8).

The user is referred to the EAGD-84 user manual for a more comprehensive discussion of the selection of dynamic response parameters.

Earthquake Ground Motion Data

The horizontal and vertical components of earthquake ground motions are read and converted into the correct EAGD-84 format by the function PRE_createEQArray. The following ground motion parameters must be defined:

Table 8 Earthquake ground motion parameters.

IHV	= 0, Compute response due to the horizontal component, only, of the ground motion. = 1, Compute response due to the vertical component, only, of the ground motion. = 2, Compute response due to the horizontal and vertical components, simultaneously, of the ground motion.
NUMREC	Number of ordinates in the ground motion record(s). The number of ordinates must be the same for both horizontal and vertical ground motion records.
dt	Time step of the ground motion record(s). The time step must be constant and the same for both horizontal and vertical ground motion records. Together, dt and NUMREC determines duration of response history computation: $DUR = NUMREC \cdot dt$.
SFAC	Scale factor for ground motion records. The scale factor must be the same for both horizontal and vertical ground motion records.
hName	File name, including extension, of the horizontal ground motion file. Example input is 'horzacc.txt'.
hNumHead	Number of header lines (rows containing non-acceleration values) in the horizontal ground motion record.
vName	File name, including extension, of the vertical ground motion file. Example input is 'vertacc.txt'.
vNumHead	Number of header lines (rows containing non-acceleration values) in the vertical ground motion record.

The acceleration files must contain acceleration values *only* (i.e. any time intervals must not be present in the file), and the acceleration values must be in units of g (acceleration due to gravity) and have a constant time step. An example of a correct acceleration file is shown in Figure 5, downloaded from the PEER Ground Motion Database. Note that the acceleration file is not limited to having any specific number of columns, i.e., even a file containing a single vector of acceleration values can be used.

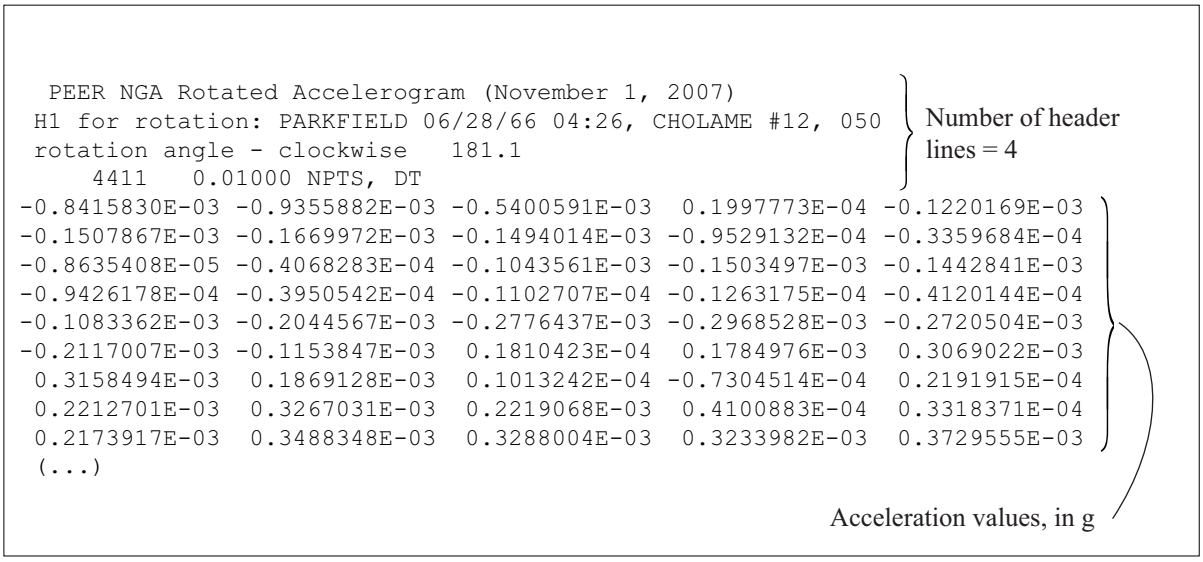

Figure 5 Example of acceleration input file.

EXAMPLES

Example 1: Using Scripts to Analyze Idealized Dam

The following example presents the necessary steps for performing a dynamic analysis of an idealized concrete gravity dam cross-section subjected to the horizontal component of Taft ground motion by using the modules directly in a Matlab script file.

The script file shown in Figure 7 is used to create the EAGD-84 input file, execute the program, and load all output into the Matlab workspace. This file contains all the necessary input for the program to run. The mesh generated by the automatic mesh generator is shown in Figure 6.

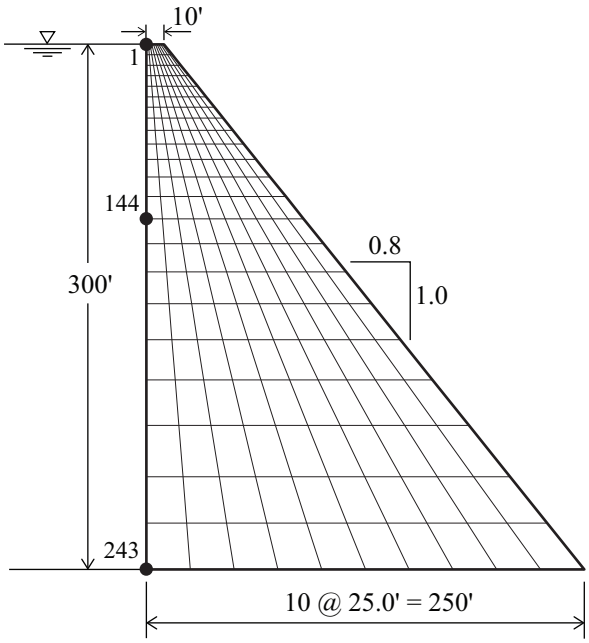

Figure 6 Mesh for idealized dam generated by PRE_createMesh, consisting of 220 (22 x 10) quadrilateral four-node elements.

```
%-------------------------------------------------------------------------%
% EXAMPLE 1: DYNAMIC ANALYSIS OF IDEALIZED CROSS SECTION
%-------------------------------------------------------------------------%
clc; clear all; close all

%% DEFINE INPUT

% 1. Define control parameters
IRES=0; ICOMB=0; IGRAV=0; IRIG=0; PSP=0.0;

% 2. Define material properties
EC=5.76e5; DENSC=4.8e-3; POISC=0.20; DAMPC=0.04; % Dam
EF=5.76e5; DENSF=5.1e-3;             DAMPF=0.04; % Foundation
ALPHA=0.75;                                      % Water

% 3. Define FE geometry using automatic mesh-generator
L1=250; L2=0; L3=10; L4=10;                        % lengths, in ft
elA=0; elB=300; elC=300; elD=300; elWL=300;        % elevations, in ft
NBASE=11;
ft=1.0;                                            % Conversion factor to ft

% 4 Define dynamic response parameters
NEV=12; NEXP=12; DT=0.01;

% 5. Define EQ ground motion data
IHV=0; NUMREC=3000; dt=0.01; SFAC=1;
hName='Taft_horz.txt'; hNumHead=1;

%% CREATE INPUT FILE

% Create finite element idealization
[COORD Element WL Spacing NUMNP NUMEL NBASE,
 NPP WatNodes BaseNodes] = PRE_createMesh(L1,L2,L3,L4, ...
 elA,elB,elC,elD,elWL,NBASE,ft);

% Create earthquake array
[EQArrayH EQArrayV] = PRE_createEQArray(IHV, NUMREC, dt, SFAC, hName, hNumHead);

% Create input file
PRE_writeInput(IRES,ICOMB,IGRAV,IRIG,PSP,EC,POISC,DENSC,DAMPC, ...
 EF,DENSF,DAMPF,ALPHA,NUMNP,NUMEL,NBASE,Spacing,WL,NPP,COORD,Element, ...
 WatNodes,BaseNodes,NEV,NEXP,DT,IHV,NUMREC,dt,EQArrayH,EQArrayV);

%% RUN EAGD-84
RUN_E1A

%% READ OUTPUT TO WORKSPACE
clear all;

% Read output file
[NUMNP NUMEL NBASE COORD Element Post] = POST_readOutput;

% Read fort.3 file
[NUMNP NUMEL Post] = POST_readFort3(Post);
```

Figure 7 Matlab script file to create input file, run EAGD-84, and read output data into the Matlab workspace.

Once the script file has been run and the output data is read into the Matlab workspace, results can easily be accessed and post-processed using the utility functions (Table 2) provided with the post-processor scripts, in addition to available built-in Matlab utility functions. A few examples of such post-processing of the program output are presented below,

- The first four mode shapes, including the corresponding vibration periods, of the dam on flexible foundation are plotted in Figure 8.
- The horizontal and vertical displacements, relative to the free-field ground motion, at three levels on the upstream face of the dam (nodal points 1, 144 and 243, see Figure 6) due to the horizontal component of Taft ground motion are shown in Figure 9.
- The distribution of envelope values of the maximum principal stresses in the dam, excluding stresses due to static loads, is plotted in Figure 10.

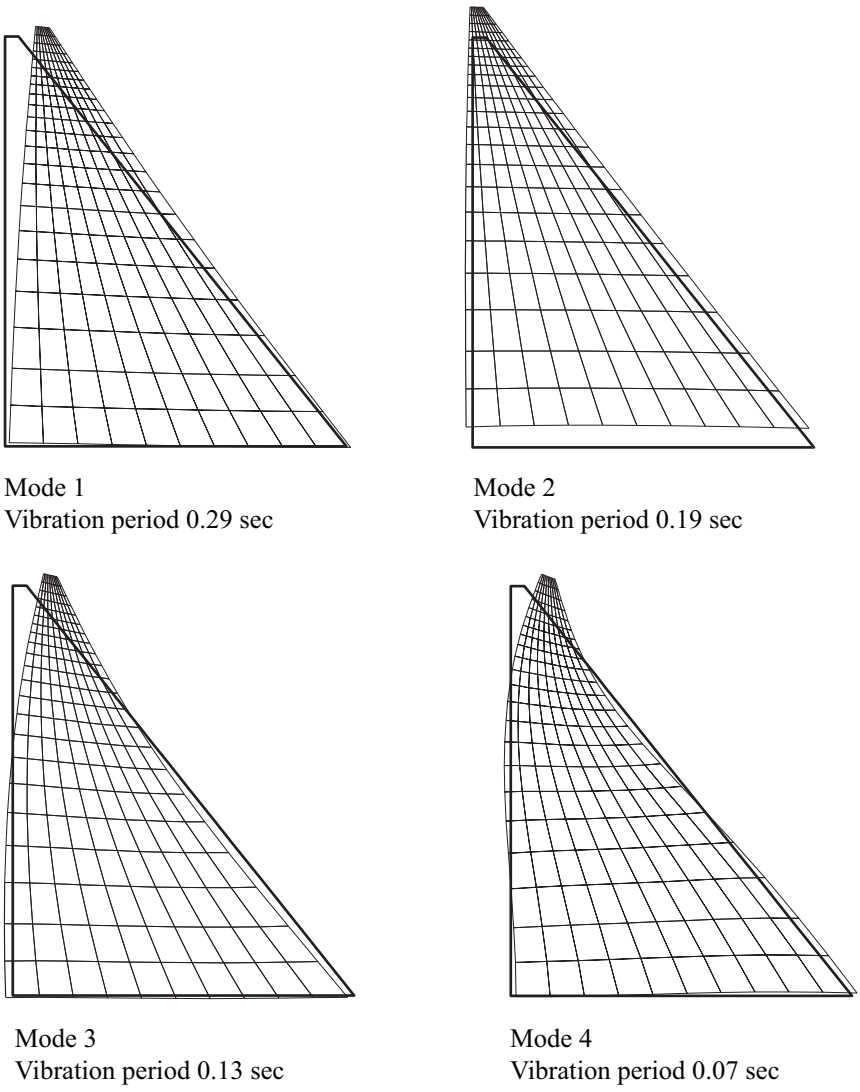

Figure 8 First four vibration modes for the associated dam-foundation system.

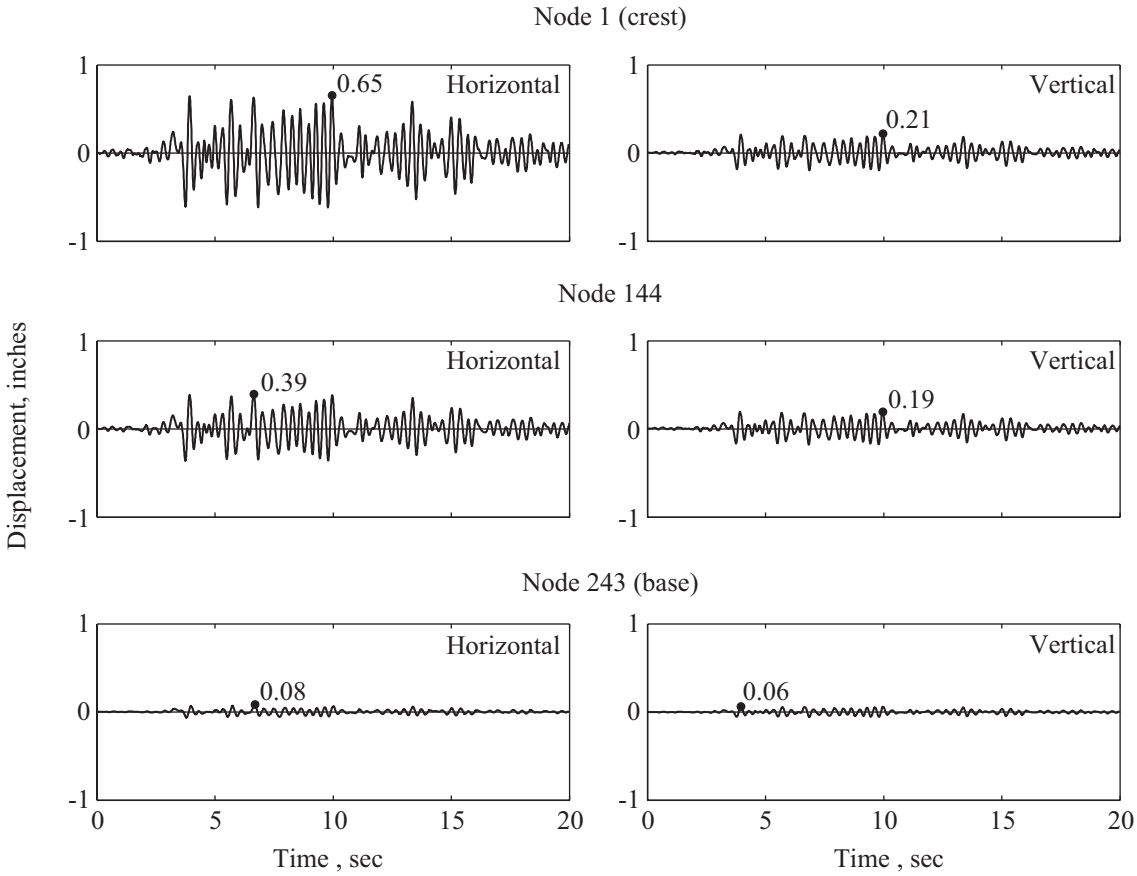

Figure 9 Displacement response histories for nodal points 1, 144 and 243.

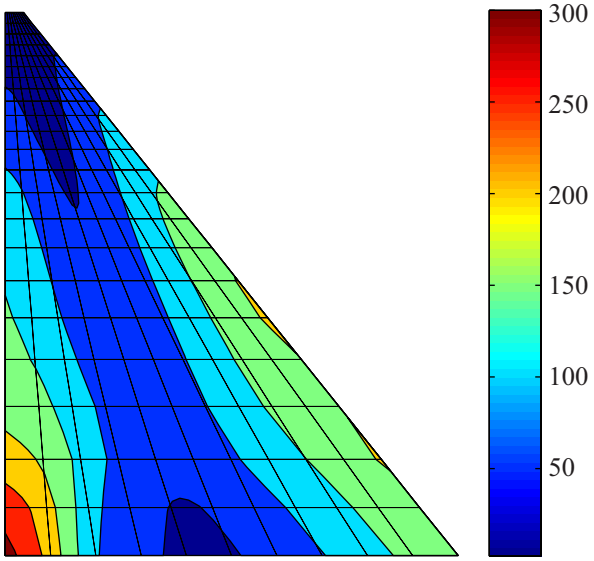

Figure 10 Filled contour plot showing envelope values of maximum principal stresses; initial static stresses are excluded.

Example 2: Using GUI to Analyze Pine Flat Dam

The following example shows how the GUI can be used to perform a dynamic analysis of Pine Flat Dam subjected to the horizontal and vertical components of Taft ground motion, simultaneously. The mesh used in the analysis is produced by the automatic mesh generator and is shown in Figure 4c. The input parameters are chosen to be the same as the example analysis presented in Fenves and Chopra (1984).

Figure 12 shows the GUI with the input parameters for Pine Flat Dam, units are in ft., ksf, and k-s^2/ft^4. The earthquake ground motion parameters and the names of the files containing acceleration values are defined in the separate window shown in Figure 11. These two windows define all input parameters necessary to run the analysis.

The GUI is run in three steps: (1) the EAGD-84 input file is created, (2) EAGD-84 is executed, and (3) the results from EAGD-84 are read into the Matlab workspace and post-processed. The response histories for horizontal and vertical displacement of nodes 1, 166 and 276, corresponding to locations at the crest, at 2/3 height, and at the base of the dam, respectively, are plotted in Figure 13; the envelope of the maximum principal stresses in the dam over the duration of the ground motion is plotted in Figure 14.

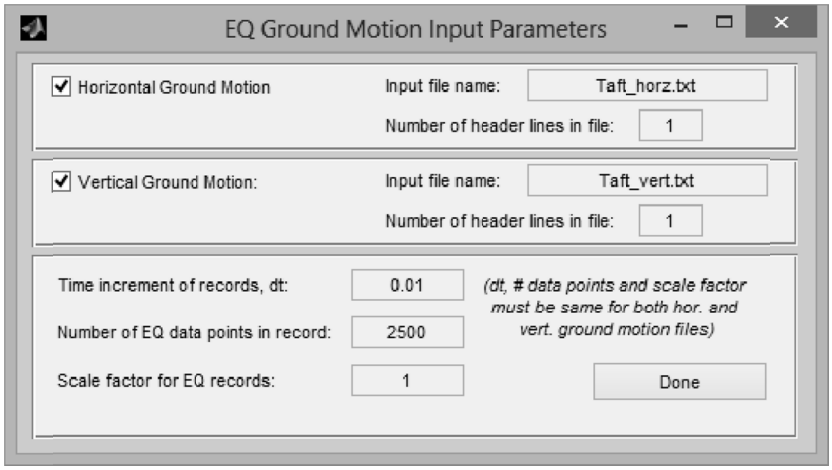

Figure 11 Window for defining earthquake ground motion in GUI.

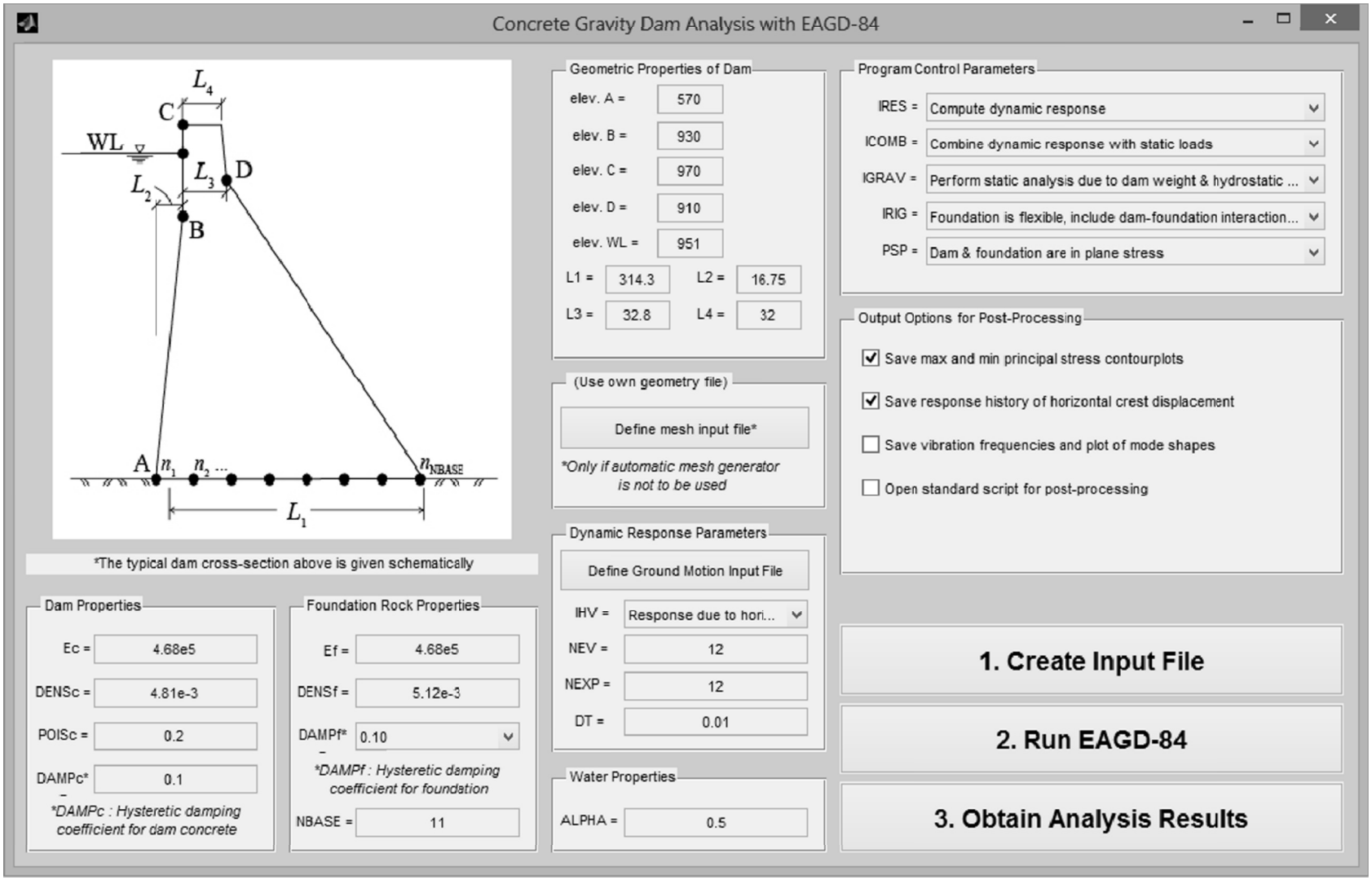

Figure 12 Main user window with input for Pine Flat Dam.

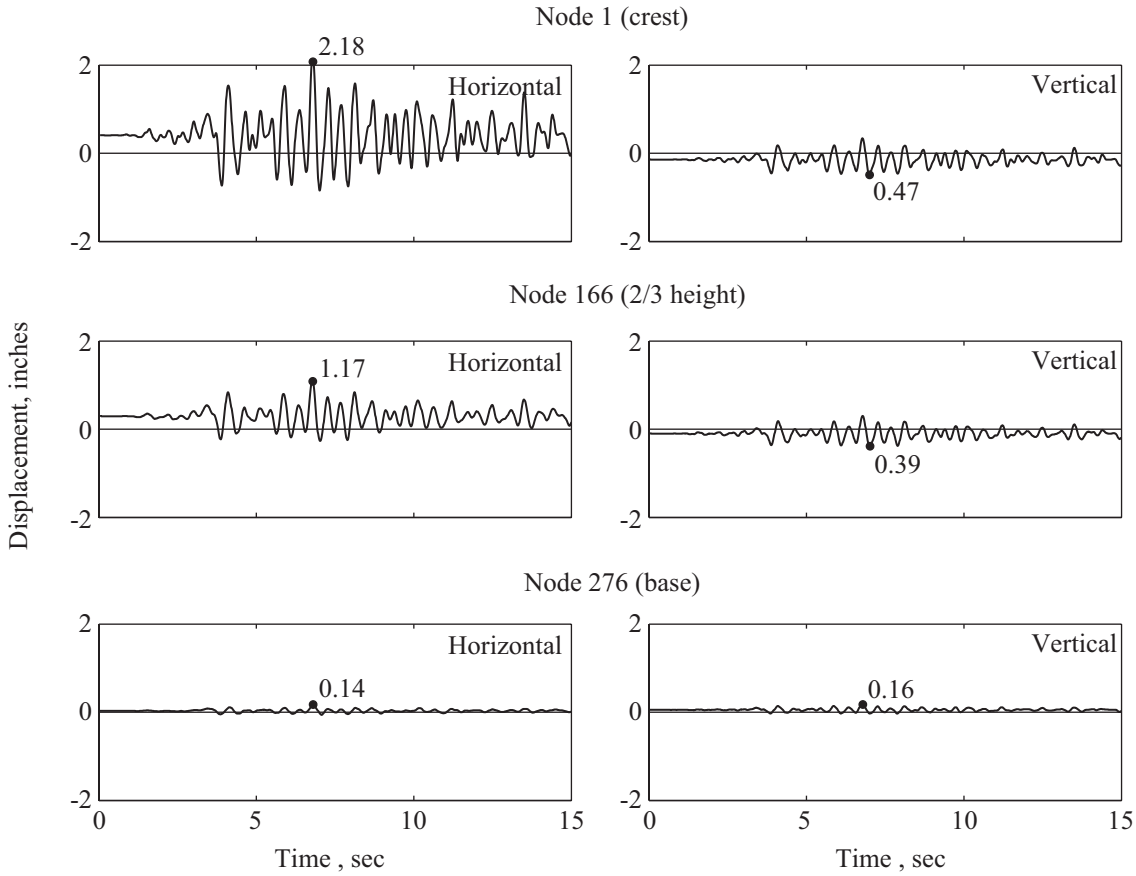

Figure 13 Displacement response of Pine Flat Dam due to horizontal and vertical components, simultaneously, of Taft ground motion; initial static displacements are included.

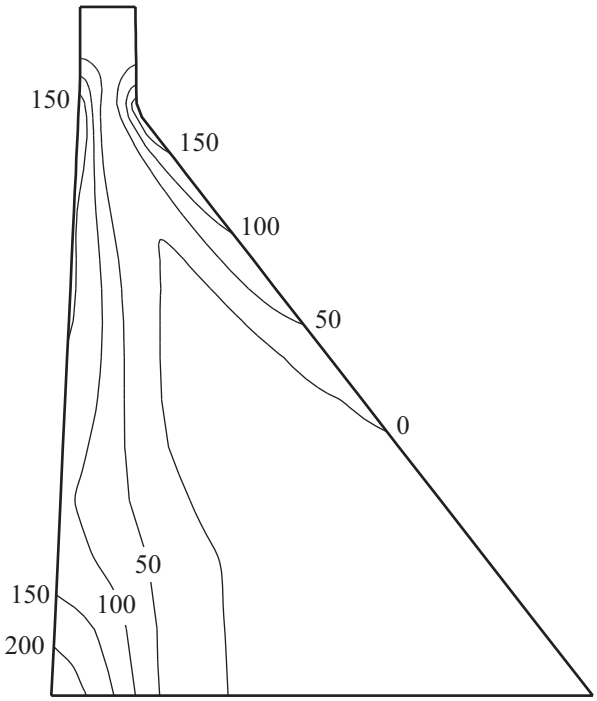

Figure 14 B/W contour plot showing envelope values of maximum principal stresses, in psi, in Pine Flat Dam due to horizontal and vertical components, simultaneously, of Taft ground motion; initial static stresses are included.

By comparing the results presented in Figures 13 and 14 with the results presented in Fenves and Chopra (1984), it is apparent – as expected – that the results are essentially identical except for minor differences due to small variances in the mesh used to compute the results.

REFERENCES

Fenves, G., and A.K. Chopra (1984). EAGD-84: A computer program for earthquake response analysis of concrete gravity dams, *Report No. UCB/EERC-84/11,* Earthquake Engineering Research Center, University of California, Berkeley, Calif., 78 pgs.

Løkke, A. and A. K. Chopra, Response spectrum analysis of concrete gravity dams including dam-water-foundation interaction, *Submitted for publication,* Pacific Earthquake Engineering Research Center, University of California, Berkeley, 2013.

APP. 1: EXAMPLE OF MESH INPUT FILE

```
      1      0.00    16.750   400.000
      2      0.00    20.750   400.000
      3      0.00    24.750   400.000
      4      0.00    28.750   400.000
      5      0.00    32.750   400.000
      6      0.00    36.750   400.000
      7      0.00    40.750   400.000
      8      0.00    44.750   400.000
      9      0.00    48.750   400.000
     10      0.00    16.750   383.000
     11      0.00    20.750   383.000

(...)

    152      0.00   253.390    32.000
    153      0.00   289.360    32.000
    154      0.00     0.000    -0.000
    155      0.00    39.290    -0.000
    156      0.00    78.580    -0.000
    157      0.00   117.870    -0.000
    158      0.00   157.160    -0.000
    159      0.00   196.450    -0.000
    160      0.00   235.740    -0.000
    161      0.00   275.030    -0.000
    162      0.00   314.320    -0.000
```

Definition of nodal points

```
    1       1    10    11     2          1
    2       2    11    12     3          1
    3       3    12    13     4          1
    4       4    13    14     5          1
    5       5    14    15     6          1
    6       6    15    16     7          1
    7       7    16    17     8          1
    8       8    17    18     9          1
    9      10    19    20    11          1
   10      11    20    21    12          1

(...)

  126     141   150   151   142          1
  127     142   151   152   143          1
  128     143   152   153   144          1
  129     145   154   155   146          1
  130     146   155   156   147          1
  131     147   156   157   148          1
  132     148   157   158   149          1
  133     149   158   159   150          1
  134     150   159   160   151          1
  135     151   160   161   152          1
  136     152   161   162   153          1
  10   19   28   37   46   55   64   73   82   91  100  109  118  127  136
  145  154
  154  155  156  157  158  159  160  161  162
```

Definition of element connectivity

Definition of nodal points in contact with water

Definition of nodal points at the dam base

Figure A1 Example (excerpts) of correct mesh input file. In this file: NUMNP=162; NUMEL=136; NBASE=9; Spacing=39.29; WL=381.0; NPP=17.

Appendix E Tables for Standard Values Used in Response Spectrum Analysis Procedure

Table E.1 Standard fundamental mode shape $\phi_1(y)$ for concrete gravity dams.

y/H_s	$\phi_1(y)$
1.0	1.000
0.95	.866
0.90	.735
0.85	.619
0.80	.530
0.75	.455
0.70	.389
0.65	.334
0.60	.284
0.55	.240
0.50	.200
0.45	.165
0.40	.135
0.35	.108
0.30	.084
0.25	.065
0.20	.047
0.15	.034
0.10	.021
0.05	.010
0	0

Table E.2(a) Standard values for R_r and ζ_r, the period lengthening ratio and added damping ratio due to hydrodynamic effects for modulus of elasticity of concrete, E_s = 5 and 4.5 million psi.

H/H_s	α	E_s = 5 million psi		E_s = 4.5 million psi	
		R_r	ζ_r	R_r	ζ_r
1.0	1.0	1.454	0	1.409	0
	0.90	1.462	.043	1.416	.030
	0.75	1.456	.060	1.412	.051
	0.50	1.355	.067	1.344	.060
	0.25	1.284	.054	1.285	.050
	0	1.261	.038	1.259	.036
0.95	1.0	1.368	0	1.323	0
	0.90	1.376	.044	1.330	.031
	0.75	1.366	.056	1.323	.049
	0.50	1.255	.060	1.256	.053
	0.25	1.208	.045	1.208	.042
	0	1.192	.032	1.191	.030
0.90	1.0	1.289	0	1.247	0
	0.90	1.297	.041	1.253	.029
	0.75	1.284	.050	1.247	.042
	0.50	1.181	.050	1.185	.044
	0.25	1.151	.036	1.152	.033
	0	1.139	.025	1.139	.023
0.85	1.0	1.215	0	1.179	0
	0.90	1.224	.033	1.185	.023
	0.75	1.206	.042	1.177	.034
	0.50	1.129	.039	1.131	.033
	0.25	1.111	.027	1.109	.025
	0	1.100	.019	1.099	.018
0.80	1.0	1.148	0	1.121	0
	0.90	1.156	.024	1.126	.015
	0.75	1.140	.032	1.121	.024
	0.50	1.092	.028	1.092	.024
	0.25	1.078	.019	1.078	.018
	0	1.071	.014	1.071	.013
0.75	1.0	1.092	0	1.078	0
	0.90	1.099	.014	1.080	.008
	0.75	1.089	.021	1.078	.014
	0.50	1.065	.018	1.064	.015
	0.25	1.055	.013	1.055	.012
	0	1.049	.009	1.050	.009

Table E.2(a) – continued.

		E_s = 5 million psi		E_s = 4.5 million psi	
H/H_s	α	R_r	ζ_r	R_r	ζ_r
0.70	1.0	1.055	0	1.048	0
	0.90	1.057	.006	1.050	.003
	0.75	1.055	.011	1.050	.007
	0.50	1.045	.011	1.044	.009
	0.25	1.038	.009	1.037	.008
	0	1.034	.006	1.035	.006
0.65	1.0	1.033	0	1.031	0
	0.90	1.034	.002	1.031	.001
	0.75	1.034	.005	1.031	.003
	0.50	1.030	.006	1.029	.005
	0.25	1.026	.005	1.027	.005
	0	1.024	.004	1.025	.004
0.60	1.0	1.020	0	1.020	0
	0.90	1.020	.001	1.020	.001
	0.75	1.020	.002	1.020	.001
	0.50	1.019	.003	1.018	.003
	0.25	1.017	.003	1.018	.003
	0	1.016	.003	1.016	.002
0.55	1.0	1.013	0	1.012	0
	0.90	1.013	.000	1.012	.000
	0.75	1.013	.001	1.012	.001
	0.50	1.013	.002	1.012	.001
	0.25	1.012	.002	1.012	.002
	0	1.011	.002	1.012	.001
0.50	1.0	1.009	0	1.008	0
	0.90	1.009	.000	1.008	.000
	0.75	1.009	.000	1.008	.000
	0.50	1.008	.001	1.008	.001
	0.25	1.008	.001	1.008	.001
	0	1.008	.001	1.008	.001

Table E.2(b) Standard values for R_r and ζ_r, the period lengthening ratio and added damping ratio due to hydrodynamic effects for modulus of elasticity of concrete, E_s = 4, 3.5 and 3 million psi.

		E_s = 4 million psi		E_s = 3.5 million psi		E_s = 3 million psi	
H/H_s	α	R_r	ζ_r	R_r	ζ_r	R_r	ζ_r
1.0	1.0	1.370	0	1.341	0	1.320	0
	0.90	1.374	.021	1.344	.013	1.319	.008
	0.75	1.374	.040	1.341	.029	1.312	.021
	0.50	1.333	.051	1.316	.042	1.289	.035
	0.25	1.285	.045	1.282	.040	1.264	.036
	0	1.259	.034	1.256	.032	1.247	.030
0.95	1.0	1.289	0	1.259	0	1.241	0
	0.90	1.292	.020	1.263	.012	1.240	.007
	0.75	1.289	.038	1.259	.027	1.233	.019
	0.50	1.247	.045	1.238	.036	1.213	.030
	0.25	1.208	.038	1.208	.033	1.194	.030
	0	1.191	.028	1.188	.026	1.181	.025
0.90	1.0	1.214	0	1.191	0	1.176	0
	0.90	1.220	.017	1.193	.010	1.176	.006
	0.75	1.214	.033	1.193	.022	1.171	.015
	0.50	1.179	.037	1.174	.029	1.155	.024
	0.25	1.152	.030	1.152	.026	1.141	.024
	0	1.139	.022	1.136	.020	1.131	.019
0.85	1.0	1.152	0	1.136	0	1.126	0
	0.90	1.157	.013	1.139	.007	1.125	.004
	0.75	1.155	.024	1.136	.016	1.122	.011
	0.50	1.129	.028	1.124	.023	1.111	.017
	0.25	1.109	.022	1.109	.020	1.101	.017
	0	1.099	.017	1.099	.016	1.093	.015
0.80	1.0	1.104	0	1.095	0	1.087	0
	0.90	1.106	.008	1.094	.004	1.087	.003
	0.75	1.106	.016	1.090	.011	1.085	.007
	0.50	1.089	.019	1.080	.016	1.079	.012
	0.25	1.078	.016	1.071	.014	1.071	.012
	0	1.071	.012	1.066	.011	1.066	.011
0.75	1.0	1.070	0	1.063	0	1.059	0
	0.90	1.069	.004	1.063	.003	1.059	.002
	0.75	1.065	.010	1.061	.006	1.058	.004
	0.50	1.056	.013	1.055	.010	1.054	.007
	0.25	1.050	.011	1.050	.010	1.050	.008
	0	1.046	.009	1.046	.008	1.046	.007

Table E.2(b) – continued.

		E_s = 4 million psi		E_s = 3.5 million psi		E_s = 3 million psi	
H/H_s	α	R_r	ζ_r	R_r	ζ_r	R_r	ζ_r
0.70	1.0	1.044	0	1.041	0	1.039	0
	0.90	1.044	.002	1.041	.001	1.039	.001
	0.75	1.042	.005	1.040	.003	1.038	.002
	0.50	1.038	.007	1.037	.006	1.036	.004
	0.25	1.034	.007	1.034	.006	1.034	.005
	0	1.031	.006	1.031	.005	1.031	.005
0.65	1.0	1.028	0	1.026	0	1.025	0
	0.90	1.028	.001	1.026	.001	1.025	.000
	0.75	1.027	.002	1.026	.002	1.025	.001
	0.50	1.025	.004	1.024	.003	1.024	.002
	0.25	1.023	.004	1.022	.004	1.022	.003
	0	1.021	.004	1.021	.003	1.021	.003
0.60	1.0	1.017	0	1.016	0	1.016	0
	0.90	1.017	.000	1.016	.000	1.016	.000
	0.75	1.017	.001	1.016	.001	1.016	.001
	0.50	1.016	.002	1.015	.002	1.015	.001
	0.25	1.015	.002	1.014	.002	1.014	.002
	0	1.013	.002	1.013	.002	1.013	.002
0.55	1.0	1.010	0	1.010	0	1.010	0
	0.90	1.010	.000	1.010	.000	1.010	.000
	0.75	1.010	.001	1.010	.000	1.010	.000
	0.50	1.010	.001	1.010	.001	1.009	.001
	0.25	1.009	.001	1.009	.001	1.009	.001
	0	1.009	.001	1.009	.001	1.009	.001
0.50	1.0	1.006	0	1.006	0	1.006	0
	0.90	1.006	.000	1.006	.000	1.006	.000
	0.75	1.006	.000	1.006	.000	1.006	.000
	0.50	1.006	.001	1.006	.001	1.006	.001
	0.25	1.005	.001	1.005	.001	1.005	.001
	0	1.005	.001	1.005	.001	1.005	.001

Table E.2(c) Standard values for R_r and ζ_r, the period lengthening ratio and added damping ratio due to hydrodynamic effects for modulus of elasticity of concrete, E_s = 2.5, 2 and 1 million psi.

		E_s = 2.5 million psi		E_s = 2 million psi		E_s = 1 million psi	
H/H_s	α	R_r	ζ_r	R_r	ζ_r	R_r	ζ_r
1.0	1.0	1.301	0	1.286	0	1.263	0
	0.90	1.301	.005	1.285	.003	1.263	.001
	0.75	1.287	.014	1.284	.009	1.262	.004
	0.50	1.283	.025	1.275	.018	1.260	.008
	0.25	1.264	.030	1.262	.024	1.256	.013
	0	1.247	.027	1.247	.024	1.247	.017
0.95	1.0	1.224	0	1.212	0	1.193	0
	0.90	1.224	.005	1.211	.003	1.193	.001
	0.75	1.221	.012	1.210	.008	1.193	.003
	0.50	1.209	.022	1.203	.015	1.191	.007
	0.25	1.194	.025	1.192	.020	1.187	.011
	0	1.181	.022	1.181	.020	1.181	.014
0.90	1.0	1.164	0	1.154	0	1.140	0
	0.90	1.163	.004	1.154	.002	1.140	.001
	0.75	1.161	.009	1.152	.006	1.140	.002
	0.50	1.152	.017	1.148	.012	1.139	.005
	0.25	1.141	.020	1.140	.016	1.136	.008
	0	1.131	.018	1.131	.016	1.131	.011
0.85	1.0	1.117	0	1.110	0	1.100	0
	0.90	1.116	.003	1.110	.002	1.100	.001
	0.75	1.115	.007	1.109	.004	1.100	.002
	0.50	1.109	.012	1.106	.009	1.100	.004
	0.25	1.101	.014	1.100	.012	1.097	.006
	0	1.093	.013	1.093	.012	1.093	.008
0.80	1.0	1.081	0	1.077	0	1.071	0
	0.90	1.081	.002	1.077	.001	1.071	.000
	0.75	1.080	.004	1.076	.003	1.071	.001
	0.50	1.076	.008	1.074	.006	1.070	.003
	0.25	1.071	.010	1.071	.008	1.069	.005
	0	1.066	.010	1.066	.008	1.066	.006
0.75	1.0	1.055	0	1.053	0	1.049	0
	0.90	1.055	.001	1.053	.001	1.049	.000
	0.75	1.054	.003	1.052	.002	1.049	.001
	0.50	1.053	.005	1.051	.004	1.048	.002
	0.25	1.050	.007	1.049	.005	1.048	.003
	0	1.046	.007	1.046	.006	1.046	.004

Table E.2(c) – continued.

		E_s = 2.5 million psi		E_s = 2 million psi		E_s = 1 million psi	
H/H_s	α	R_r	ζ_r	R_r	ζ_r	R_r	ζ_r
0.70	1.0	1.037	0	1.035	0	1.033	0
	0.90	1.037	.001	1.035	.000	1.033	.000
	0.75	1.037	.002	1.035	.001	1.033	.000
	0.50	1.035	.003	1.034	.002	1.033	.001
	0.25	1.033	.004	1.033	.004	1.032	.002
	0	1.031	.004	1.031	.004	1.031	.003
0.65	1.0	1.024	0	1.023	0	1.022	0
	0.90	1.024	.000	1.023	.000	1.022	.000
	0.75	1.024	.001	1.023	.001	1.022	.000
	0.50	1.023	.002	1.023	.001	1.022	.001
	0.25	1.022	.003	1.022	.002	1.021	.001
	0	1.021	.003	1.021	.003	1.021	.002
0.60	1.0	1.016	0	1.016	0	1.014	0
	0.90	1.016	.000	1.016	.000	1.014	.000
	0.75	1.016	.001	1.016	.001	1.014	.000
	0.50	1.015	.001	1.015	.001	1.014	.000
	0.25	1.014	.002	1.014	.002	1.014	.001
	0	1.013	.002	1.013	.002	1.013	.001
0.55	1.0	1.009	0	1.009	0	1.009	0
	0.90	1.009	.000	1.009	.000	1.009	.000
	0.75	1.009	.000	1.009	.000	1.009	.000
	0.50	1.009	.001	1.009	.000	1.009	.000
	0.25	1.009	.001	1.009	.001	1.009	.000
	0	1.009	.001	1.009	.001	1.009	.001
0.50	1.0	1.006	0	1.006	0	1.005	0
	0.90	1.006	.000	1.006	.000	1.005	.000
	0.75	1.006	.000	1.006	.000	1.005	.000
	0.50	1.006	.000	1.005	.000	1.005	.000
	0.25	1.005	.000	1.005	.000	1.005	.000
	0	1.005	.001	1.005	.000	1.005	.000

Table E.3 Standard values for R_f and ζ_f, the period lengthening ratio and added damping ratio due to dam-foundation interaction.

		Added damping ratio, ζ_f									
E_f / E_s	R_f	η_f =.01	η_f =.02	η_f =.03	η_f =.04	η_f =.05	η_f =.06	η_f =.07	η_f =.08	η_f =.09	η_f =.10
5.0	1.044	.011	.011	.011	.012	.012	.013	.013	.013	.014	.014
4.5	1.049	.012	.012	.013	.013	.014	.014	.015	.015	.015	.016
4.0	1.054	.013	.014	.014	.015	.015	.016	.016	.017	.017	.018
3.5	1.061	.016	.016	.017	.017	.018	.018	.019	.019	.020	.020
3.0	1.070	.018	.019	.020	.020	.021	.021	.022	.023	.023	.024
2.5	1.083	.022	.023	.024	.024	.025	.026	.026	.027	.028	.028
2.0	1.102	.028	.029	.030	.030	.031	.032	.033	.034	.035	.035
1.5	1.131	.037	.038	.039	.040	.041	.042	.043	.045	.046	.047
1.4	1.139	.040	.041	.042	.043	.044	.045	.046	.048	.049	.050
1.3	1.149	.043	.044	.045	.046	.047	.049	.050	.051	.052	.053
1.2	1.159	.046	.047	.049	.050	.051	.052	.054	.055	.056	.057
1.1	1.172	.050	.051	.053	.054	.055	.057	.058	.059	.061	.062
1.0	1.187	.054	.056	.057	.059	.060	.062	.063	.065	.066	.067
0.9	1.204	.060	.062	.063	.065	.066	.068	.069	.071	.072	.074
0.8	1.225	.066	.068	.070	.072	.073	.075	.077	.078	.080	.082
0.7	1.252	.075	.076	.078	.080	.082	.084	.086	.087	.089	.091
0.6	1.286	.085	.087	.089	.091	.093	.095	.097	.099	.101	.103
0.5	1.332	.097	.100	.102	.104	.107	.109	.111	.114	.116	.118
0.4	1.396	.115	.117	.120	.123	.125	.128	.130	.133	.136	.138
0.3	1.495	.138	.141	.145	.148	.151	.154	.157	.160	.163	.166
0.2	1.670	.173	.177	.181	.185	.189	.193	.197	.201	.205	.208

Table E.3 – continued.

	Added damping ratio, ζ_f						
E_f / E_s	η_f =0.12	η_f =0.14	η_f =0.16	η_f =0.18	η_f =0.20	η_f =0.25	η_f =0.50
5.0	.015	.016	.016	.017	.018	.019	.025
4.5	.017	.017	.018	.019	.020	.021	.027
4.0	.019	.020	.020	.021	.022	.024	.030
3.5	.021	.022	.023	.024	.025	.027	.035
3.0	.025	.026	.027	.028	.029	.032	.040
2.5	.030	.031	.032	.034	.035	.038	.047
2.0	.037	.039	.040	.042	.043	.046	.058
1.5	.049	.051	.052	.054	.056	.060	.075
1.4	.052	.054	.056	.058	.060	.064	.080
1.3	.055	.058	.060	.062	.064	.068	.085
1.2	.060	.062	.064	.066	.068	.073	.091
1.1	.064	.067	.069	.072	.074	.079	.098
1.0	.070	.073	.075	.078	.080	.086	.107
0.9	.077	.080	.082	.085	.088	.094	.117
0.8	.085	.088	.091	.094	.097	.104	.129
0.7	.095	.098	.101	.105	.108	.115	.143
0.6	.107	.111	.114	.118	.121	.130	.162
0.5	.122	.127	.131	.135	.139	.149	.186
0.4	.143	.148	.153	.158	.163	.174	.220
0.3	.172	.179	.185	.191	.196	.211	.269
0.2	.216	.224	.232	.240	.247	.266	.351

Table E.4(a) Standard values for the hydrodynamic pressure function $p(\hat{y})$ for full reservoir, i.e., $H/H_s = 1$; $\alpha = 1.0$.

	Value of $gp(\hat{y}) / wH$												
$\hat{y} = y / H$	$R_w \leq .5$	$R_w = .7$	$R_w = .8$	$R_w = .85$	$R_w = .90$	$R_w = .92$	$R_w = .93$	$R_w = .94$	$R_w = .95$	$R_w = .96$	$R_w = .97$	$R_w = .98$	$R_w = .99$
1.00	0	0	0	0	0	0	0	0	0	0	0	0	0
0.95	.070	.073	.076	.079	.083	.086	.088	.090	.092	.096	.102	.111	.133
0.90	.112	.118	.124	.129	.138	.143	.147	.151	.157	.164	.176	.195	.238
0.85	.127	.135	.144	.152	.164	.172	.178	.184	.193	.204	.221	.249	.313
0.80	.133	.144	.155	.165	.182	.193	.200	.208	.220	.235	.257	.295	.379
0.75	.141	.154	.168	.180	.201	.214	.223	.234	.248	.267	.294	.340	.445
0.70	.145	.161	.178	.192	.216	.232	.242	.255	.272	.294	.327	.382	.506
0.65	.143	.161	.180	.197	.224	.242	.254	.269	.288	.313	.351	.414	.558
0.60	.139	.159	.180	.199	.230	.250	.264	.280	.301	.330	.373	.444	.605
0.55	.137	.159	.183	.203	.237	.260	.274	.293	.316	.348	.395	.473	.651
0.50	.135	.159	.184	.206	.244	.269	.284	.304	.329	.364	.415	.500	.694
0.45	.130	.155	.182	.206	.246	.272	.289	.310	.338	.375	.430	.522	.730
0.40	.124	.151	.179	.204	.247	.275	.293	.315	.345	.384	.442	.540	.762
0.35	.121	.149	.179	.205	.250	.279	.298	.322	.353	.395	.456	.559	.793
0.30	.118	.147	.178	.206	.252	.283	.303	.328	.360	.403	.467	.575	.820
0.25	.113	.143	.175	.204	.252	.284	.304	.330	.363	.408	.475	.587	.840
0.20	.109	.139	.172	.202	.252	.284	.305	.332	.366	.412	.481	.596	.856
0.15	.107	.138	.172	.202	.252	.286	.307	.334	.369	.417	.487	.604	.871
0.10	.106	.137	.172	.202	.253	.287	.309	.337	.372	.420	.491	.611	.881
0.05	.103	.135	.169	.200	.252	.286	.308	.336	.372	.420	.492	.613	.886
0	.100	.133	.168	.198	.251	.285	.307	.335	.371	.420	.492	.613	.886

Table E.4(b) Standard values for the hydrodynamic pressure function $p(\hat{y})$ for full reservoir, i.e., $H/H_s = 1;\ \alpha = 0.90$.

	Value of $gp(\hat{y})/wH$								
$\hat{y} = y/H$	$R_w \leq .5$	$R_w = .7$	$R_w = .8$	$R_w = .9$	$R_w = .95$	$R_w = 1.0$	$R_w = 1.05$	$R_w = 1.1$	$R_w = 1.2$
1.00	0	0	0	0	0	0	0	0	0
0.95	.070	.073	.076	.082	.088	.089	.069	.064	.062
0.90	.112	.118	.124	.136	.149	.149	.110	.100	.095
0.85	.127	.135	.144	.162	.181	.181	.123	.108	.101
0.80	.133	.144	.155	.179	.204	.205	.127	.107	.098
0.75	.141	.154	.168	.197	.228	.229	.133	.108	.097
0.70	.145	.161	.177	.212	.249	.249	.135	.105	.092
0.65	.143	.161	.179	.219	.261	.262	.130	.096	.081
0.60	.139	.159	.179	.234	.271	.272	.124	.085	.067
0.55	.137	.159	.182	.231	.283	.283	.119	.076	.057
0.50	.135	.159	.183	.236	.293	.292	.114	.067	.046
0.45	.130	.155	.181	.238	.299	.298	.106	.055	.032
0.40	.124	.150	.178	.238	.303	.301	.097	.044	.019
0.35	.121	.148	.177	.241	.309	.307	.091	.035	.009
0.30	.118	.146	.177	.243	.313	.311	.086	.027	.000
0.25	.113	.142	.174	.242	.315	.312	.078	.017	.000
0.20	.109	.139	.171	.241	.316	.312	.071	.008	.000
0.15	.107	.137	.170	.242	.318	.313	.067	.003	.000
0.10	.106	.136	.170	.242	.320	.313	.064	.000	.000
0.05	.103	.134	.167	.241	.318	.311	.059	.000	.000
0	.101	.133	.166	.239	.317	.309	.056	.000	.000

Table E.4(c) Standard values for the hydrodynamic pressure function $p(\hat{y})$ for full reservoir, i.e., $H/H_s = 1;\ \alpha = 0.75$.

	Value of $gp(\hat{y}) / wH$								
$\hat{y} = y / H$	$R_w \leq .5$	$R_w = .7$	$R_w = .8$	$R_w = .9$	$R_w = .95$	$R_w = 1.0$	$R_w = 1.05$	$R_w = 1.1$	$R_w = 1.2$
1.00	0	0	0	0	0	0	0	0	0
0.95	.070	.073	.075	.079	.080	.078	.073	.068	.065
0.90	.112	.118	.122	.129	.132	.128	.118	.101	.101
0.85	.127	.133	.140	.151	.154	.150	.134	.121	.110
0.80	.133	.143	.152	.166	.171	.163	.142	.125	.110
0.75	.140	.153	.164	.181	.187	.177	.151	.130	.110
0.70	.145	.159	.173	.193	.200	.188	.157	.131	.108
0.65	.143	.159	.174	.197	.205	.191	.155	.126	.099
0.60	.139	.157	.174	.199	.208	.192	.151	.118	.088
0.55	.137	.157	.175	.203	.213	.195	.150	.113	.079
0.50	.135	.156	.176	.206	.216	.196	.147	.107	.070
0.45	.129	.152	.173	.205	.216	.194	.140	.097	.058
0.40	.123	.147	.170	.203	.214	.191	.134	.088	.045
0.35	.120	.145	.169	.204	.215	.190	.129	.080	.036
0.30	.117	.143	.168	.204	.215	.188	.125	.074	.027
0.25	.112	.139	.164	.201	.212	.184	.118	.065	.016
0.20	.108	.135	.161	.199	.209	.180	.111	.056	.007
0.15	.106	.134	.159	.198	.208	.177	.107	.051	.001
0.10	.104	.133	.158	.197	.207	.175	.103	.046	.000
0.05	.102	.130	.156	.194	.204	.171	.098	.040	.000
0	.100	.128	.154	.192	.201	.167	.093	.036	.000

Table E.4(d) Standard values for the hydrodynamic pressure function $p(\hat{y})$ for full reservoir, i.e., $H/H_s = 1;\ \alpha = 0.50$.

	Value of $gp(\hat{y})/wH$								
$\hat{y} = y/H$	$R_w \leq .5$	$R_w = .7$	$R_w = .8$	$R_w = .9$	$R_w = .95$	$R_w = 1.0$	$R_w = 1.05$	$R_w = 1.1$	$R_w = 1.2$
1.00	0	0	0	0	0	0	0	0	0
0.95	.071	.072	.073	.074	.074	.073	.072	.070	.068
0.90	.112	.116	.118	.119	.119	.118	.116	.113	.108
0.85	.125	.132	.135	.136	.135	.134	.130	.127	.120
0.80	.132	.139	.143	.146	.145	.143	.138	.133	.123
0.75	.139	.148	.153	.156	.155	.152	.146	.139	.127
0.70	.144	.154	.160	.163	.162	.158	.151	.143	.128
0.65	.141	.152	.159	.163	.161	.156	.148	.138	.122
0.60	.137	.149	.157	.162	.160	.153	.143	.132	.113
0.55	.135	.148	.156	.161	.158	.151	.141	.128	.107
0.50	.133	.147	.155	.159	.156	.148	.137	.123	.099
0.45	.127	.142	.150	.154	.151	.142	.129	.115	.088
0.40	.121	.136	.145	.149	.145	.136	.122	.106	.077
0.35	.117	.133	.143	.146	.142	.131	.116	.099	.069
0.30	.114	.131	.140	.143	.137	.126	.110	.092	.060
0.25	.109	.126	.135	.137	.131	.119	.102	.083	.050
0.20	.104	.121	.130	.132	.125	.112	.094	.074	.040
0.15	.102	.119	.127	.128	.121	.108	.089	.068	.033
0.10	.100	.117	.125	.125	.118	.104	.083	.062	.026
0.05	.098	.114	.121	.121	.113	.098	.077	.055	.018
0	.096	.111	.119	.117	.108	.093	.072	.049	.012

Table E.4(e) Standard values for the hydrodynamic pressure function $p(\hat{y})$ for full reservoir, i.e., $H/H_s = 1;\ \alpha = 0.25$.

	Value of $gp(\hat{y}) / wH$								
$\hat{y} = y / H$	$R_w \leq .5$	$R_w = .7$	$R_w = .8$	$R_w = .9$	$R_w = .95$	$R_w = 1.0$	$R_w = 1.05$	$R_w = 1.1$	$R_w = 1.2$
1.00	0	0	0	0	0	0	0	0	0
0.95	.069	.070	.071	.071	.071	.071	.070	.070	.070
0.90	.111	.113	.114	.114	.114	.114	.113	.113	.111
0.85	.124	.127	.128	.129	.129	.128	.127	.127	.125
0.80	.130	.133	.134	.135	.135	.134	.133	.132	.129
0.75	.137	.141	.142	.143	.142	.141	.140	.138	.135
0.70	.141	.145	.147	.147	.146	.145	.143	.141	.137
0.65	.137	.142	.144	.144	.143	.142	.140	.137	.131
0.60	.133	.138	.140	.139	.138	.136	.134	.131	.124
0.55	.131	.136	.137	.136	.135	.133	.130	.126	.118
0.50	.128	.133	.134	.133	.131	.128	.125	.121	.112
0.45	.121	.126	.127	.126	.124	.120	.116	.112	.101
0.40	.115	.120	.120	.118	.115	.112	.107	.102	.091
0.35	.111	.116	.116	.113	.110	.106	.100	.095	.082
0.30	.107	.111	.111	.107	.104	.099	.093	.087	.074
0.25	.101	.105	.104	.100	.096	.091	.084	.077	.063
0.20	.096	.099	.098	.093	.088	.082	.076	.068	.052
0.15	.094	.096	.094	.088	.083	.076	.069	.061	.044
0.10	.092	.096	.090	.083	.078	.071	.063	.054	.037
0.05	.088	.088	.085	.077	.071	.064	.055	.046	.028
0	.086	.085	.081	.072	.065	.057	.048	.039	.020

Table E.4(f) Standard values for the hydrodynamic pressure function $p(\hat{y})$ for full reservoir, i.e., $H/H_s = 1;\ \alpha = 0$.

	Value of $gp(\hat{y}) / wH$								
$\hat{y} = y / H$	$R_w \leq .5$	$R_w = .7$	$R_w = .8$	$R_w = .9$	$R_w = .95$	$R_w = 1.0$	$R_w = 1.05$	$R_w = 1.1$	$R_w = 1.2$
1.00	0	0	0	0	0	0	0	0	0
0.95	.069	.069	.069	.069	.069	.069	.070	.070	.070
0.90	.109	.110	.110	.111	.111	.111	.112	.112	.112
0.85	.122	.123	.124	.125	.125	.125	.126	.126	.126
0.80	.127	.128	.128	.129	.129	.129	.130	.130	.130
0.75	.133	.134	.134	.135	.135	.135	.136	.136	.136
0.70	.135	.136	.137	.138	.138	.138	.139	.139	.139
0.65	.132	.133	.133	.133	.133	.133	.134	.134	.134
0.60	.127	.127	.127	.127	.127	.127	.127	.127	.127
0.55	.123	.123	.123	.123	.123	.123	.122	.122	.121
0.50	.120	.119	.118	.118	.118	.117	.116	.116	.115
0.45	.113	.111	.110	.109	.109	.108	.107	.106	.105
0.40	.105	.103	.102	.100	.099	.098	.097	.096	.094
0.35	.101	.098	.096	.094	.092	.091	.090	.088	.085
0.30	.096	.092	.090	.087	.085	.084	.082	.080	.076
0.25	.090	.085	.082	.078	.076	.074	.072	.069	.065
0.20	.084	.078	.074	.070	.067	.065	.062	.059	.053
0.15	.080	.073	.068	.064	.061	.058	.055	.051	.045
0.10	.077	.069	.064	.058	.054	.051	.048	.044	.036
0.05	.073	.063	.057	.050	.046	.043	.039	.035	.026
0	.070	.058	.052	.044	.040	.036	.031	.027	.017

Table E.5(a) Standard values for A_p, the hydrodynamic force coefficient in $\tilde{L}_1$; $\alpha = 1.0$.

R_w	Value of A_p for α=1
0.99	1.242
0.98	.893
0.97	.739
0.96	.647
0.95	.585
0.94	.539
0.93	.503
0.92	.474
0.90	.431
0.85	.364
0.80	.324
0.70	.279
≤ 0.50	.237

Table E.5(b) Standard values for A_p, the hydrodynamic force coefficient in $\tilde{L}_1$; $\alpha = 0.90$, 0.75, 0.50, 0.25 and 0.

	Value of A_p				
R_w	α=0.90	α=0.75	α=0.50	α=0.25	α=0
1.20	.071	.111	.159	.178	.181
1.10	.110	.177	.204	.197	.186
1.05	.194	.249	.229	.205	.189
1.00	.515	.340	.252	.213	.191
0.95	.518	.378	.267	.219	.193
0.90	.417	.361	.274	.224	.195
0.80	.322	.309	.269	.229	.198
0.70	.278	.274	.256	.228	.201
≤ 0.50	.237	.236	.231	.222	.206

Table E.6 Standard values for the hydrodynamic pressure function $p_0(\hat{y})$.

$\hat{y} = y / H$	gp_0 / wH
1.0	0
0.95	.137
0.90	.224
0.85	.301
0.80	.362
0.75	.418
0.70	.465
0.65	.509
0.60	.546
0.55	.580
0.50	.610
0.45	.637
0.40	.659
0.35	.680
0.30	.696
0.25	.711
0.20	.722
0.15	.731
0.10	.737
0.05	.741
0	.742